RWTH AACHEN UNIVERSITY

Design of a Test Rig and its Testing Methods for Rotation and Expansion Performing Assemblies in Parabolic Trough Collector Power Plants

MASTER'S THESIS

presented by

Andreas Plumpe

Energy Engineering (M.Sc.)

carried out and presented at the

German Aerospace Center (DLR)

Institute of Solar Research

Supervision and Assessment

Univ.-Prof. Dr.-Ing. Bernhard Hoffschmidt

Dipl.-Ing. Christoph Hilgert

Almería, April 13, 2016

Declaration of Academic Honesty / Eidesstattliche Erklärung

I hereby declare to have written the present master's thesis on my own, having used no other resources and tools than the listed. All contents cited from published or nonpublished documents are indicated as such.

Hiermit erkläre ich, dass ich die vorliegende Masterarbeit selbständig verfasst und keine anderen als die angegebenen Hilfsmittel verwendet habe. Alle Inhalte, die wörtlich oder sinngemäß aus veröffentlichten oder nicht veröffentlichten Schriften entnommen sind, sind als solche kenntlich gemacht.

Ort, Datum

Unterschrift

Abstract

The present master's thesis deals with the design of a new test rig for the investigation of durability and failure mechanisms of flexible pipe connections – so called Rotation and Expansion Performing Assemblies (REPAs) –, which are utilized in Parabolic Trough Collector power plants. Said assemblies compensate for the motion of the absorber tubes relative to the fixed piping of the header connection. The work focusses on the test rig's design in view of a realistic simulation of all loads a REPA is exposed to in commercial applications. To achieve this, all possible requirements of the components, which are supposed to endure a lifetime of up to 30 years in power plants, are depicted. A literature research is carried out in order to investigate and evaluate existing test rigs for REPAs or their single components. By means of the findings, a specification sheet is derived.

The test rig is composed of two main assemblies. On the one hand, a *Kinematics Unit* is used to reproduce the cyclic rotational and translational motions of a Parabolic Trough Collector. On the other hand, an *HTF cycle* (Heat Transfer Fluid cycle) conduces to set up pressure, temperature and flow rate circulating through the test specimens. The main part of the thesis contributes to the integration of the externally designed Kinematics Unit into the HTF cycle – taking into consideration realistic operation conditions and a complete and precise measurement of all parameters. Special emphasis is put on an accurate acquisition of the mechanical loads the test objects have to cope with.

As a result of this work, a test rig is erected enabling realistic endurance tests of two serially connected REPAs in less than three months. The hydraulic properties are adjustable in terms of mass flow ($6-60\ {}^{m^3}/_{h}$), pressure (up to 40 bars) and temperature (up to 450 $°C$). The investigations can be tailored to customized applications of the REPA concept (Ball Joint Assemblies or Rotary Flex Hose Assemblies) and the collector geometry (e.g. focal length).

Kurzfassung

Die vorliegende Masterarbeit beschreibt die Auslegung eines Prüfstands zur Untersuchung von Lebensdauer und Versagensmechanismen flexibler Rohrverbinder – sog. REPAs (Rotation and Expansion Performing Assemblies) –, die in solarthermischen Parabolrinnenkraftwerken zum Einsatz kommen. Diese Vorrichtungen werden zur Verbindung der sich bewegenden Absorberrohre und der feststehenden Rohrleitung eingesetzt. Ziel der Arbeit ist die Auslegung des Prüfstands hinsichtlich einer möglichst realitätsnahen Abbildung der Beanspruchungen, denen die Testobjekte im kommerziellen Anwendungsfall ausgesetzt sind. Um dies zu gewährleisten, werden sämtliche Anforderungen an die Komponenten, die im Kraftwerk eine Lebensdauer von bis zu 30 Jahren aufweisen sollen, untersucht. Zugleich bietet die Arbeit eine Literaturrecherche mit dem Ziel, bereits existierende Prüfstande zur Untersuchung von REPAs bzw. deren Einzelkomponenten zu beurteilen. Aus den gewonnenen Erkenntnissen wird ein Lastenheft abgeleitet, nach dessen Vorgaben die Auslegung der Anlage stattfindet.

Der Prüfstand besteht aus zwei Baugruppen: einer sog. *Kinematikeinheit*, die die zyklischen Rotations- und Translationsbewegungen eines Parabolrinnenkollektors präzise nachstellt, und einem *Wärmeträgerkreislauf*, über den Druck, Temperatur und Massenstrom an den Prüflingen eingestellt werden können. Der Schwerpunkt der Arbeit liegt auf der Integration der vorausgelegten Kinematikeinheit in den Wärmeträgerkreislauf – unter dem Gesichtspunkt eines anwendungsgetreuen Betriebs der REPAs und der möglichst vollständigen und präzisen Messung aller Betriebsparameter. Besondere Beachtung kommt dabei der Erfassung der mechanischen Belastungen zu, die die Testobjekte während des Betriebs erfahren.

Im Zuge dieser Arbeit wird eine Anlage in Betrieb genommen, die realitätsgetreue Lebensdauerstests zweier seriell verbundener REPAs ermöglicht. Dabei lassen sich mittels Durchflussrate ($6 - 60\ {}^{m^3}/_{h}$), Systemdruck (bis zu 40 bar) und Temperatur des Wärmeträgeröls (bis zu 450 $°C$) sämtliche Anwendungsfälle moderner Parabolrinnenkraftwerke simulieren. Die Untersuchungen werden im Hinblick auf das REPA-Konzept (sog. Ball Joint Assemblies oder Rotary Flex Hose Assemblies) und die Kollektorgeometrie (z.B. Fokallänge) maßgeschneidert an die jeweilige Anwendung angepasst.

Contents

List of Tables

List of Figures

Nomenclature

Greek Symbols

Symbol	Unit	Signification
α	$^1/_K$	coefficient of thermal expansion
α	$^W/_{m^2K}$	heat transfer coefficient
α	$^\circ$	angle (angular expansion joint)
δ	$^\circ$	conical angle
δ	mm	dilatation (axial expansion joint)
Δ	-	difference
ϵ	-	emissivity
ζ	-	resistance coefficient
ϑ	K	temperature
λ	-	pipe friction coefficient
ξ	-	coefficient (change of cross section)
ρ	$^{kg}/_{m^3}$	density
σ	$5.669 \cdot 10^{-8}$ $^W/_{m^2K^4}$	Stefan-Boltzmann constant

Roman Symbols

Symbol	Unit	Signification
c	$^{N}/_{mm}$	spring rate
d	mm	diameter
DN	mm	pipe nominal diameter
F	N	force
g	9.81 $^{m}/_{s^2}$	standard gravity
H	m	differential head
I_0	1367 $^{W}/_{m^2}$	solar constant
$\vec{I}$	$^{kg \cdot m}/_{s}$	momentum
k	$^{W}/_{mK}$	thermal transmission coefficient
L	m	length
M	Nm	torque
$\vec{n}$	-	normal
p	bar	pressure
$\dot{q}''$	$^{W}/_{m^2}$	specific heat flux (per unit area)
$\dot{q}'$	$^{W}/_{m}$	specific heat flux (per unit length)
$\dot{Q}$	W	heat flux
r	mm	radius (pipe bend)
t	-	time
T	K / $°C$	temperature
V	m^3	volume
$\dot{V}$	$^{m^3}/_{h}$	volume flow
w	$^{m}/_{s}$	velocity
$\vec{w}$	$^{m}/_{s}$	velocity (vectorial)
x, y, z	-	coordinates of the Cartesian coordinate system

Acronyms and Abbreviations

ASME	American Society of Mechanical Engineers
BJA	Ball Joint Assembly
CAD	Computer-Aided Design
CAE	Computer-Aided Engineering
CIEMAT	Centro de Investigaciones Energéticas, Medioambientales y Tecnológicas
CSP	Concentrated Solar Power
DIN	Deutsches Institut für Normung (German Institute for Standardization)
DLR	Deutsches Zentrum für Luft- und Raumfahrt (German Aerospace Center)
DNI	Direct Normal Irradiation
DP-DPO	Diphenyl-Diphenyl Oxide
DSG	Direct Steam Generation
EJ	Expansion Joint
ET	EuroTrough
FFPT	Fixed Focus Parabolic Trough
HCE	Heat Collector Element
HTF	Heat Transfer Fluid
LS	Luz System
PTC	Parabolic Trough Collector
PSA	Plataforma Solar de Almería
REPA	Rotation and Expansion Performing Assembly
RFHA	Rotary Flex Hose Assembly
SCA	Solar Collector Assembly
SCE	Solar Collector Element
SEGS	Solar Energy Generating Systems

Subscripts

amb	ambient
b	bend
cs	cross section
con	convection
def	deflection
e	electrical
flex	flexible
fr	friction
g	gravity
i	inner (diameter)
in	inlet
ins	insulation
is	intersection
L	length
max	maximum
min	minimum
o	outer (diameter)
out	outlet
p	pipe
p	pressure
pre	pre-tension
rad	radiation
S	sun
th	thermal
v	valve

Chapter 1

Introduction

The qualification department of the Institute of Solar Research, member of the German Aerospace Center, deals with the characterization of key components like, for instance, solar mirrors, parabolic trough receivers and flexible pipe connections, as well as with the evaluation of the system performance of collectors and solar fields. Therefore, measurement techniques are developed which can be used to study and evaluate the performance of said components. The results are used to identify and apply possible improvements on the components or systems, leading to a more efficient, cost-effective and durable Concentrated Solar Power (CSP) technology.

The present master's thesis comprises the design of a test rig and its testing methods for the investigation of durability and failure mechanisms of flexible pipe connections, so called Rotation and Expansion Performing Assemblies (REPAs), which are installed in Parabolic Trough Collector (PTC) power plants. Those key components are applied to maintain a connection between the fixed piping on the one hand and the moving absorber tube on the other hand. Since they are exposed to high pressures and temperatures of the Heat Transfer Fluid (HTF), repeated motion, mechanical stresses and concentrated solar radiation, REPAs are highly stressed components.

The purpose of the test rig is to enable an accelerated, yet realistic, durability test of two serially connected REPAs. In order to achieve this, the test rig consists of two assemblies: a *Kinematics Unit*, utilized to reproduce the cyclic rotational and translational motion of a Parabolic Trough Collector, whereas an *HTF cycle* ensures boundary conditions – such as temperature, pressure and mass flow – similar to those of commercial power plants. Key activity of the present work is the integration of the externally designed Kinematics Unit into the HTF cycle, taking into account realistic operation of the REPAs and a complete and precise acquisition of all relevant operating parameters.

Initially, an overview of CSP technologies will be presented with emphasis on PTCs and their relevant components. Afterwards, the State of the Art in regard to testing methods of REPAs will serve to disclose the necessity for a more sophisticated test rig. Then, all possible requirements and loads a REPA has to cope with during operation will be revealed and a specification sheet for the test rig will be determined. Finally, the design of the HTF cycle and its interaction with the Kinematics Unit will be presented; special attention will be given to the acquisition of mechanical loads the REPAs are exposed to.

Chapter 2

Fundamentals

The subsequent chapter provides an overview of solar thermal background knowledge. After explaining basic principles of solar radiation, different concepts of its thermal conversion and its employing in today's energy economy are presented. The focus will be on Parabolic Trough Collectors (PTCs) and testing of PTC specific components, which is the superior topic of the present thesis. Special attention will be given to the collector's interconnections, so called Rotation and Expansion Performing Assemblies (REPAs).

2.1 Solar Radiation

All life on earth derives from solar radiation. Within six hours the world's deserts receive more energy from the sun than humankind consumes within a year [1]. Hence, it is our ultimate source of life which has the potential to cover substantial amounts of mankind's energy demands.

Considering the sun as a black body, the characteristics of its emittance can be described by the Stefan-Boltzmann equation [2]

$$\dot{q}''_S = \sigma \cdot T^4 \tag{2.1}$$

Based on sun's surface temperature of $T \approx 5777K$ and the Stefan-Boltzmann constant ($\sigma = 5.669 \cdot 10^{-8}\ {}^{W}/_{m^2K^4}$), the specific heat emittance is obtained as $\dot{q}''_S = 61.9\ {}^{MW}/_{m^2}$. Taking into account the spatial relationship between the sun and the earth, the extraterrestrial solar radiation is given by

$$I_0 \approx 1367\ {}^{W}/_{m^2} = 12\ {}^{MWh}/_{m^2a} \tag{2.2}$$

This value – the *solar constant* – constitutes the amount of radiation vertically penetrating a surface outside the earth's atmosphere [3]. Yet, the effective amount of terrestrial radiation is lower due to reflection and absorption effects in the atmosphere. Moreover, scattering effects (e.g. Rayleigh- and Mie-Scattering) caused by micro particles of the atmosphere decrease the radiation on its way to the earth's surface. Additionally, the distribution of terrestrial solar radiation varies substantially throughout the world due to climatic distinctions, see figure 2.1.

2.2 Concentrating Solar Power

A promising way of harnessing solar energy can be accomplished by converting solar radiation into heat which in turn is utilized in a conventional thermodynamic cycle (e.g. Carnot Cycle) and converted to gather electricity. For most of these energy conversion processes, it is crucial to provide thermal energy at high temperature levels. This is achieved by concentrating sunlight from a large surface onto a small surface or, technically spoken, by increasing the ratio of collector area to absorber area [4].

A major commonality of all Concentrated Solar Power (CSP) technologies derives from the fact, that they are only capable of focussing radiation from one single direction, in other words: Direct Normal Irradiation (DNI) is concentrated. Figure 2.1 shows the average worldwide DNI. Having a closer look at the illustration reveals possible locations for CSP, since the economic sense for erecting CSP power plants is given above a DNI threshold of minimum 2000 $^{kWh}/_{m^2 \cdot a}$ [5].

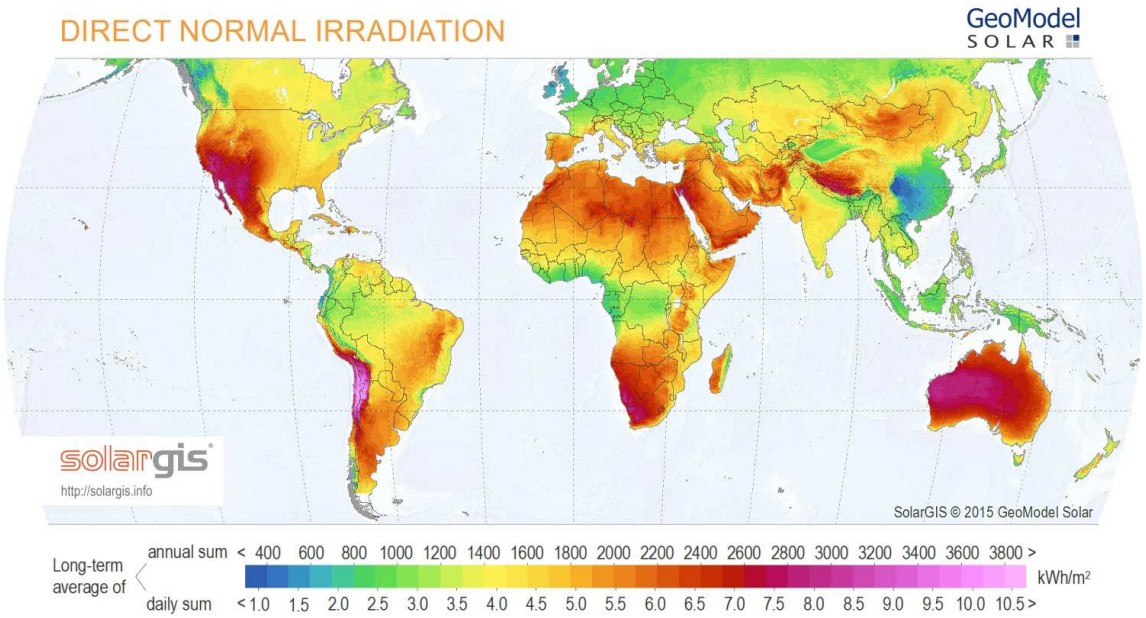

Figure 2.1: Average worldwide annual and daily DNI on a horizontal plane in kWh/m^2 [6]

In addition, being solely able to concentrate DNI discloses the necessity of mechanical sun-tracking systems. A general distinction can be made between point-focussing (e.g. Solar Tower and Solar Dish) and line-focussing systems (e.g. Parabolic Trough and Linear Fresnel), see figure 2.2 and figure 2.3, respectively. Though all point-focussing systems require two-axes suntracking, they can achieve thousandfold concentration and therefore higher temperatures compared to line-focussing systems. The following subchapters serve to provide an overview regarding nowadays CSP technologies. Afterwards, an individual chapter is dedicated to Parabolic Trough Collectors.

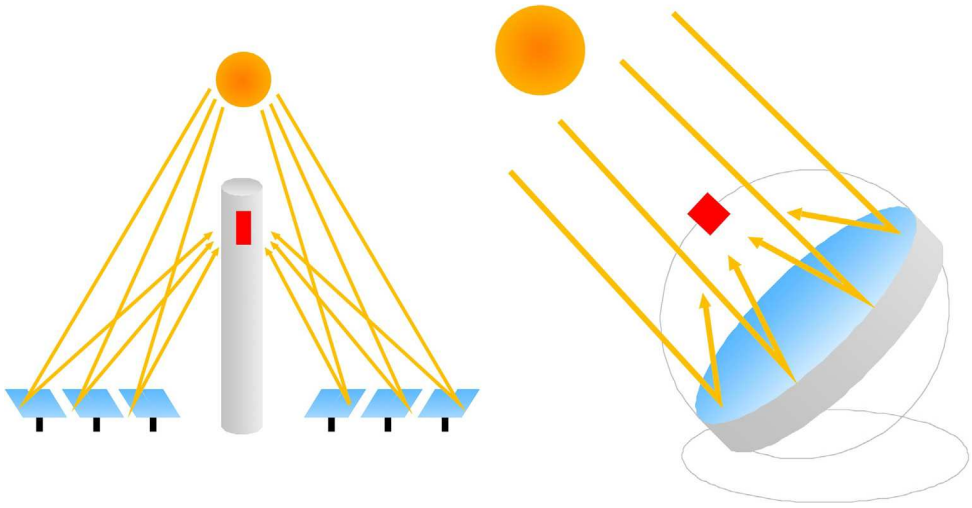

Figure 2.2: Scheme of Solar Tower (left) and Solar Dish (right) [7]

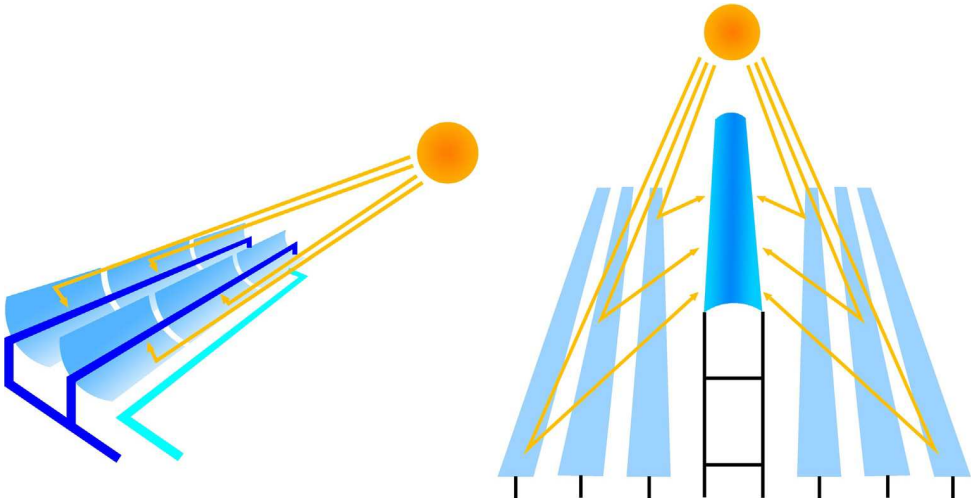

Figure 2.3: Scheme of Parabolic Trough (left) and Linear Fresnel (right) [7]

2.2.1 Solar Tower

Solar Tower systems consist of a large-scale field of plane reflectors (heliostats) focussing sunlight on a tower-mounted central receiver. Heliostats are slightly concave curved mirror assemblies which provide concentration of radiation onto a focal spot (receiver) on the tower. Using this technology, concentration factors of up to a thousandfold are feasible. Due to the high solar flux, temperatures of up to 1200 $°C$ can be achieved at the absorber. It is pressurized with Heat Transfer Fluid (HTF) carrying the enthalpy in either a Rankine cycle, a Brayton cycle or a combination of both (combined cycle). Either way, a steam or gas turbine serves to generate electricity. Solar Tower power plants also distinguish between the utilized HTF and the corresponding thermal storage system. Figure 2.4, for instance, depicts a plant schematics example of an open volumetric air receiver, as it has been erected in Jülich (*Solar Thermal Test and Demonstation Power Plant Jülich*). The

air cycle, featuring a storage system filled with a packing of ceramic elements, is connected to a conventional Rankine cycle converting thermal power into electricity [8] [9].

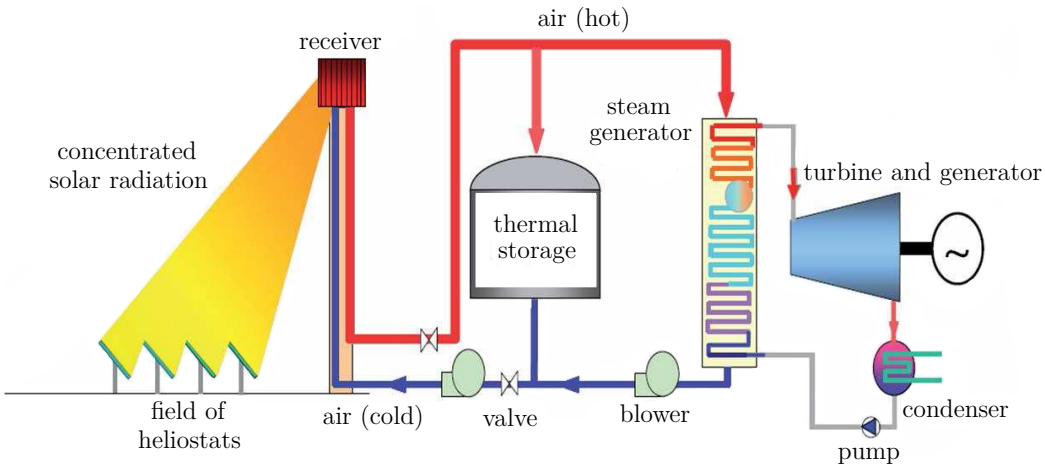

Figure 2.4: Schema of a Solar Tower power plant using a volumetric air receiver [8]

There are different concepts to design a field of heliostats. Whilst there are configurations that consist of a multitude of heliostats arranged in an 180° area northwards of the receiver (north field), 360° solar fields surround the tower in circles, see figure 2.5. The choice of the concept is highly dependent on the degree of latitude as well as of the receiver design.

Figure 2.5: Areal view of the Gemasolar power plant surrounded by a 360° solar field consisting of 2.650 heliostats (Photo: *Torresol Energy*) [10]

2.2.2 Solar Dish

Solar dish systems use an extensive point-focussing concentrator with a rotationally symmetric shape, the so-called *Dish*. The high concentration ratio obtains an elevated temperature range at the receiver, operating a stirling engine to produce electricity . Owing to the fact that only direct radiation can be focussed, there is a necessity of two-axis tracking. Dish systems usually have electric capacities between 10 and 50 kW; thus they are suitable for small stand-alone applications and compete in some sense directly with photovoltaics. Yet, dish systems can be connected in grids to satisfy energy demands up to several Megawatts. These characteristics make them applicable in wide ranges [11]. However, photovoltaics is so far a significantly more established technology in regard to cost competitiveness on the energy market.

Figure 2.6 illustrates the main components of a Solar Dish facility. The paraboloid dish mirror is exposed to solar radiation, whereupon the light is redirected onto the focal point. Next to the focal point there is a heat receiver of a downstream stirling engine, which converts the thermal energy into mechanical energy. Electrical power is retrieved by a generator attached to the stirling engine's crankshaft.

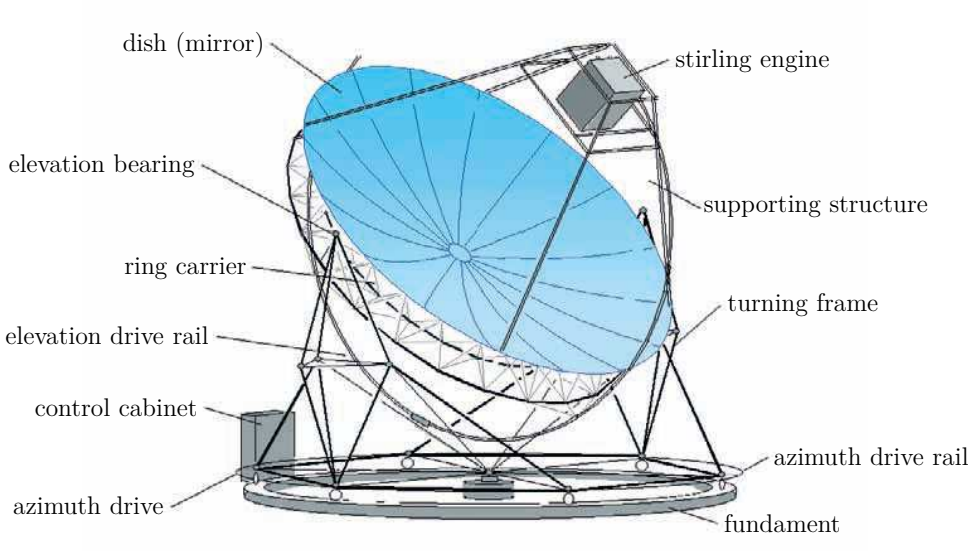

Figure 2.6: Principle of a Solar Dish assembly [11]

2.2.3 Linear Fresnel

The Linear Fresnel collector comprises a single-axis tracked and line-focussing CSP technology. Its working scheme is depicted in figure 2.7. Several optical surfaces (mirror rows) are aligned in a way that reflects the sunlight towards a receiver line, which is represented by an absorber tube. A series of almost flat, narrow-curvature mirrors are used to focus sunlight onto the absorber tube by means of a second stage concentrator. In contrast to Parabolic Trough collectors, the position of the absorber tube is stationary whilst the mirrors track the sun. In commercial applications, water is used as HTF which is being evaporated and superheated. The superheated steam in turn is employed in a steam turbine coupled with a generator to provide electricity.

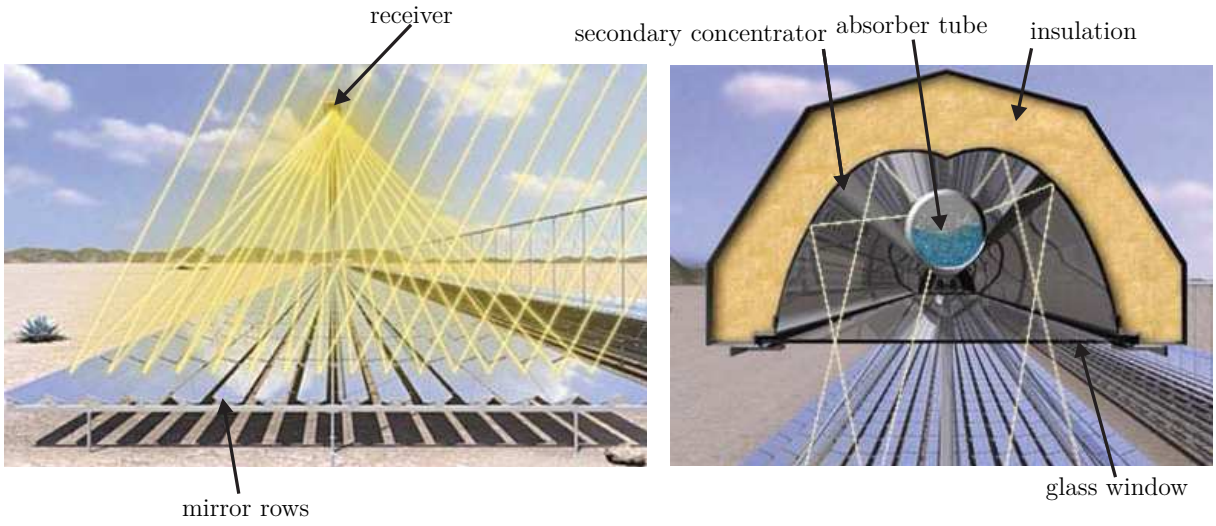

Figure 2.7: Linear Fresnel working scheme [12]

The required parts necessary to erect a Linear Fresnel power plant are, with a high share, standard components enabling a high amount of local added value. Even though all CSP technologies benefit from this, it is a particular advantage of the Linear Fresnel technology [13]. In addition, the plane arrangement of the mirrors diminishes wind loads significantly compared to Parabolic Trough Collectors. Yet, there is little experience with this kind of technology, since the worldwide capacity of Linear Fresnel is only 45.5 MW (2013) [14]. Due to cosine losses, blocking and shading, the optical efficiency of a Linear Fresnel is lower with respect to Parabolic Trough collectors [15]. This results in a more "peaky" efficiency curve, since Linear Fresnel applications attain the highest yields during solar noon.

2.3 Parabolic Trough Collectors

2.3.1 General Information

The first efforts of exploiting solar radiation using Parabolic Trough Collectors (PTCs) date back to the early 20th century. By 1913, PTCs were employed to produce steam driving a 45 kW engine in Meadi, Egypt. However, further developments were postponed until the 1980s, when the oil crisis and growing consciousness about global warning required alternative and independent energy sources. Later in the 1980s, the first commercial power plants, the so called *Solar Energy Generating Systems* (SEGS), were erected in California (USA) having a total net output of more than 300 MW_e [8]. The *Andasol I* power plant near Granada (Spain) was built in 2009 as the first parabolic trough power plant in Europe. Meanwhile, there are three units at this location (*Andasol I-III*) with an installed power of 50 MW_e each. Regarding nowadays large-scale CSP energy generation, the PTC is the most mature technology on the market. A list of worldwide PTC power plants is depicted in appendix C.

Despite the heat source, the operation principle of a PTC power plant is similar to conventional power plants which use steam in a Rankine cycle. Figure 2.8 displays the circuit diagram of the *Andasol* power plants. Heated up by a multitude of collectors arranged in a solar field, heat is transported by a HTF which serves to drive an adjacent Rankine cycle. For an optimum efficiency, there are four different counterflow heat exchangers: After passing a solar preheater, the water is vaporized in a steam generator in order to then be superheated. Having passed the high-pressure turbine, the steam is reheated and runs through the low-pressure turbine. Said turbine is connected to a generator producing electricity. Moreover, there is a storage system enabling full-time operation of the power plant. Using molten salt in a two-tank system, surplus enthalpy can be collected during hours of high solar radiation. Once this radiation decreases the tank is depleted, e.g. assuring electricity generation during the night. This ability of shifting the load responding to demand fluctuations in the grid is also called *dispatchability*. It constitutes a major benefit of PTC power plants with storage, making them a competitive technology on the energy market.

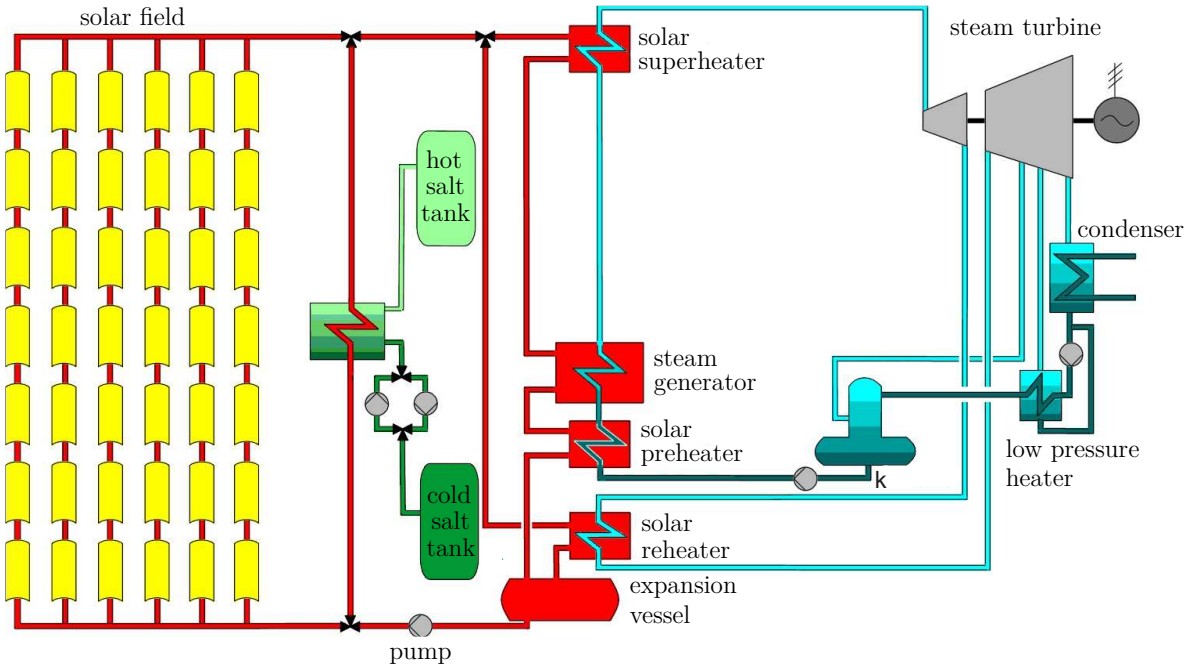

Figure 2.8: Circuit diagram of the *Andasol I* power plant [8]

The concentrator (mirror) of a PTC comprises a multitude of mirror facets. It is formed like a parabolic cylinder and focusses the sunlight up to a hundredfold onto a straight focal line. Therefore, the symmetry plane – the aperture – has to be directed perpendicularly towards the sun. This is accomplished by one-axes tracking systems. A tubular element – the so called Heat Collector Element (HCE) – is located in the focal line absorbing the concentrated sunlight and conducting it to a flowing HTF inside the tube. The HCE is depicted in figure 2.9 and consists of an inner absorber tube and an outer glass cover tube. The outer surface of the absorber tube is selectively coated to maximize the absorption of short-waved radiation whilst minimizing the emissivity of long-waved thermal radiation. Convective losses are constrained by a vacuum (evacuated annulus) in between the inner steel tube and the outer glass tube. The bellows serve to compensate for the offset in thermal dilatation between the glass and the steel tube. By this means, temperatures of up to 400 $°C$ are feasible, depending on mass flow, HTF type and concentration factor [15]. Increasing the temperature beyond the threshold of 400 $°C$ hinges on finding a HTF with sufficient thermal stability.

The HTF in PTC applications is usually a thermal oil of which the thermal energy is being transferred in a heat exchanger for steam generation. There have been further efforts of using water as HTF which is directly vaporized in the absorber tubes. This Direct Steam Generation (DSG) is capable of reaching higher temperatures whilst having lower losses due to the omission of a heat exchanger. However, this technology is still developing, and therefore not yet established in large-scale applications[1]. A different approach is using

[1]There is one 5 MW power plant in Thailand using DSG [10]

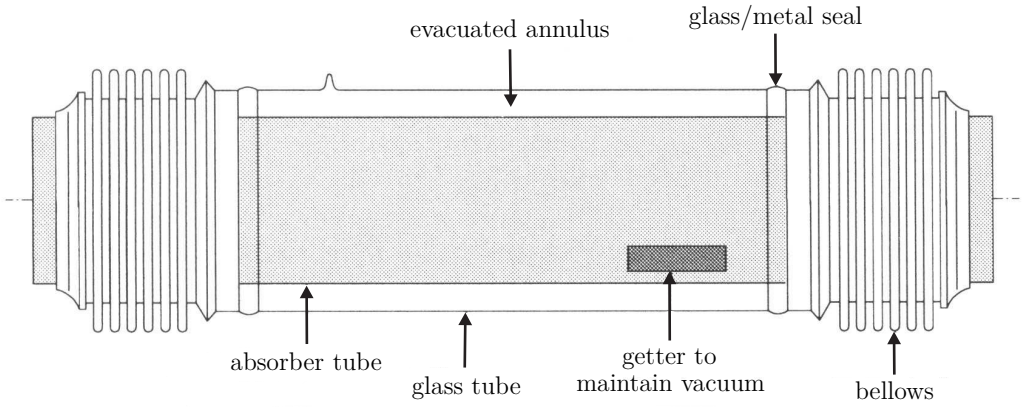

Figure 2.9: Schematic sketch of a Heat Collector Element for PTC power plants [8]

molten salt as HTF, which already serves as heat storage medium in parabolic trough power plants to enable power generation during hours of low or even no radiation. Hence, the use of molten salt avoids the intermediate heat exchanger between the HTF and the storage medium, because both are the same substance. Further, an increase of the operating temperature is feasible, enabling higher efficiencies (Carnot cycle). However, the commonly used molten salt has a melting point of 238 $°C$; therefore, arrangements have to be made to prevent the salt from freezing in the widespread piping system of the solar field. Further information on different HTFs is given in chapter 2.3.4.

2.3.2 Collector Design

Figure 2.10 shows a photo of four serially connected *EuroTrough* Solar Collector Elements (SCEs). For ensuring sufficient stiffness of the assembly – therefore optical efficiency –, the mirrors are attached to a steel frame. Concerning the *EuroTrough* SCE, the term "torque box" has established. This supporting structure is anchored to the ground using steel pylons. The drive unit / drive pylon serves to accomplish one-axes tracking of the sun. Depending on the location the orientation of SCEs is either north-south (optimized tracking of the sun's azimuth angle) or east-west in higher degrees of latitude (optimized tracking of the sun's elevation angle). In commercial applications, mostly north-south orientated collectors prevail; this is due to higher annual average yields that can be obtained. However, east-west orientated collectors are especially suitable for testing purposes: During solar noon, the sun is directly perpendicular to the mirror apertures and thus cosine losses are negligible.

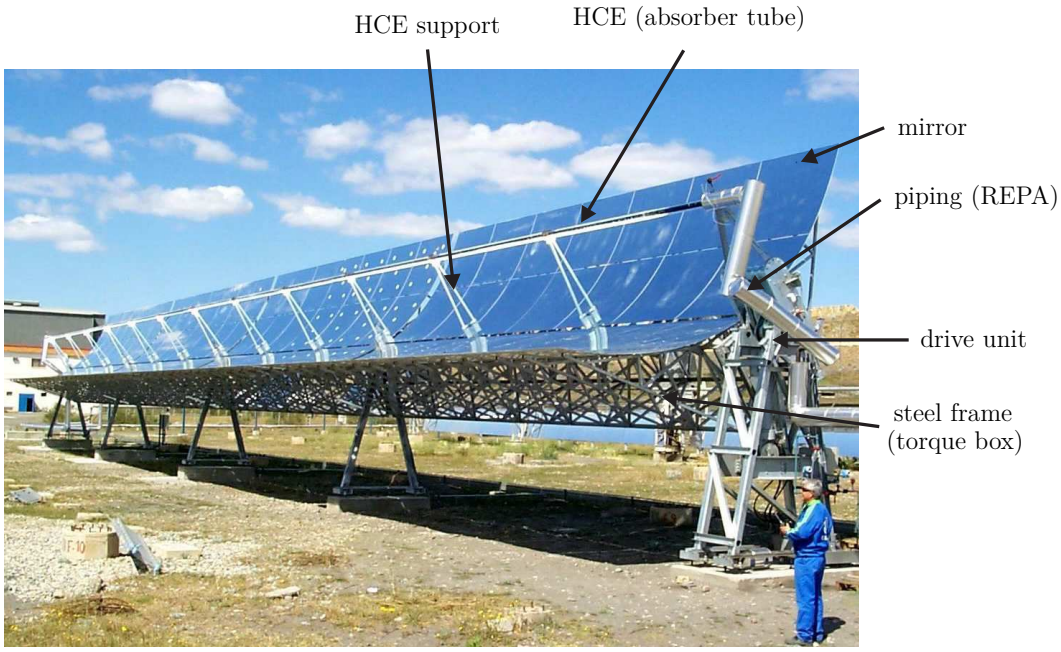

Figure 2.10: (Four) *EuroTrough* Solar Collector Element(s) (SCE) (cf. [9])

Table 2.1 summarizes different PTC generations. It can be noted that efforts aim to expand the spatial dimensions: not only has the aperture width been continuously increased to maximize the thermal and therefore the economical efficiency, but also Solar Collector Assembly (SCA) length. The latter can be traced back to a longitudinal extension of SCEs. By this means, the quantity of steel pylons and concrete foundations can be decreased significantly.

Table 2.1: Different Solar Collector Assemblies [16] [9] [17] [18]

		LS-1	LS-2	LS-3	*EuroTrough*	*HelioTrough*®	*Ultimate Trough*™
development		1984	1985	1989	1998	2005	2009
SCE length	[m]	6.3	8	12	12	19	24.5
HCEs per SCE	[-]	2	2	3	3	4	5
SCEs per SCA	[-]	8	6	8	12	10	10
SCA length	[m]	50.2	49	99	150	191	247
aperture width	[m]	2.5	5	5.76	5.76	6.78	7.51
SCA aperture area	[m^2]	126	245	570	865	1288	1802
focal length	[m]	0.94	1.49	1.71	1.71	1.71	1.71/1.878[2]
drive		gear	gear	hydraulic	hydraulic	hydraulic	hydraulic

[2]The inner mirror's focal length is 1.71 m, the outer mirror's 1.878 m.

2.3.3 Solar Field Design

In commercial parabolic trough power plants a plurality of SCEs is mounted in a row in order to form a SCA, see figure 2.11. The pylons serve to connect the SCEs with each other stiffly, so that, for instance, the length of a *EuroTrough* SCA is 150 m.

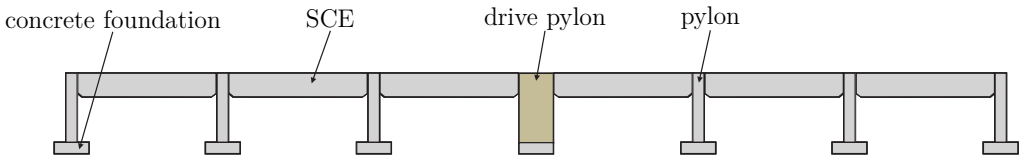

Figure 2.11: Schematic illustration of a Solar Collector Assembly (SCA)

Figure 2.12 depicts a section of the assembly situation in commercial parabolic trough power plants. There is a pair of HTF pipes conveying the HTF through the solar field, the so called header pipes. Emitting from the power block, the cold header pipe supplies a multitude of groups of serially connected SCAs, each of them heating the fluid up from inlet temperature to outlet temperature. As the fluid is circulating, this assembly is commonly designated as a *collector loop*. The increase of temperature is approx. the same in all loops. The HTF in turn is led back through the hot header pipe entering the power block. A multitude of loops is arranged parallel forming a solar field. In most power plants, two to three SCAs are connected in a row; two parallel rows thus forming a collector loop [19].

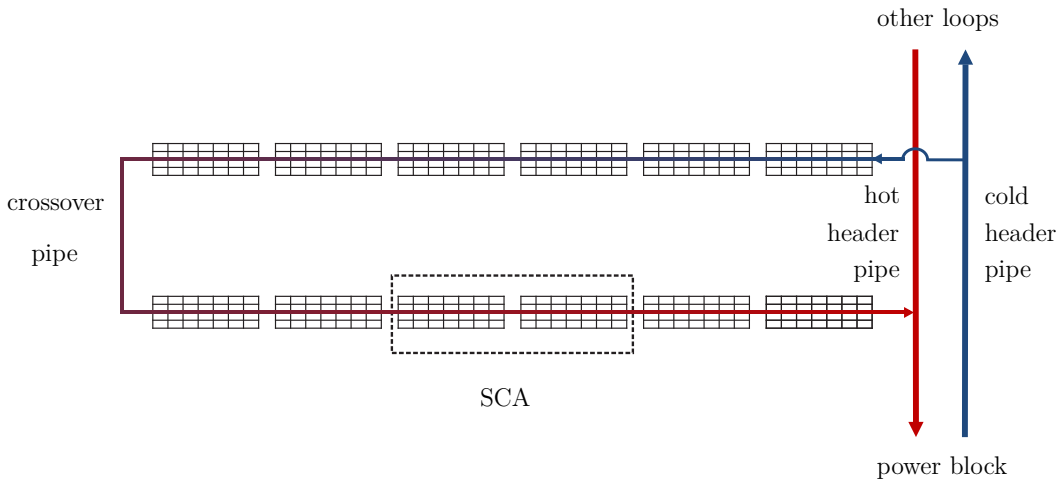

Figure 2.12: Schematic illustration of a Collector Loop and its connection to the header piping

The solar field's layout hinges significantly on minimizing both investment costs and energy losses. This applies particularly to the piping length in the solar field, since the purpose is to find a design which minimizes the investment, heat losses and pumping

parasitics. In commercial applications, solar fields are divided in sections. Whilst the quantity of those sections is depending on the power output, there are three different arrangements according to the configuration of the header piping: I-, U- and H-layout, see figure 2.13. In addition, figure 2.14 shows a aerial view of the three *Andasol* power plants near Granada, Spain. The superimposed header structure (blue and red line) reveals the typical H-layout, which encloses the power block as well as the thermal storage system. Due to its minimized piping lengths, the H-layout is the most established [20].

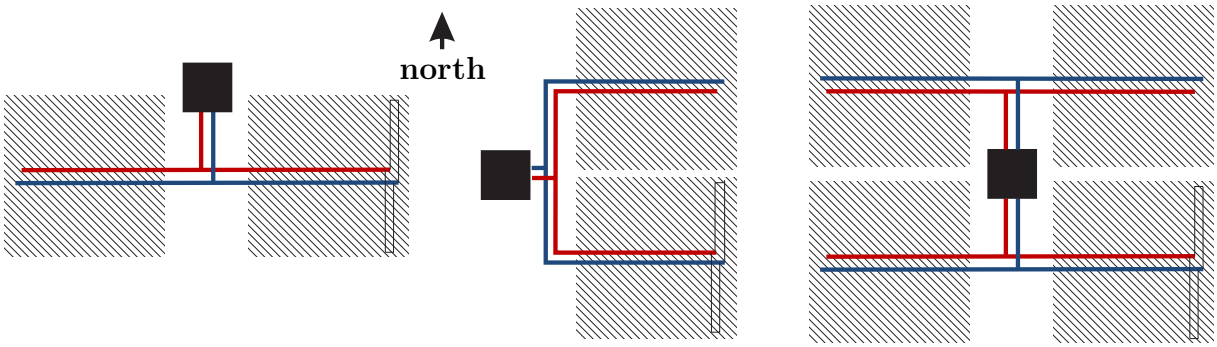

Figure 2.13: Schematic illustration of different solar field configurations: I-layout (left), U-layout (middle) and H-layout (right) (cf. [20])

Figure 2.14: Aerial view from northeast of *Andasol I-III* PTC power plants with superimposed field and header structure (three loops are indicated) [20]

2.3.4 Heat Transfer Fluids in Parabolic Trough Collectors

Since the HTF is carrying the yielded thermal energy from the solar field to the power block, it is a key component in PTC power plants. Therefore, it must fulfil different properties in order to ensure a maximized efficiency of the system. Those are, on the one hand, a high operation temperature along with good thermal stability. On the other hand, a high volumetric heat capacity accompanied with high thermal conductivity enables low pump consumption and optimized heat transfer, respectively. Moreover, low freezing points allow the omission of trace heating systems. The HTF must be available cost-efficiently and in high quantities whilst being harmless to both humandkind and environment. This also applies to its non-flammability under standard conditions [9]. Table 2.2 summarizes characteristics of eligible HTFs in PTC applications.

Diphenyl-Diphenyl Oxide (DP-DPO)

The most widespread HTFs in PTC applications comprises an eutectic mixture of 73.5% diphenyl oxide ($C_{12}H_{10}O$) and 26.5% diphenyl ($C_{12}H_{10}$) by weight. This organic substance is commonly abbreviated DP-DPO and was patented in 1932 [21]. Main suppliers are *Dow Chemicals* (*DOWTHERM A*), *Lanxess* (*Diphyl*®) and *Eastman*[3] (*Therminol*® *VP-1*). The latter is the most widespread HTF in PTC applications. In power plants, DP-DPO can be utilized up to a maximum bulk temperature of 400 $°C$ whilst having a freezing point at 12 $°C$. Since the vast majority of PTC power plants utilizes DP-DPO, it is the state of the art HTF [22].

However, there are several disadvantages in using DP-DPO. Its maximum operation temperature of 400 $°C$, for instance, is – up to the present day – the limiting factor of the power plant's efficiency. Additionally, DP-DPO's freezing point of 12 $°C$ requires a freeze protection system to prevent the HTF from solidifying. This is achieved by a constant circulation even when the solar field is not operating, e.g. during the night or in the winter. Also, its use as storage medium is economically not feasible, since its vapour pressure beyond 250 $°C$ is greater than 1 bar; hence, a pressurized storage tank would be required. Moreover, long-term operation may cause cracking of organic compounds. This leads to, on the one hand, an accumulation of particles increasing the HTF's viscosity and, on the other hand, it causes carcinogenic decomposition products to occur, e.g. benzene. The odor treshold for DP-DPO in air is 9 parts per billion (ppb) combined with unpleasant smell. DP-DPO suffers from higher costs compared to other HTFs[4]. [23] [9] [24]

[3] former *Solutia Inc.*
[4] HTF costs represent 5% of total costs at *Andasol III*

Silicone Oils

In contrast to the above presented DP-DPO, which represents a synthetic fluid of organic origin, silicon oils consist of siloxane-based chain molecules, so called polydimethylsiloxanes. Silicone oils are odorless, exhibit low oral toxicity, high thermal stability and freezing points far below 0 $°C$. The latter is accompanied with good pumpability even at low temperatures; this is why silicone fluids are frequently chosen for test facilities, since long downtimes do not affect the fluid's performance. At Plataforma Solar de Almería (PSA), for instance, the vast majority of parabolic trough test facilities operate using *Syltherm 800* made by *Dow Chemicals*. Another promising silicone oil for future applications is *HELISOL® 5A* from *Wacker Chemie AG*, as it offers an elevated maximum operation temperature of 430 $°C$. Hence, this newly introduced HTF is likely to play a significant role in future power plants. Another benefit of silicone oils is that it can be applied without major modifications in existing power plant designs. [21]

Yet, the commercial establishment of silicone oils in PTC applications is still obstructed by high costs compared to DP-DPO.

Molten Salts

Molten salts as HTFs in PTC power plants are not yet commercially established. However, several R&D projects are dedicated to its commercialization. The main incentive for developing solar power plants operating with molten salt is its elevated temperature stability compared to the above-mentioned silicone oils and DP-DPO. Solar field output temperatures can be raised up to 500 $°C$ causing distinct increases of the Rankine cycle's efficiency [10]. Since nowadays PTC power plants merely operate with molten salt storages, it could serve as both heat transfer and storage medium. Hence, construction costs can be decreased due to the omission of a heat exchanger. This is also accompanied with diminished heat losses. Moreover, molten salt is less expensive as well as less harmful to the environment compared to DP-DPO in particular. Yet, its implementation into the technical process turns out to be difficult, because it has a corrosive impact on the piping. Above that and derived from its freezing point (*Solar Salt*: 238 $°C$), the necessity of a trace heating is given increasing both investment costs and energy consumption [25]. The freezing point may even be increased due to ageing [9]. Also, its establishment hinges on finding a suitable REPA that withstands the high pressures and temperatures, see chapter 3.4.

There are three different generations of molten salts for PTC applications. Those are:

- *Solar Salt* (60% $NaNO_3$, 40% KNO_3)
- *Hitec*® (7% $NaNO_3$, 53% KNO_3, 40% $NaNO_2$)
- *Hitec*® *XL* (48% $Ca(NO_3)_2$, 7% $NaNO_3$, 45% KNO_3)

Main incentive for the development of *Hitec*® and *Hitec*® *XL* was a temperature setback of the freezing point, see table 2.2.

Steam

A different approach is the use of water as HTF in PTC power plants. Using this so called Direct Steam Generation (DSG) the collector evaporates and superheats water feeding the turbine directly. Hence, an intermediate HTF system as well as sophisticated heat exchanger systems (cf. figure 2.8) can be omitted. This leads to a simplification in plant design [26]. Yet, handling the layered two phase flow inside the absorber tubes is one of the major challenges. Since the vaporization of water is accompanied by different flow patterns, there may occur different temperature profiles in the pipe cross-section. Consequently, thermal stresses occur in the HCE, which have to be avoided necessarily. In addition, DSG requires a more complex control system in particular during periods of DNI fluctuations [27]. The REPA Test Rig will not be designed for utilizing steam as HTF.

Physical and Chemical Properties

Table 2.2 summarizes the above mentioned HTFs – except from steam – in regard to their physical and chemical properties as well as their expenses (ordinal scale).

Table 2.2: Characteristics of HTFs in PTC applications [9] [10]

		Therminol® *VP-1*	*Syltherm 800*	*HELISOL*® *5A*	*Solar Salt*	*HITEC*®	*HITEC*® *XL*
freezing point	$[°C]$	12	−40	−65	220	142	120
max. temp.	$[°C]$	400	400	430	600	535	500
ρ (300 °C)	$[kg/m^3]$	815	671	656	1899	1640	1992
η (300 °C)	$[mPa \cdot s]$	0.20	0.47	0.20	3.26	3.16	6.37
c_p (300 °C)	$[J/kgK]$	2319	2086	2235	1495	1560	1447
costs	[-]	high	very high	high	low	medium	medium

2.4 Rotation and Expansion Performing Assemblies

Since the axis of rotation of a PTC is commonly not aligned with its focal line, an interface between the movable HCE and the fixed piping is crucial. In addition, temperature cycles of up to 400°C require a linear compensation of the HCE's thermal expansion and contraction. Using flexible pipe connections, the accommodation of thermal expansion as well as of the SCA's rotary movement is ensured. These intermediate interfaces established the term **R**otation and **E**xpansion **P**erforming **A**ssembly (**REPA**) in terminology. In general, there are two commercially successful concepts for REPAs, Ball Joint Assemblies (BJAs) and Rotary Flex Hose Assemblies (RFHAs).

2.4.1 Rotary Flex Hose Assemblies

Rotary Flex Hose Assemblies are composed of a corrugated metal hose, a swivel joint and a torque transmitting connection which is referred to as *torque sword* – as it is often a flat steel beam. Figure 2.15 shows a photo of said assembly. The corrugated hose consists of cylindrical components with a corrugated structure in its longitudinal section. So as to avoid heat losses, it is thermally insulated. The swivel joint, also called rotary joint, serves to connect the twisting part – the corrugated tube driven by the *torque sword* – to the fixed pipe. In doing so, it depicts an anchor point, because it is screwed to a rigid support. The swivel joint has only one degree of freedom (rotationally). The torque sword conduces to maintain an interface between the SCA's axis of rotation and the swivel joint. Consequently, the RFHA is indirectly connected to and driven by the drive unit of the related SCA.

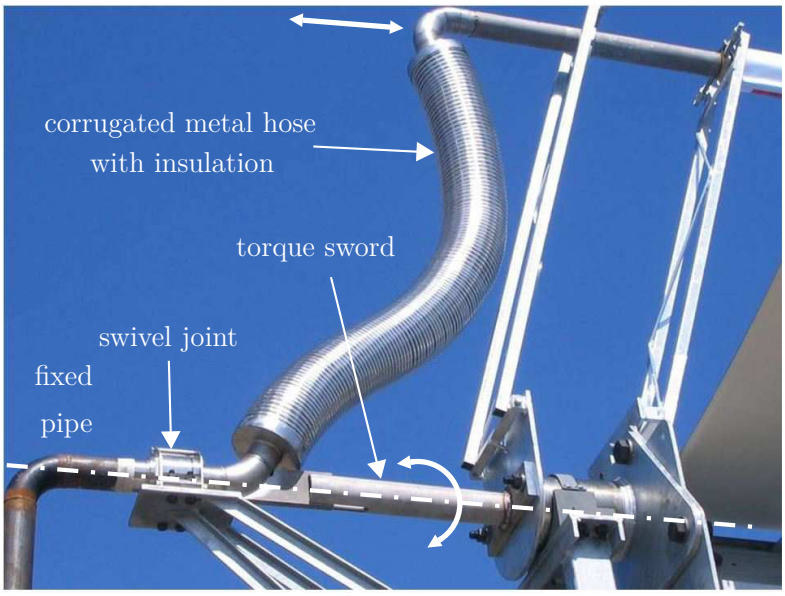

Figure 2.15: Rotary Flex Hose Assembly

2.4.2 Ball Joint Assemblies

Whilst RFHA deflect the combination of axial elongation and rotation separately, BJAs work differently. An assembly of three ball joints – which is commonly employed – has the capability to both compensate for rotation and expansion of the SCA. BJAs cause lower hydraulic pressure drops in the solar field which results in a higher efficiency of the power plant due to lower pumping parasitics [28].

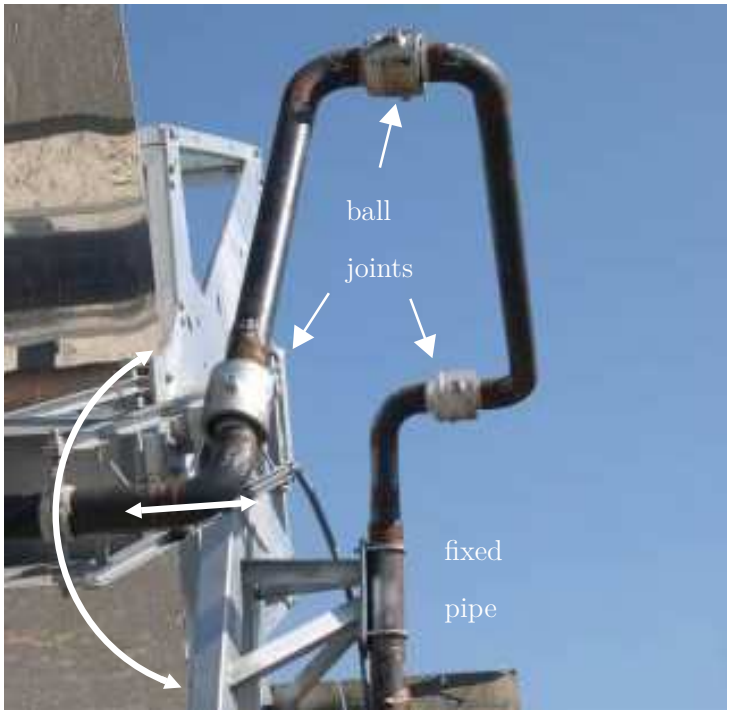

Figure 2.16: Ball Joint Assembly (not insulated)

Figure 2.17 shows a photo of a ball joint cutaway consisting of two main parts: a transition casing and a ball which is pivoted inside. There are inner and outer compression seals made of ductile iron to enable operation up to 426 $°C$. They retain a softer sealing material in between. This injectable seal consists of a reinforced graphite in order to reduce friction and to avoid leakage. Since it gets dissipated during operation, it needs to be refilled by means of a packing injection port (screwed). Most BJAs allow injections of additional graphite under operating pressure, hence a system shutdown can be avoided. Ball joints allow 360° of intermittent rotation as well as double-digit degrees of rocking motions [29] [30].

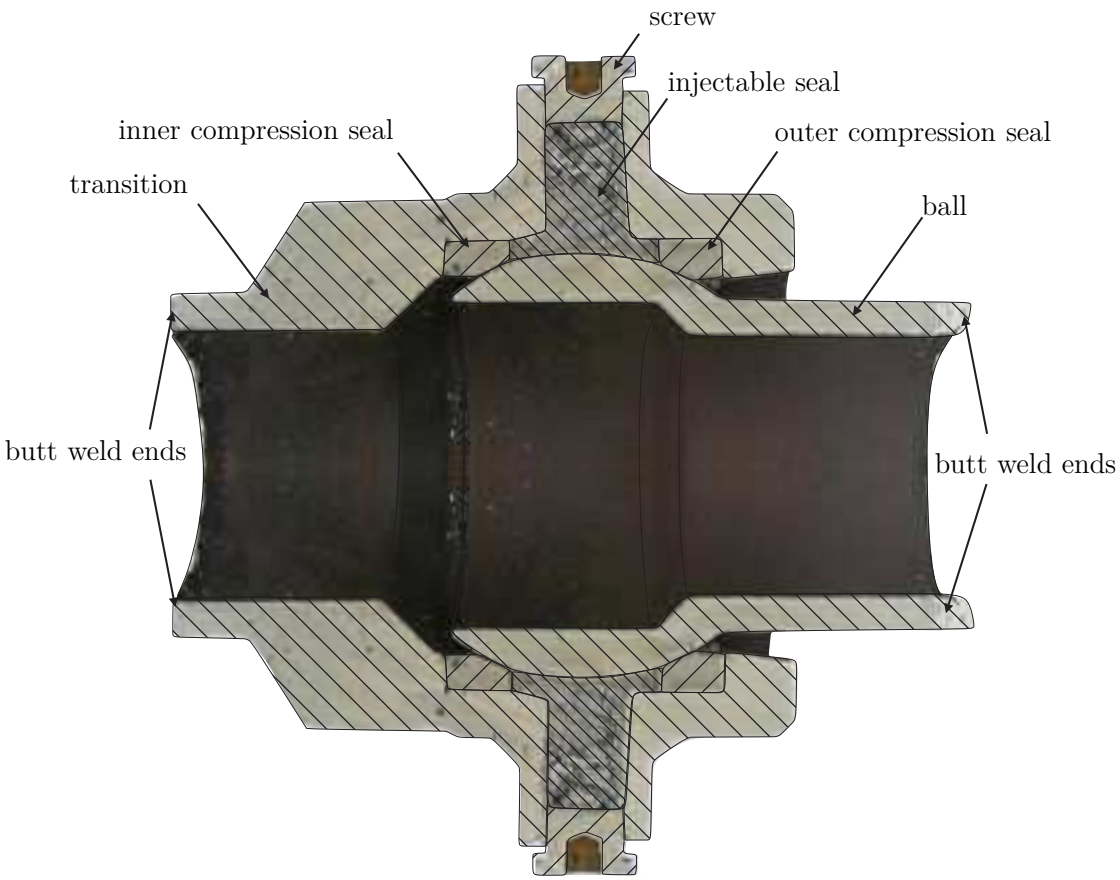

Figure 2.17: Ball Joint cutaway [9]

2.4.3 History and Market Situation

Appendices C.1 and C.2 provide a list of PTC power plants and their equipment (incomplete) in regard to REPAs. The first Solar Energy Generating Systems (SEGS) have been erected using simple flex hoses made by *Senior Flexonics GmbH*[5]. Those corrugated tubes coped without rotary joints. Instead, they carried both the collector's rotation and the thermal elongation of the absorber tube simultaneously. With the development of advanced solar collector assemblies having larger focal lengths, however, fatigue failures occurred causing HTF leakage [28]. Consequently, different options were pursued and Ball Joint Assemblies have been established gradually from 1994 onward (substituting flex hoses in the SEGS power plants to some extent). Before the development of first Rotary Flex Hose Assemblies (*RotationFlex® I* made by *Senior Flexonics GmbH*) in 1998, BJAs had been prevalent (global market leader is *Advanced Thermal Systems, Inc.* (ATS)). At the present day, RFHA and BJA are competing products.

[5]former *Senior Berghöfer GmbH*

2.5 Fixed Focus Parabolic Trough

A different approach, the Fixed Focus Parabolic Trough (FFPT), is characterized by a mass distribution which enables the SCE's focal line to interfere with the center of mass. Unlike the PTC's, the FFPT's mirror surfaces is segmented in three pairs of different fragments with various focal lengths. Figure 2.18 demonstrates the spatial alignment of the mirrors concentrating the sunlight onto the focal line (left) and the corresponding CAD model[6] (right). The mirror elements are incorporated into a lightweight, yet stiff, structure rotating around the focal line. A big advantage of FFPTs is the omission of REPAs, since the HCE is steady state; hence there is no necessity of a flexible connection to the adjacent piping to compensate rotational offsets. However, the use of a flexible connection is still mandatory, since the thermal dilatation of the HCEs must be taken into account. Furthermore, the use of several peripheral drives, rather than a central drive unit, diminishes the demands on torsion stiffness of the structure. Consequently, the installed power of the drives as well as the weight (=price) of the supporting structure (steel frames) can be reduced.

A negative impact of this new concept is a significant reduction of the optical efficiency due to blocking and shading of structural elements mounted between the mirrors and the absorber tube [31]. So far there is no full scale prototype of this collector built. Also, this concept might lead to other issues; for example, the bearing which is compelled to be penetrated by the evacuated glass envelope.

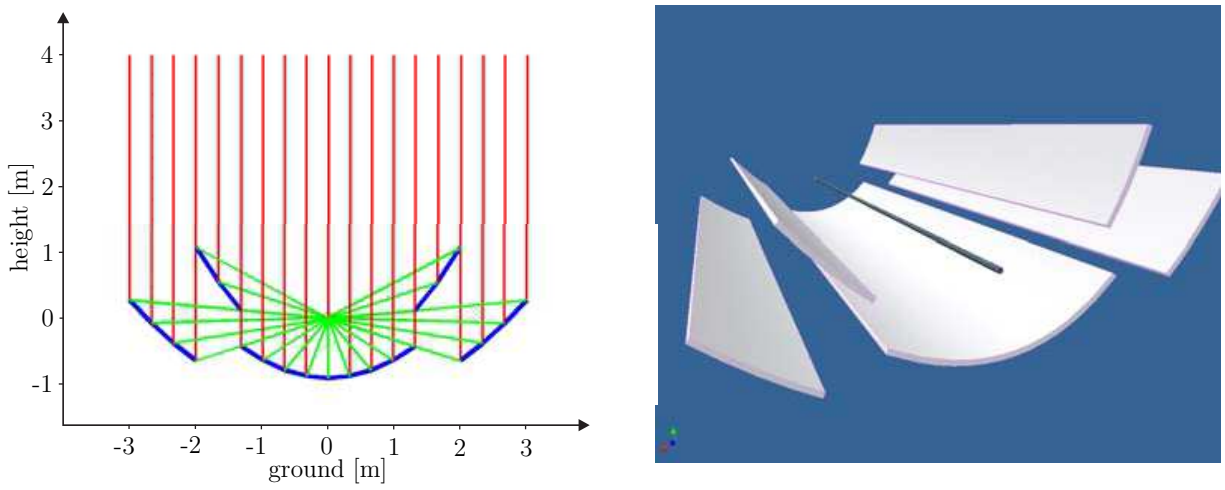

Figure 2.18: Mirror alignment in zenith position (left) and 3D model (right) of a FFPT collector [32]

[6]The structural elements connecting the mirrors panels are not depicted

2.6 Plataforma Solar de Almería / DLR

The present master thesis was written during a six months stay at the Plataforma Solar de Almería (PSA) in Andalusia, Spain. It was accompanied by a previous, four months internship. The PSA is the world's largest center devoted to research and development of solar thermal concentrating systems. It is owned and operated by CIEMAT[7], the Spanish Research Center for Energy, Environment and Technology. Located in the Tabernas Desert in south-eastern Spain (37°05′27.8″ north and 2°21′19″ west), it offers excellent boundary conditions for CSP research with respect to a DNI of more than 1900 $^{kWh}/_{m^2}$ per year and an average annual temperature of around 17 $°C$.

The research activities at the PSAs are structured around three units:

- Solar Concentrating Systems
- Solar Desalination
- Solar Treatment of Water

In regard to Solar Concentrating Systems, a large variety of test facilities has been erected throughout the years. Those are (selection) [33]:

- *CESA-1* (Solar Tower, 7 MW_{th})
- *SSPS-CRS* (Solar Tower, 2.5 MW_{th})
- *DISS* (DSG PTC test loop, 2.5 MW_{th})
- *FRESDEMO* (Linear Fresnel test loop)
- *PTTL* (Parabolic Trough Test Loop; no collectors installed yet)
- *HTF Test Loop* (Parabolic Trough test loop)
- *Prometeo Test Loop* (Parabolic Trough test loop)
- *KONTAS* (Rotary test bench for parabolic trough collector components)

[7] Centro de Investigaciones Energéticas, Medioambientales y Tecnológicas

Chapter 3

State of the Art

Prior to the conception and the design of a new test rig, the following chapter provides an overview of existing test rigs for flexible connections in PTC power plant applications. Initially, short summaries of three REPA component test rigs are depicted. These rigs only enable testing of a single component each. Afterwards, three different assembly test rigs are presented. In the course of this survey, possible drawbacks of the simulation are revealed, exposing the motivation to design a more sophisticated test rig.

3.1 REPA Component Test Rigs

ATS - Flex Torque Test Rig

Advanced Thermal Systems, Inc. (ATS), world leader in the supply (self-titled) of ball joints for solar applications, built a so called *Flex Torque Test Stand*. Each manufactured ball joint (series *P2* and *S2*) is tested for quality assurance. The ball joints are deflected through their full flex angle measuring the applied force, see figure 3.1.

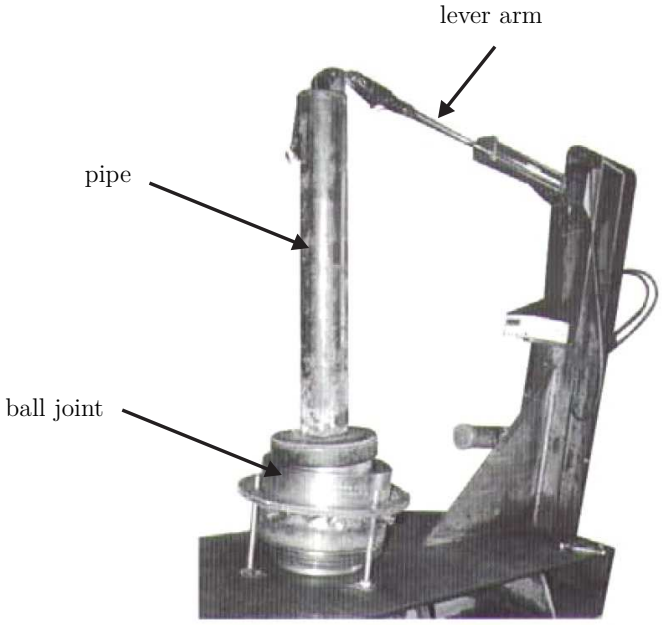

Figure 3.1: ATS Test Rig [29]

Hyspan - Durability Test Rig

Hyspan Precision Products, Inc. is a US-American manufacturer of flexible tubular metal products. The company operates an endurance test rig for testing ball joints, see figure 3.2. Using *DOWTHERM A* (cf. chapter 2.3.4), the ball joint is statically wetted (no mass flow) with a pressure of up to 30 bars at the HTF's maximum temperature of 393 $°C$. These values are close to operating conditions in solar fields. The test objects are cyclically strained with a rotation of 215 ° and ±7 ° angular deflection simultaneously. One cycle has a duration of approx. one minute. It consists of back and forth angular motion from $-7°$ to $+7°$ and of $0°$ to $215°$ rotation, back and forth. There are torque sensors installed to measure both the rotational and the angular torque. Also, pressure and temperature are continuously monitored. Designed to perform more than 1000 cycles per day, the endurance testing comprises 11.000 cycles in total which is equivalent to 30 years of power plant operation. The operation / test conditions – representing inlet and outlet of a loop in a solar field – are as follows:

- Condition 1 ("cold header", 6667 cycles): 30 bars and 293 $°C$
- Condition 2 ("hot header", 4428 cycles): 23 bars and 393 $°C$

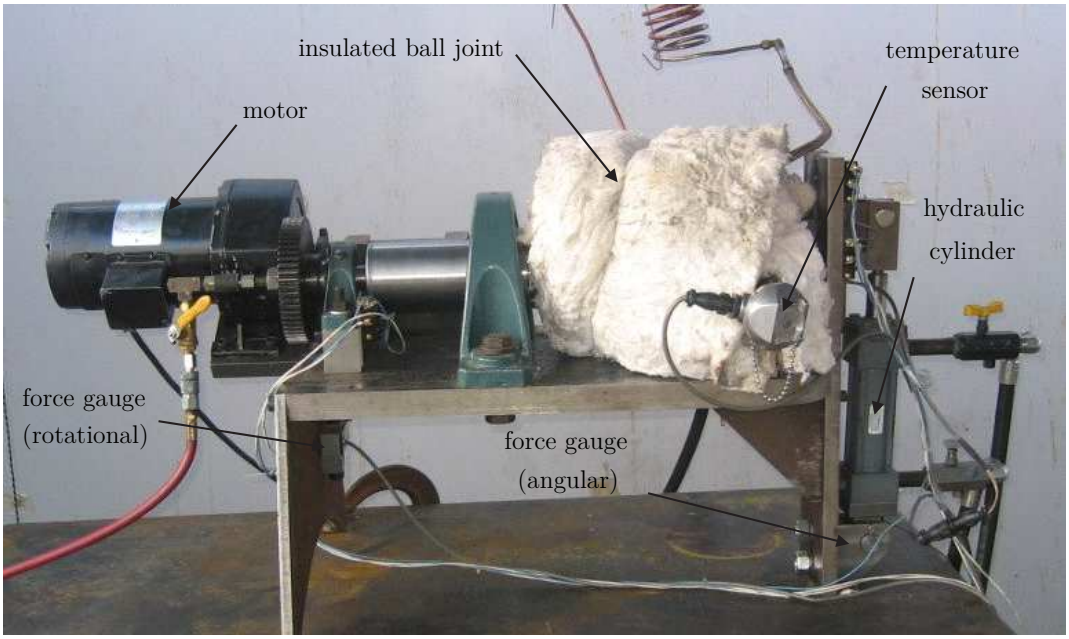

Figure 3.2: Hyspan Test Rig [34]

In spite of the fact that it offers full life cycle testing of ball joints, there are also disadvantageous aspects of this test rig. Ball Joint Assemblies regularly comprise three ball joints performing combined motions. Hence, each of the three ball joint carries out a different (location specific) motion which does not accord with the whole range.

IRAtec - durability test rig

Using a rubbing wear test rig, *IRAtec*, a German engineering services provider, investigates the leakage of swivel joints. Therefore, clamping plates are welded on both butt weld ends of the swivel joint. Figure 3.3 (left) shows a swivel joint in its delivery condition (apart from the welded clamping plates). The same swivel joint is shown in dismantled condition after the test (right). A screwed socket is mounted (to ensure oil supply) as well as two nozzles holding thermocouples.

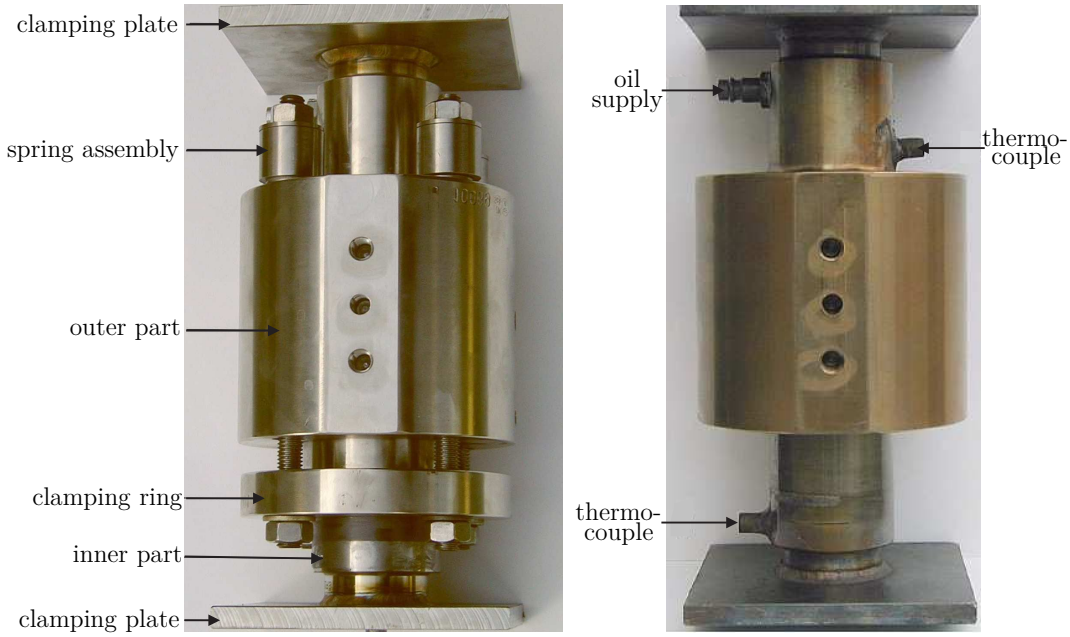

Figure 3.3: Swivel joint delivery condition (left) and with measuring points (right)

The test object it is filled with HTF (*Therminol® VP-1*) and then installed on the test rig, see figure 3.4. A temperature of 345 $°C$ is maintained by electrical heaters in the clamping plates, whereas a pressure of 6 bars is applied using a hydraulic hand pump. 15.000 rotation cycles of 20 degrees each (back and forth) are tested. 2000 cycles per day are feasible. There is a load cell measuring the friction force required to perform the rotation. The corresponding torque can be obtained by the length of lever arm between the load cell and the center of rotation. Furthermore, both before and after the test a leakage check by immersing the ball joint in water is performed. Therefore, the ball joint is pressurized with air of 6 bars. Size and quantity of occurring air bubbles are criteria for evaluation.

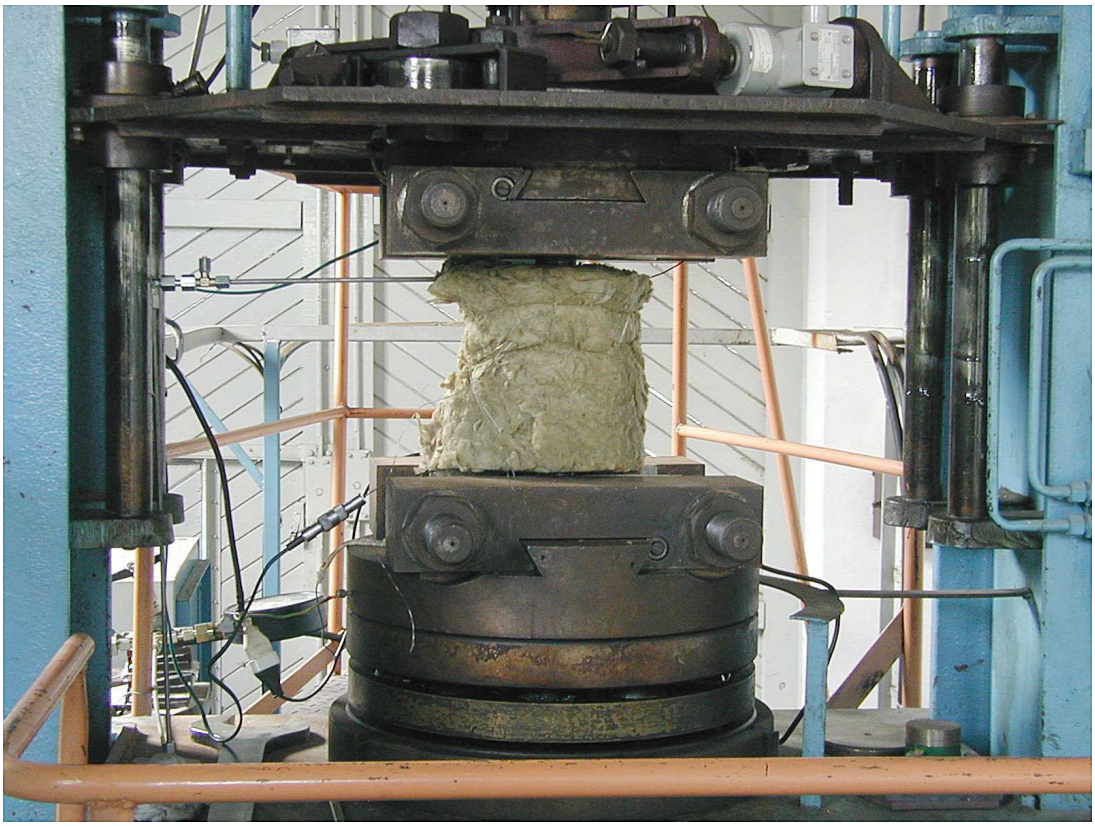

Figure 3.4: Insulated swivel joint on IRAtec test rig

A major drawback of the *IRAtec* test rig is the pressurization of the swivel joint. The hand pump is only capable to maintain a fluid pressure of 6 bars, which is significantly below PTC loop working pressures (approx. 20 - 30 bars). Furthermore, this is accompanied by an HTF temperature limit, since the vapour pressure of the fluid (around 11 bars at 400 $°C$ [23]) must not exceed the working pressure of 6 bars in the swivel joint. Hence, the temperature is capped at 345 $°C$ which is too low in order to be able to represent all possible PTC operation conditions. The leakage check is, above that, done with air at 6 bars at ambient temperature; consequently, this test cannot assure seal tightness at real working conditions.

Besides thermodynamic properties, the applied motion cycles of 20 ° are not conform with those that appear in power plants. SCAs rather perform rotational motions of up to 120° (distance between vertical position and stow position) in each direction.

3.2 DLR - Accelerated Ageing of RFHA

In contrast to the above mentioned testing methods which are targeted on investigating only single components of REPAs, *DLR* used an existing facility testing an entire Rotary Flex Hose Assembly. The tests were carried out at a HTF test loop at PSA, which consists of six prototype SCEs with a total length of 75m (east-west orientation). The existing REPA at the outlet was substituted with a *RotationFlex*®[8] system made by *Senior Flexonics GmbH*, see figure 3.5. The purpose was to gain more detailed information about long term operation properties of the REPA. The RFHA was strained both thermally and mechanically. Heat was provided by focussing the collector to the sun and temperatures were measured both of the HTF at the collector outlet and at the outer surface of the insulated flexible hose.

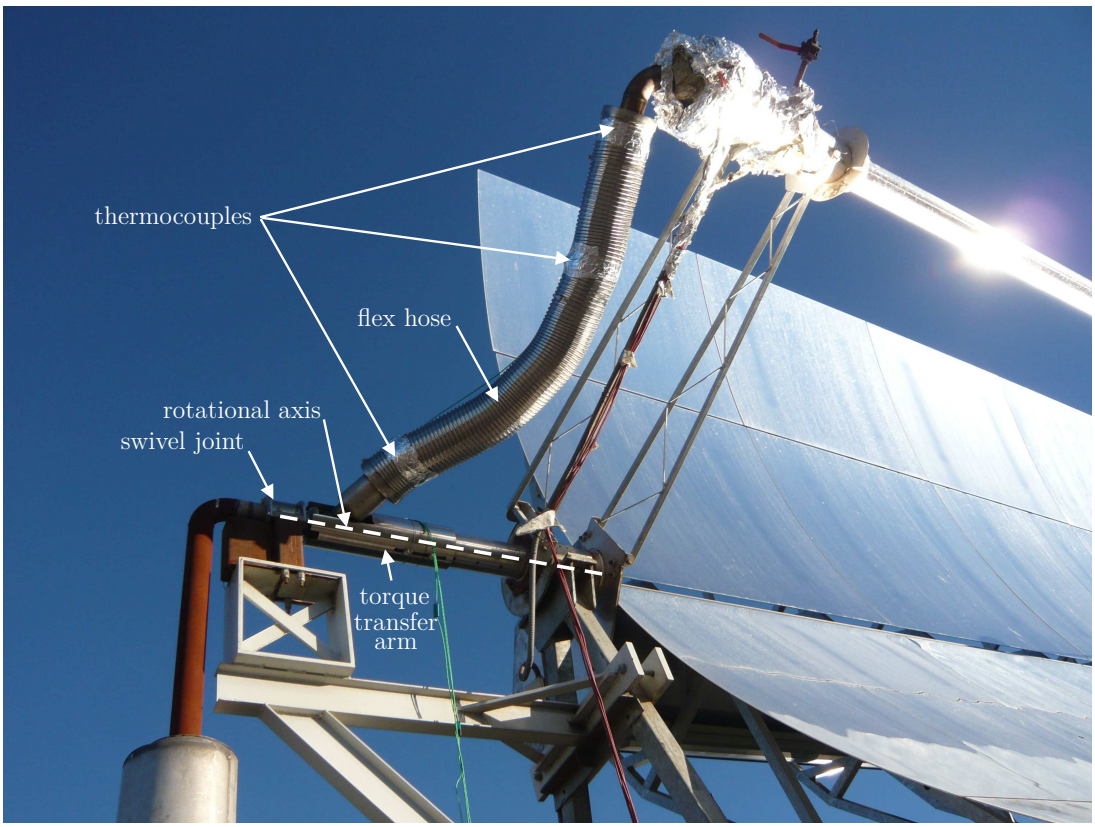

Figure 3.5: RFHA prototype incorporated into a test collector demo loop (*HTF Test Loop*) at PSA during heat up

After heating up the HTF to 350 $°C$ which is flowing through both the SCA and the REPA with a pressure of approx. 20 bars, the *EuroTrough* SCA commences its movement cycles. Based on a rotation cycle defined from 170° (northernmost) to −25° (stow) back and forth, which lasts about 30 minutes, up to nine movement cycles in the course of one day are feasible. By contrast, only one temperature cycle per day can be performed,

[8] company's brand name for RFHA

since the HTF is heated up to operating temperature in the morning and cooled down to ambient temperature in the evening. As there is no auxiliary heating element, the tests are highly dependent on the weather conditions [35].

There are several disadvantages that make this type of test rig unsuitable for durability testing of REPAs. First of all, since the drive is only likely to realize up to nine cycles per day, it would take more than three years to simulate the desired 10.000 cycles of its intended life time. Furthermore, it is highly dependent on weather conditions influencing the progress. It is, above that, impossible the have an influence on the thermal expansion cycles. Also, testing is limited to REPAs for *EuroTrough* geometry, i.e. the focal length is fixed. Consequently, this kind of testing in not suitable for a realistic, yet accelerated, REPA life time testing in regard to different collector types and time efficiency.

3.3 Senior Flexonics GmbH - Assembly Test Rig

Senior Flexonics GmbH, manufacturer of, amongst other things, flexible connections for CSP applications, utilizes a kinematics test rig for RFHA, see figure 3.6. The swivel joints are wetted with stagnant HTF, heated up to max. 550 $°C$ and pressurized up to max. 40 bars. The flexible hose is filled with water at ambient temperature and pressurized up to max. 40 bars. The rotation is applied from $-120°$ (stow position) to $120°$ (end position) and backwards, which represents one cycle. Simultaneously, the thermal expansion movement is performed from maximum cold position at $-14.5°$ (equivalent to 20 $°C$) to maximum hot position at $+5.5°$ (equivalent to 400 $°C$ in a PTC application). There are two force/torque sensors; one between the fixture of rotary joint and support (interface 230mm below the roatation axis) and one between the upper end of the flexible hose and the HCE interface [36] [19].

The lack of a mass flow circulating through the test rig diminishes the reliability of the test procedure, since it is to be expected that shear forces due to pipe wall friction have a distinct influence on the lifetime.

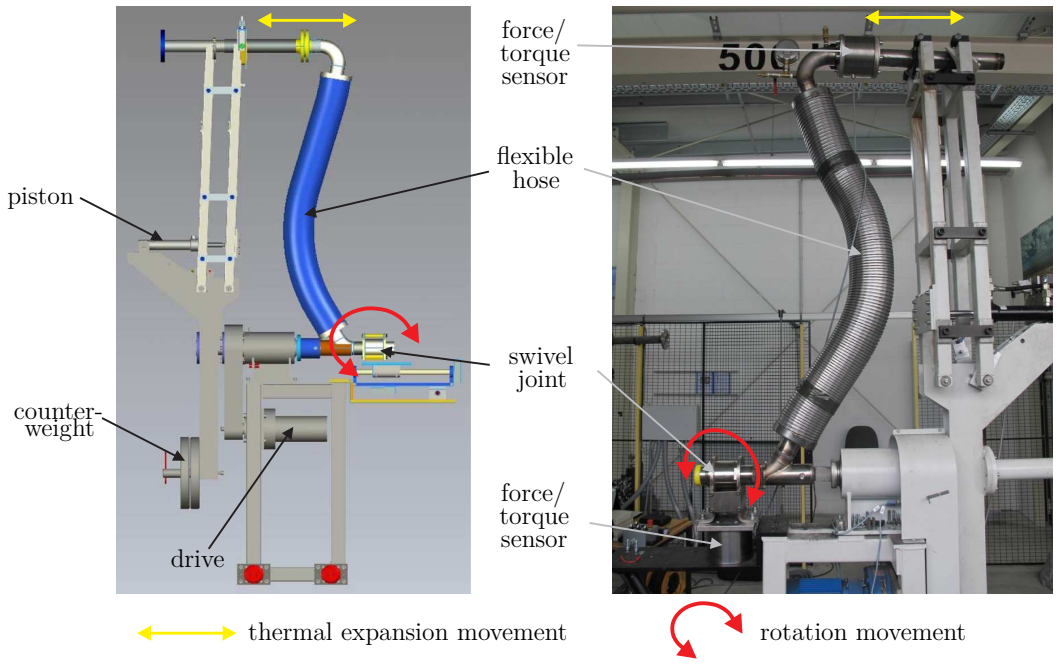

Figure 3.6: Rotary Flex Hose Assembly test rig by *Senior Flexonics GmbH*; CAD model (left) and photo (right)

In addition, *Senior Flexonics GmbH* utilizes a durability test rig for flexible hoses. Exposed to circulating HTF with a temperature of up to 450 $°C$ and a pressure of up to 40 bars, the test rig simulates the daily thermal expansion of the absorber tubes. However, rotation cycles cannot be applied.

3.4 Abengoa Solar - Assembly Test Rig

Associated with the development of molten salt HTF technology in PTC power plants, *Abengoa Solar* erected a test rig investigating REPAs, see figure 3.7. Whilst being entirely instrumented with torque, force, temperature, pressure and salt level sensors, the facility exposes the test objects to stagnant molten salt at operating pressure and temperatures similar to desired operation conditions of future commercial plants. Using Solar Salt (60% $NaNO_3$ and 40% KNO_3, cf. chapter 2.3.4), the test objects can be pressurized with up to 40 bars, which is equivalent to one and a half times the maximum application pressure. A maximum temperature of up to 500 $°C$ can be reached. The test rig enables a rotational movement of 215° which is induced by a drive unit. The thermal expansion movement can be performed from maximum cold position at 0 mm (ambient temperature) to maximum hot position at 600 mm (500 $°C$). Yet, after one initial movement from 0 mm - 600 mm, the normal operating range for testing is set to 200 mm - 600 mm. Rotational and expansion movement are performed simultaneously with a duration of two minutes per cycle. The success criterion was specified to 11.000 cycles (30 years of operation) with zero leakage [37].

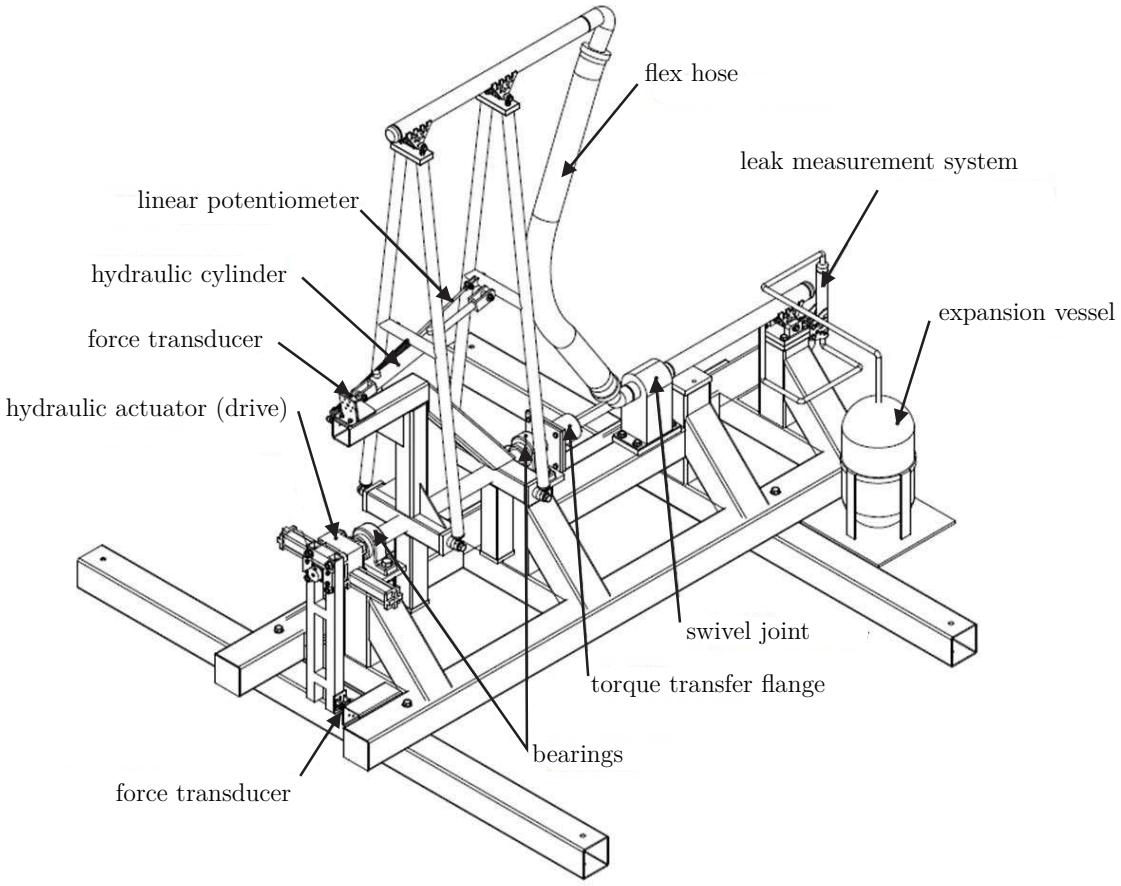

Figure 3.7: Technical drawing of the Abengoa test rig [38]

The first testing phase revealed that exposing the REPAs to the maximum pressure (40 bars) and temperature (500 $°C$) leads to plentiful failures. Hence, a more sophisticated testing plan was developed implementing step by step increases of the boundary conditions. Additionally, a distinction was made according to hot and cold header conditions, cf. chapter 2.3.3.

There have been tests with various BJAs and RFHAs, yet no configuration proved to withstand the boundary conditions. According to *Abengoa Solar*, the development depends on finding a pliable seal material that is qualified for 500 $°C$ molten salt. It could be manifested that no BJA was successfully tested at elevated temperatures due to exalted leak rates. Yet, there was partial success in testing RFHA: Using a swivel joint with face seal design, a cycle testing was successfully carried out in 10 $°C$ temperature increments up to 480 $°C$. The leak rate was less than one gram per hour. Furthermore, a life cycle test showed that 2855 cycles could be performed before the leak rate of the swivel joint exceeded the allowable level of 10 grams per hour.

Moreover, *Abengoar Solar* mentions a different, yet promising REPA technology omitting swivel or ball joints in general. Instead, it consists of two flexible hoses and a "torque transfer arm". However, first designs failed quickly.

Figure 3.8: Photo of the Abengoa test rig with installed RFHA (left) and BJA (right) [38]

3.5 Summary and Conclusions for a new Test Rig

Table 3.1 summarizes the test rigs' specifications as mentioned above. Based on this literature research, it can be said that there are various efforts of investigating the durability of REPAs. Those test facilities enable examinations from simple quality checks (*ATS*) to endurance testing of individual parts of REPAs (*Hyspan* and *IRAtec*) to entire life time analysis of the test objects in specially built test rigs (*Abengoa Solar* and *Senior Flexonics GmbH*).

Table 3.1: Overview of existing test rigs

	REPA	HTF	p_{max} [*bar*]	T [°*C*]	cycles
ATS	BJ	-	-	-	-
Hyspan	BJ	*DOWTHERM A*	<30	393	11.000
IRAtec	SJ	*Therminol VP-1*	6	345	15.000
DLR	RFHA	*Syltherm 800*	20	300	321
Abengoa Solar	RFHA/BJA	*Solar Salt*	25	550	11.000
Senior Flexonics	RFHA	water/ *Therminol VP-1*[9]	30	25	ca. 11.000

However, the above discussed test rigs suffer from several limitations. One the one hand, testing of REPAs in real-scale loops (*DLR*, cf. chapter 3.2) is highly dependent on weather conditions as well as on velocities of the collector drives. Since about eleven thousand cycles are necessary to approximate 30 years of solar operation, the use of real-scale loops is inadequate. One the other hand, the mentioned kinematics test rigs (*Senior Flexonics GmbH* and *Abengoa Solar*, cf. chapter 3.3 and 3.4) are not able to represent the exact hydraulic conditions of a solar field. Consequently, a new test bench will be designed and commissioned which overcomes the limitation of necessary test time for durability tests in a real-scale loop and the approximation of existing test benches not being capable to simulate flow conditions. Furthermore, it enables testing and comparison of two REPAs at the same time.

[9] interchangeable

Chapter 4

Requirements

Most PTC designs have a focal line different to the axis of rotation. For realizing an independent movement of individual parabolic trough collectors (SCAs), compensation of thermal linear expansion of absorber tubes and because of the fact that the focal line does not remain steady state in the course of a day, special flexible piping connections (REPAs) are crucial.

The target of the present work is the design of a test rig and its testing methods for rotation and expansion performing assemblies, so called REPAs, cf. chapter 2.4. Whilst being connected to a HTF cycle, the test rig simulates the motion of parabolic trough collectors, thus moving the REPA just the way they would move in a real collector. Owing to the fact that future PTC power plants using silicone oils (see also chapter 2.3.4) may achieve working temperatures of up to 450 $°C$, the REPA Test Rig's design incorporates this parameter, in order not to be the limiting factor no matter which HTF is used. Additionally, working pressures of up to 40 bars are feasible. Testing of Ball Joint Assemblies as well as of Flexible Hose Assemblies is enabled.

So as to be proficient to design the test rig, all impacts such as constraints, loads and outside influences that affect the REPAs have to be emphasized in the following subchapter. Afterwards, the acquired knowledge contributes to derive and determine the features the test rig has to incorporate by means of a specification sheet.

4.1 Requirements for REPAs

In order to design a test rig for a certain component or assembly ensuring its realistic simulation, it is indispensable to be aware of all occurring loads it has to endure during operation. Subsequently, this thesis serves to implement the gained knowledge into the REPA Test Rig design.

As mentioned in chapter 2.4, a REPA is the hydraulic connection link between the moving absorber tube (HCE) and the adjacent, fixed piping. It has to perform both a rotational and a linear dilatational (translational) movement. Meanwhile, it is exposed to hydraulic loads by means of the HTF, external loads induced by its interfaces to adjacent components and environmental loads (e.g. concentrated sunlight). Lastly, a REPA has to fulfil several security regulations. The listed impacts are illustrated in figure 4.1.

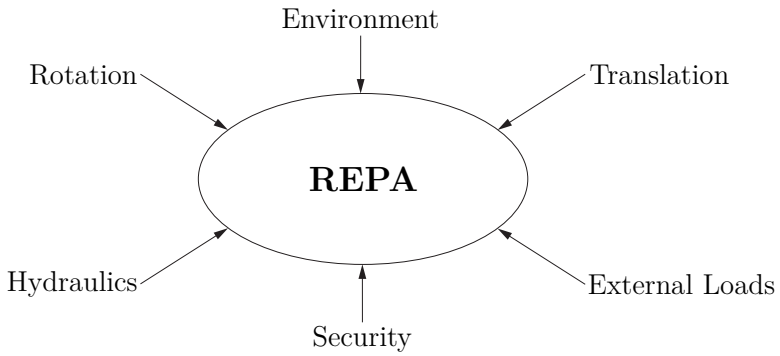

Figure 4.1: Impacts on a Rotation and Expansion Performing Assembly

4.1.1 Rotational Motion

Rotation is induced by the SCA tracking the sun. Figure 4.2 illustrates a daily rotation cycle of a SCA. The figure depicts the regime of the collector angle α. When not operating – for instance during the night, but also during maintenance or high wind loads – the collector maintains in its stow position (α_{stow}). Once operation begins, the drive moves the HCE to its start position (sunrise; α_r). Accordingly, the SCA commences a daily cycle by means of a tracking system. After sunset (α_s), the collector is being moved back to its stow position.

Main purpose of a tracking system is to maintain the aperture area perpendicular to the sunbeams and therefore to maximize the optical efficiency. This can be either ensured by algorithms for the approximate solar position (e.g. Michalsky algorithm [39]) or direct measurement technologies. Direct systems measure the current sun position by either inclinometers or magnetic strips monitoring the current collector angle. The latter value is compared to the sun's position and a new set point is calculated. If the collector

angle's actual value distinguishes from the set value, it is adjusted by the drive unit. The procedure is repeated every 20-40 seconds. Hence, the collectors do not perform a continuous but an incremental rotational movement.

The PTCs of a power plant are performing one of these cycles every day of operation. Assuming four to six weeks of downtime per year due to weather influences and maintenance[10], a power plant is operating 46 to 48 weeks (322 to 336 days) per year. Demanding a durability of all components of 30 years, a REPA will perform approx. 10.000 cycles in its lifetime.

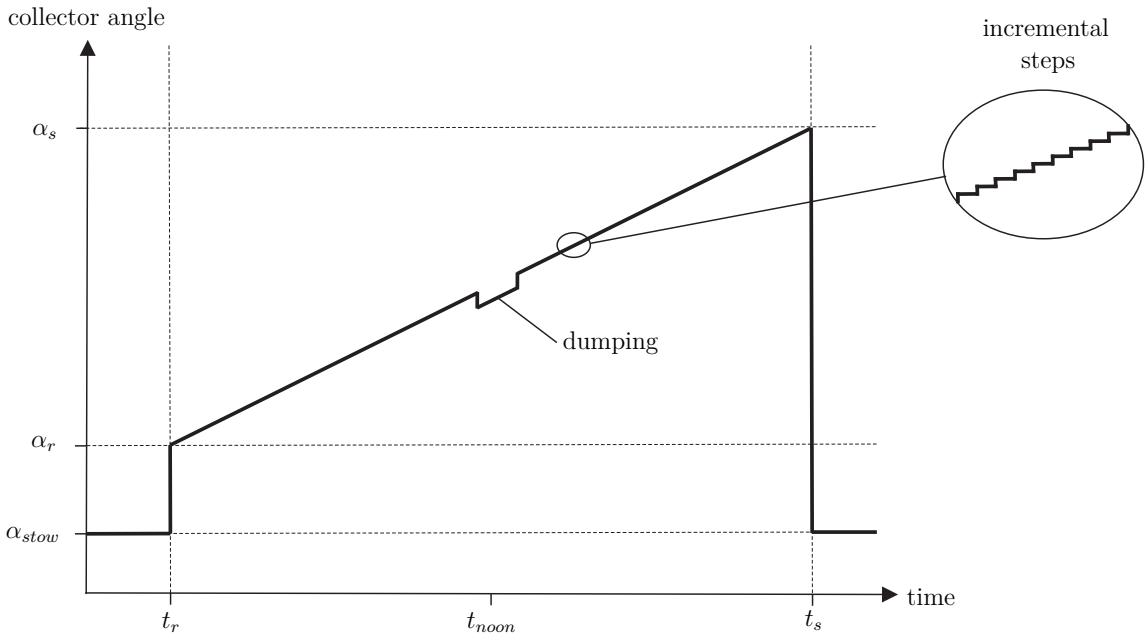

Figure 4.2: Illustation of a PTC (north-south orientation) tracking the sun

Yet, there may occur phenomenons that impede this ideal sequence of movements. There is a permanent adjustment between the current collector angle and the sun position derived from an algorithm controlling the collector's position. The discrepancy between the accurate tracking algorithm one the one hand and the defined increment of the drive unit on the other hand may lead to so called *tracking errors*. This can be manifested in reverse motion of the SCA when, for instance, the increment of the drive exceeds the set point. The extent of tracking errors is also highly dependent on the chosen drive unit. Likewise, local tracking errors may increase with the distance between the drive unit and the SCE: The *EuroTrough*, for instance, consists of 12 SCEs, i.e. six SCEs on each side of the drive. Consequently, friction torques cause elastic distortions by which means the outer SCEs are not synchronous to the drive unit. This event implies an increase of tracking errors.

The so called *dumping* of solar collectors in terms of tracking is a different phenomenon.

[10]The real amount of downtime is highly dependent on the location and other influences.

Dumping of concentrated solar radiation signifies intentionally increasing the spillage by not tracking the sun precisely. Since most HTFs have a maximum temperature, which must not be exceeded due to losses of thermal stability, a temperature control for each loop is realized. When, i.e. during solar noon, solar radiation is at its maximum, the HTF temperature in the last SCAs at the end of each loop may overrun this maximum temperature[11], see figure 2.12. In order to avoid this event, a control makes the SCA (partially) defocus the sun, see figure 4.2. Moreover, dumping can be an important factor for power plants without thermal storage: during periods of high solar radiation - when the turbine yet operates on it's limit - the solar field may deliver more energy than required (solar multiple) which cannot be used producing electricity; thus, defocussing of SCAs is required [40] [20]. Provided that this type of control works properly, there is no impact on the number of REPA cycles, since the movement of the SCA is just delaying. At one point, for instance, the collector stops tracking the sun and resumes some time later, when power is needed again.

As described above, the use of low precision control systems may cause unintentional rotation of the collector. Figure 4.3 shows power plant operation data of *Andasol III* in the course of one day: The graph depicts the temperature in the inlet of a loop, in the crossover pipe and in the outlet, as well as the corresponding collector angle in the outlet of the loop. Additionally, the DNI is displayed. The vertical axis represents the time during the day. Whilst the first SCA at the loop's inlet performs approximately a continuous rotation (no disturbance effects), the outlet SCA has several discontinuities in the course of the shown day. These phenomenons illustrate the above mentioned *dumping errors*: once the outlet temperature exceeds 400 $°C$, the last collector is defocussed in order not to exceed the maximum HTF temperature; this temperature is rather maintained below 400 $°C$. Yet, in this case the quantity of dumping is too high resulting in an unintended temperature drop. This effect can be traced back to malfunctioning tracking algorithms.

The above mentioned dumping (offset in tracking) is accompanied with an additional collector movement - and thus REPA movement. Consequently, it must be assumed that dumping may add additional cycles on the associated REPAs: Figure 4.3 reveals that the procedure of defocussing is repeated up to nine times between 10:30 and 11:30. The mean dumping angle is approx. 5° causing additional 90° of rotational motion of the SCA and therefore of the connected REPAs. The same procedure is evident in the afternoon between 15:45 and 16:45 as well as between 17:30 and 18:30. Accordingly, it is apparent that the effect of dumping must be taken into account when designing appropriate and realistic testing methods for REPAs.

[11] assuming constant mass flow

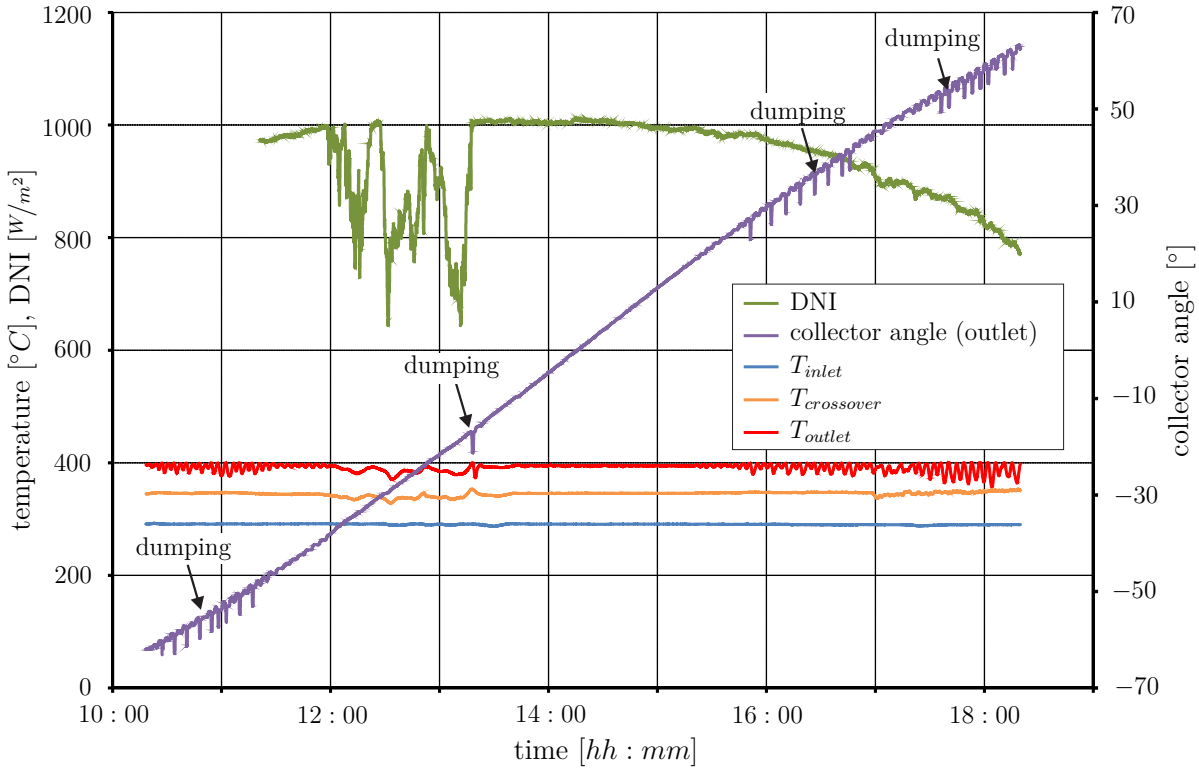

Figure 4.3: DNI, temperature profiles (inlet, crossover, outlet) and collector angle (outlet) of a loop in a 50 MW PTC power plant in Spain (01/04/2015)

4.1.2 Translational Motion

In general, the longitudinal dilatation ΔL of the HCEs can be obtained by

$$\Delta L = \alpha \cdot L \cdot \Delta\vartheta \tag{4.1}$$

- α = coefficient of linear thermal expansion (material dependent)
- L = SCA length
- $\Delta\vartheta$ = temperature difference

Consequently, the elongation is dependent on the SCA's length on the one hand and on the temperature difference on the other hand. For instance, a *EuroTrough* SCA (consisting of 12 SCEs) with its length of 150m (cf. table 2.1) has a thermal elongation of max. 550 mm [19]. Therefore, REPAs have to compensate 225 mm each. Based on ideal boundary conditions, a SCA will be heated up in the morning and cool down in the evening which ideally leads to one cycle per day. Yet, the effective thermal dilatation will differ, since there are phenomenons interfering with this ideal case:

DNI Fluctuations

The occurrence and disappearance of atmospheric influences - i.e. clouds - lead to fluctuations of solar radiation and therefore fluctuations of HCE's temperature and length. Figure 4.4 depicts the qualitative profile of a HCE's length during the course of a day. There is a trajectory for the idealized length (no outside influences) as well as for the effective length (realistic conditions, due to e.g. clouds and fluctuating DNI). Whilst the HCE length of the idealized curve remains steady state after being heated up, the effective length exhibits several gradients in the course of a day. This is derived from fluctuation of the DNI by means of clouds. The temperature trajectory in figure 4.3 shows noticeable fluctuation in the outlet of the loop between 12:00 and 13:30. Concerning this phenomenon there is a significant correlation to the DNI which is dropping from 1000 $^{W}/_{m^2}$ to values of 650 $^{W}/_{m^2}$. As a result of this, all shadowed HCEs in the solar field experience further cycles of linear thermal dilatation. Estimating a temperature decrease of approx. $50K$, the thermal dilatation varies about 3 cm.

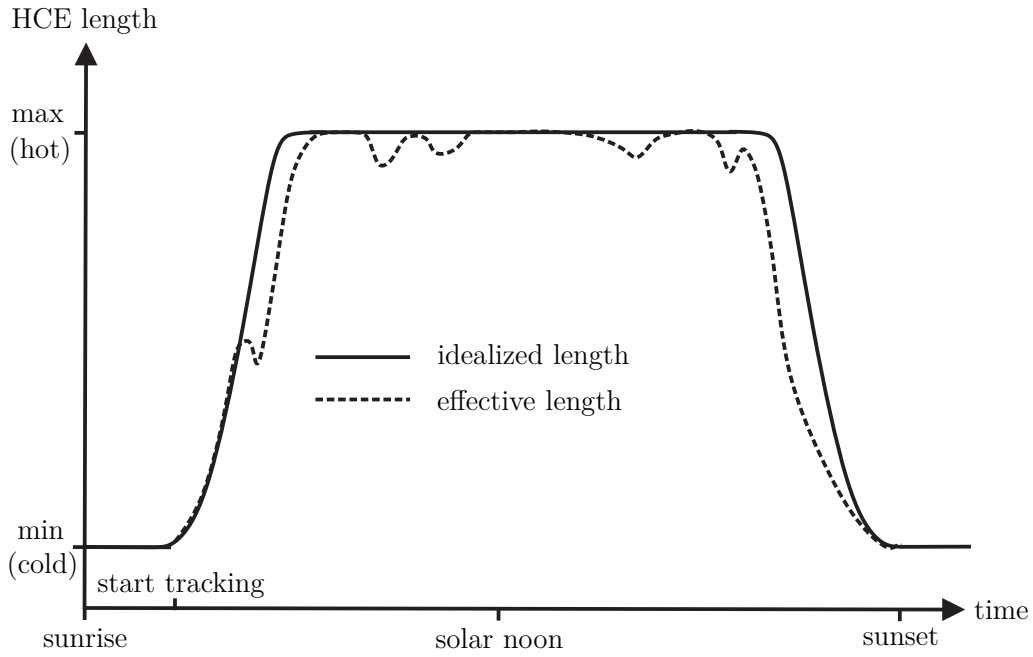

Figure 4.4: Comparison of idealized and effective HCE length affected by clouds during the day

Dumping and Tracking Errors

Dumping of collectors, as mentioned above, may cause additional thermal dilatation cycles. Having another look at figure 4.3 defocussing of a complete SCA and causes a temperature decrease of the HTF and therefore the HCE. Consequently, thermal dilatation cycles are added, even though those are only approx. 13 %[12] of the total dilatation.

[12] $^{50K}/_{380K} \approx 13\%$

4.1.3 External Loads

At first, the distinction between the two established REPA types (see chapter 2.4) must be taken up, as their mode of operation differs. In contrast to Ball Joint Assemblies, Rotary Flex Hose Assemblies derive benefit from a reduction of torque forces on the HCE: the necessary force to introduce the rotation movement is not transmitted by the absorber tube but by the torque transfer arm which is directly connected to the rotating axis of the swivel joint (see figure 3.5). Hence, the HCE is only partially stressed by the weight force of the corrugated tube. In comparison to ball joints, the cease of breakaway torques reduces those forces – introduced into the HCE – substantially. Despite these advantages Rotary Flex Hose Assemblies place higher demands on geometrical tolerances in general, as the swivel joint axis must be precisely aligned with the SCA axis. On the other hand, BJA are not subject to these requirements, since each Ball Joint is independent of other axes. This derives from an additional degree of freedom compared to swivel joints. Therefore Ball Joint Assemblies require lower precision levels in view of tolerances of position.

Another external impact to REPAs can be introduced by the adjacent piping. The pipe section – for instance between a loop's inlet and the header connection, see figure 4.5 – undergoes a thermal expansion when exposed to hot HTF. If not properly constrained by pipe bends and additional supports or pipe bends in the vicinity of the collector, the REPA must cope with additional forces. This applies particularly to RFHA, as their swivel joint depicts a location bearing carrying all external forces stemming from the adjacent piping.

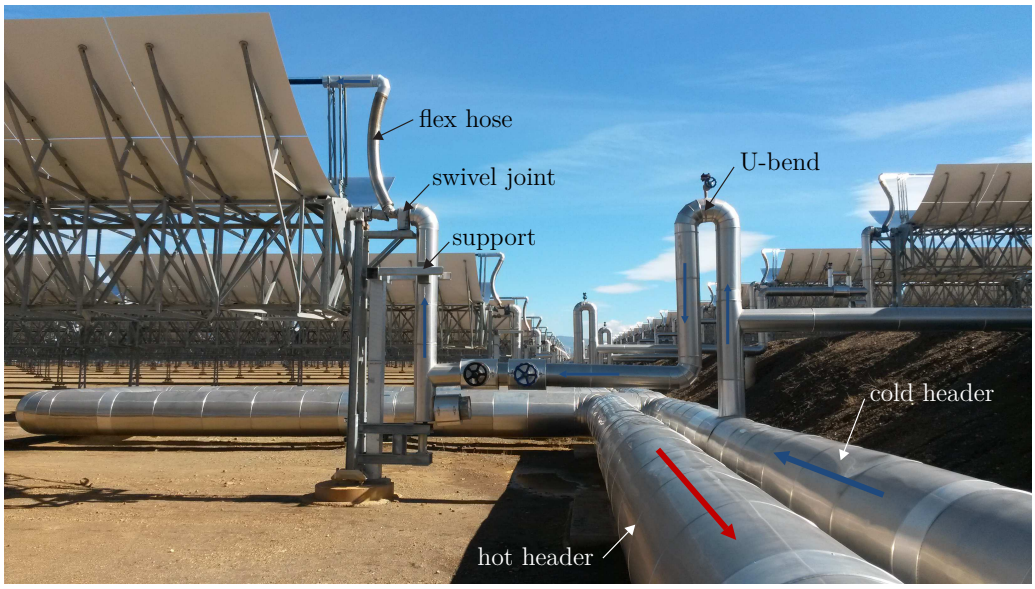

Figure 4.5: Connection between cold header pipe and loop inlet in a 50 MW PTC power plant in Spain

4.1.4 Hydraulic Loads

Forces due to Mass Flow and Fluid Velocity

REPAs contain at least two pipe bends which redirect the volume flow. Said redirection of HTF is causing reaction forces that have to be carried by the anchor points, e.g. the swivel joint of a RFHA. So as to emphasize the relevance of this impact, the conservation of momentum is outlined using the example of a RFHA. Figure 4.6 depicts a RFHA with a superimposed control volume (CV) at its bottom pipe bend. Neglecting both pressure-induced forces $\vec{F}_p$ (carried by the piping), gravitational forces $\vec{F}_g$ and friction forces $\vec{F}_{fr}$, the differential equation is given as (cf. [41])

$$\frac{d\vec{I}}{dt} = \int_A \rho\vec{w}(\vec{w}\cdot\vec{n})dA = \underbrace{\vec{F}_p}_{\approx 0} + \underbrace{\vec{F}_g}_{\approx 0} + \underbrace{\vec{F}_{fr}}_{\approx 0} + \vec{F}_{def} = \vec{F}_{def} \tag{4.2}$$

with the deflection force

$$\vec{F}_{def} = \begin{pmatrix} F_x \\ F_y \end{pmatrix} \tag{4.3}$$

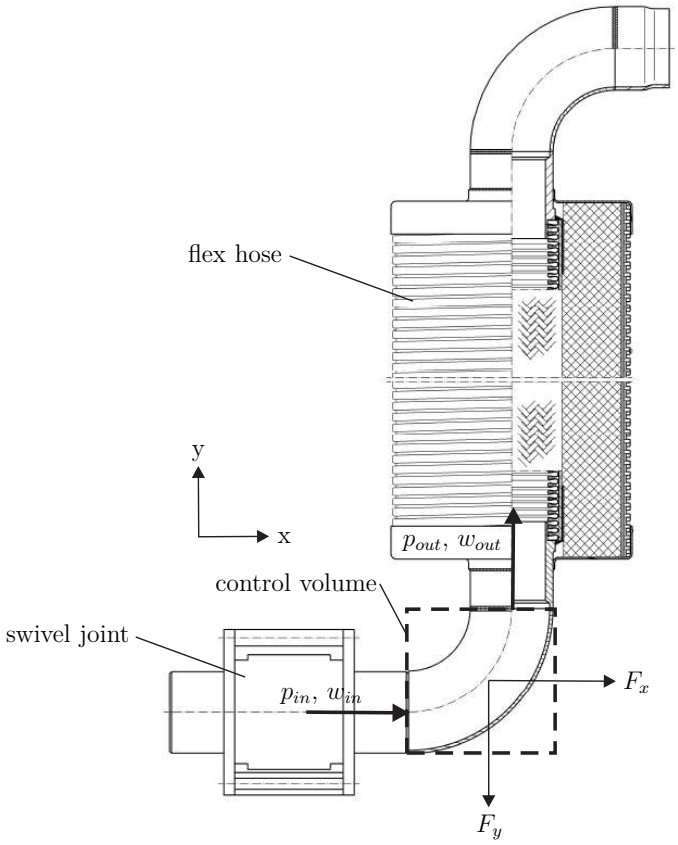

Figure 4.6: Deflection forces in a RFHA pipe bend (cf. [19])

The flow conditions in the RFHA are steady state ($\frac{dw}{dt} = 0$) and the cross-sections A in the inlet and outlet of the control volume are equal ($w_{in} = w_{out} = w$). Assuming a volume flow of 60 $^{m^3}/_h$ at ambient temperature (25 $°C$, density of *Therminol® VP-1* $\rho = 1061\ ^{kg}/_{m^3}$) and a REPA nominal diameter of $DN65$ ($d_i = 0.06m$, $w = 5.1^{m}/_{s}$), the forces are obtained as

$$\begin{aligned}\begin{pmatrix} F_x \\ F_y \end{pmatrix} &= \int_A \rho\vec{w}(\vec{w}\cdot\vec{n})dA = \rho\cdot\dot{V}\cdot\vec{w} + \underbrace{\rho\cdot V\cdot\dot{\vec{w}}}_{=0} = \rho\cdot\frac{\pi}{4}\cdot d_i^2\cdot\vec{w}^2 \\ &= \begin{pmatrix} \rho\cdot\frac{\pi}{4}\cdot d_i^2\cdot w^2 \\ -\rho\cdot\frac{\pi}{4}\cdot d_i^2\cdot w^2 \end{pmatrix} = \begin{pmatrix} 0.11\ kN \\ -0.11\ kN \end{pmatrix}\end{aligned} \tag{4.4}$$

Consequently, the said deflection forces are not negligible. Implementing them into the REPA Test Rig requires the design of an HTF cycle which supplies the test specimens with an adjustable volume flow.

Location Dependency of a REPA

In a PTC loop, REPAs occur at three different locations (see also figure 2.12):

- connection between header piping and loop
  - inlet (cold end)
  - outlet (hot end)
- interconnection between adjacent SCAs inside a loop
- connection between SCAs and the crossover pipe connecting parallel SCAs

Comparing these locations in respect to mechanical loads it is apparent that not all REPAs will carry the same amount of forces and torques, but rather will differ a lot. Despite the fact that all REPAs in a loop are quite similar in construction, boundary conditions are varying depending on the position within the collector loop. On the one hand, the geometry or rather the spatial dimensions of the interface between the fixed pipe and the REPA distinguish between the above mentioned locations. This makes an impact on the distribution of forces introduced to the REPA due to, for instance, thermal dilatation of the pipes. On the other hand, hydraulic influences have to be regarded, particularly implying pressures and temperatures: Whilst the temperature of the HTF increases inside a loop, the temperature drops along the line of a PTC power plant. Typical operating conditions at the inlet of a loop are approx. 30 bars and 300 $°C$, the temperature at the outlet increases to 400 $°C$ while the pressure drops to 20 bars [36].

HTF Influences

The type of HTF may have an influence on the REPA performance and its lifetime. Even though not all HTFs mentioned chapter 2.3.4 are state of the art in PTC power plants, their possible impacts on REPAs must be discussed:

- **Diphenyl-Diphenyl Oxide** (*Therminol® VP-1* and *DOWTHERM A*)
  Since DP-DPO is clearly the most mature and most widespread HTF on the market, the development for oil-conveying REPAs is evolved. Its environmental harmfulness puts special demands on the ball joint's and swivel joint's impermeability in regard to vapours.

- **Silicone Oils** (*Syltherm 800* and *HELISOL® 5A*)
  Derived from their promising properties for PTC applications and ongoing research projects, the REPA Test Rig will be designed for utilizing both *Syltherm 800* and *HELISOL® 5A*. This applies particularly to the elevated temperature of *HELISOL® 5A* of up to 430 $°C$.

- **Molten Salts** (*Solar Salt*, *Hitec®* and *Hitec® XL*)
  Since the efforts of using molten salt as HTF in PTC power plants are ongoing (see chapter 2.3.4), the development of a suitable REPA has been accompanied. Until now, no solution for a seal material came up withstanding temperatures of 500 $°C$ (cf. chapter 3.4). BJAs, in particular, turned out not to be applicable in said temperature levels. This can be traced back to insufficient material stability of the ball joint's seals. Yet, it is mentioned that the consequences of salt spill are less severe than of oil, as molten salt is neither inflammable nor harmful to the environment. Apart from that, the chemical properties of molten salt cause corrosion on the piping components. In addition, there will be a need for trace heating systems in molten salt PTC power plants, since its melting point is far beyond ambient temperature: the common used Solar Salt, for example, has a freezing point at 220 $°C$ (cf. table 2.2). Solidifying of molten salt inside a power plant's piping system can be caused by a malfunction of the trace heating system. It can result in serious damage to the solar field and its components, e.g. REPAs.

- **Steam / Water**
  Using steam as HTF, the REPAs have to face considerably higher pressures in contrast to other HTFs. Since those operation pressures can reach up to 100 bars and more, high demands are put on the seals. In addition, the water passes a phase transition while travelling through the absorber tube of the collector loop. Therefore, the vaporization is not a sudden event but a process; this is why REPAs in a loop may cope with different stages of the vaporization.

4.1.5 Environmental Loads

Derived from the fact that PTC power plants are detached (freestanding) facilities in plane areas, they sometimes have to face rough external (weather) conditions. This requirement also applies to the REPA's ability to withstand those outer impacts. In most cases, PTC power plants are erected in desertlike ares. Nevertheless, it is obligate that no dust and water particles penetrate the ball joint's or swivel joint's seals. In addition, the occurrence of rain and heavy wind forces has to be regarded. Another major issue forcing PTC power plants to enable zero leakage are the environmental affects by means of the HTF.

A different requirement derives from concentrated solar radiation in particular during lower solar altitudes, which have a large deviation from the zenith. Based on a north-south orientated SCA and during times of low azimuth angles – on the northern hemisphere especially in winter – a certain amount of solar radiation is deflected along the longitudinal focal line causing a "longitudinal focus deviation", i.e. *end losses*. Despite the associated efficiency losses of a PTC power plant, there is an impact on the interconnections, too. Depending on the azimuth angle this effect can cause an exposure of the REPA's components to concentrated solar radiation. Figure 4.7 shows a photo of the same prototype collector depicted in chapter 3.2. The upper connection between the flex hose and the HCE is directly irradiated by concentrated solar light causing smoke formation at the insulated parts. Even though this assembly depicts a temporary measurement setup that is only protected with aluminium foil, the occurrence of smoke illustrates the substantial thermal loads on the REPA and its thermal insulation. As a consequence of this, the REPA components – including thermal insulations and surfaces – must be designed to withstand concentrated sunlight.

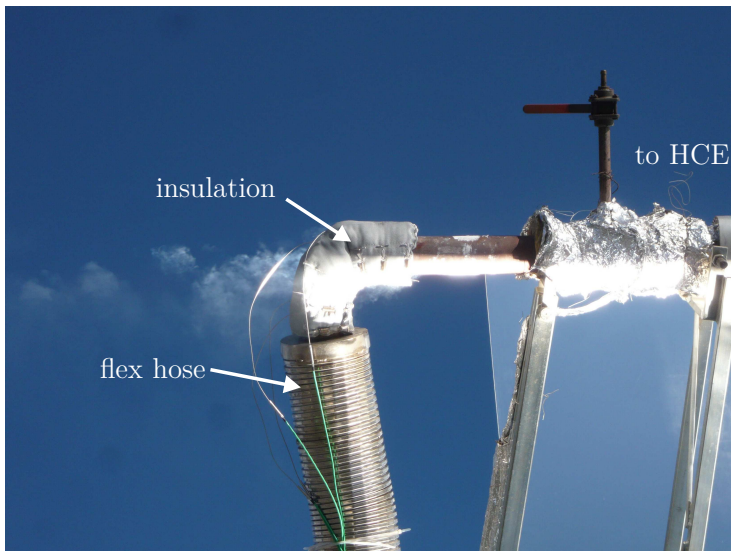

Figure 4.7: End losses at the REPA interconnection to the HCE

4.1.6 Security

The majority of PTC power plants applies the eutectic mixture of DP-DPO as HTF (cf. chapter 2.3.4). Since this fluid has a flash point below desired working temperatures, it is mandatory that every component, which is in direct contact to the HTF, ensures zero leakage. For instance, the flash point of *VP1* is at 110 $°C$ according to *DIN EN 22719*, which is significantly below the regular working temperature of 400 $°C$ [23]. The ability to show no failure even after long-term operation applies in particular to REPAs being highly stressed parts. Even though sudden failures are an absolute exception, the absence of any ignition sources in close vicinity to the REPAs must be guaranteed. Minor leakages of HTF are frequently visible due to smoke formation and thus can be noticed and repaired.

4.2 Requirements for the Test Rig

Based on the design of other test rigs (see chapter 3) and the above findings with respect to requirements and specifications for REPAs, the following section serves to contribute the derived characteristics of the REPA Test Rig. Beyond a Kinematics Unit, which conduces to realize accelerated motion cycles of the test objects, the properties of an accompanied HTF cycle must be specified. The latter serves to wet the REPA with HTF at working conditions.

4.2.1 HTF Circuit

In order to carry out realistic and application relevant tests, the REPA must be at least wetted – better flushed – with HTF. A first feasible solution is a static pressurization of the test components with hot HTF. This is, for instance, done by *Senior Flexonics GmbH*, see chapter 3.3. Yet, and in order to be able to carry out a simulation that is as similar to power plant conditions as possible, it is necessary to integrate the REPA in a circulating HTF assembly. The occurrence of a REPA leakage is a relevant failure indicator. Hence, not only "in-field" temperatures and pressure must be ensured, but also the mass flow, which has considerable influences on the forces introduced to the REPAs pipe bends, cf. chapter 4.1.4.

The REPA Test Rig and its components must be designed to enable operation with three different HTFs: *Therminol® VP-1*, *Syltherm 800* and *HELISOL® 5A*. It will neither be designed to convey molten salts nor steam / water. Their utilization would require additional HTF circuits. The associated expenses are – given the low establishment and relevance of those fluids in commercial PTC applications – not justifiable.

Since today's solar thermal R&D is targeted at improving the thermal efficiency of solar fields, there are efforts aimed at increasing the HTF temperature. Until now, said increase has been inhibited due to thermal instability of synthetic oils beyond 400 $°C$. With the development of new HTFs (i.e. silicone oils such as *HELISOL®*), temperature of up to 430 $°C$ are already feasible regarding the chemical decomposition in absence of oxygen. A further raise in temperature has an impact on the fluid viscosity and is therefore tending to induce higher demands on the seals to prevent leakage. Because of the higher quantity of seals, this represents a challenge especially for Ball Joint Assemblies compared to Rotary Flex Hose Assemblies. Even though the utilization of temperatures above 400 $°C$ has not yet been proven in commercial PTC applications, the REPA Test Rig must be designed to meet working temperatures of up to 450 $°C$. This feature enables the assembly to respond to future developments with respect to new HTFs. Since the three mentioned HTFs are non-corrosive, all seals and gaskets must cope with the above mentioned working

conditions of the different HTFs avoiding a possible exchange of said seals.

4.2.2 Kinematics Unit

The kinematics part of the REPA Test Rig has to accommodate the test objects complying with varying and therefore adjustable geometries, e.g. focal lengths. It must accomplish both rotational and translational movements. These movements have to be speeded up distinctly for the purpose of simulating accelerated life cycles of REPAs. Further, the occurrence of tracking errors (see chapter 4.1.1), which interferes with the intended accelerated tracking movements, are recurring phenomenons in PTC power plants. Since these issues may affect the durability of a REPA, a possibility to simulate them is crucial in order to achieve a realistic simulation. To make this possible, the drive must be able to depict smaller, intermediate steps as well as continuous motion. One objective of the REPA Test Rig is to find out how these phenomenons and their induced additional mechanical motions affect the lifetime of a REPA.

The first Solar Energy Generating Systems (SEGS) have been erected with *LS-1* and *LS-2* collector types using gear drives (cf. table 2.1). Nowadays state of the art SCAs operate merely with hydraulic drive units; especially the *EuroTrough*, *HelioTrough*® and *Ultimate Trough*™ collectors are driven hydraulically. Consequently, a hydraulic drive unit will be applied to the test rig, since its application in PTC power plants is widespread and since it is an adequate approach to simulate motions just the way they are introduced commercially. The drive pylon – the core of the Kinematics Unit – will be similar to those of a commercial *EuroTrough* SCA. Yet, the hydraulics system must be different compared to the customary application. On the one hand, the REPA Test Rig must be enabled to perform regular collector movements, which occur in commercial PTC power plants. On the other hand, the implementation of a servo motor driving the hydraulic pump (rather than a three-phase motor) allows to realize accelerated incremental movements whilst taking into account the lifetime of all hydraulic components.

4.3 Specification Sheet

The specifications of the test rig, as listed below, are designed in a way that – as far as possible – all realistic operation conditions of REPAs can be reproduced. The individual testing procedures for a specific REPA can and must be adapted to its particular application. Not all operation parameters can be set independently (e.g. the working pressure must always be greater than the HTF's vapour pressure). However, they are variable and can be combined in accordance with the test objects and their individual application.

1. **HTF Cycle**
   - HTF: DP-DPO (e.g. *Therminol VP-1* or similar) and Silicone Oils (e.g. *Syltherm 800* and *HELISOL® 5A*)
   - volume flow: $6 - 60\ {}^{m^3}/_{h}$
   - working pressure: $1 - 40$ bars
   - design pressure: 45 bars
   - working temperature: $20 - 450\ {}^{\circ}C$
   - design temperature: $500\ {}^{\circ}C$
2. **Kinematics**
   - rotation
     - range of the rotation: 210°
     - increment rotationally: up to 0.25°
     - rotational radius (focal length): adjustable for different REPAs in a range between 1500 mm and 2300 mm
     - drive type: hydraulic, two pistons
   - translation
     - maximum stroke : 500 mm
     - drive type: hydraulic, two parallel pistons

3. **Operation**
    - operating mode: endurance test, tailored to specific application
    - maximum number of cycles per day: approx. 400
    - cycling: stepwise along the whole rotation and back to initial position; simultaneous translational motion to cover the thermal dilatation of HCEs
    - representative simulation of the REPA's assembly situation
4. **Measurement**
    - temperature sensors
        - upstream the pump
        - downstream the heater
        - expansion vessel (fluid phase)
        - expansion vessel (head phase)
    - pressure sensors
        - upstream the pump
        - downstream the pump
        - downstream the Kinematics Unit
        - expansion vessel
    - expansion vessel level switch
    - volume flow (main HTF cycle)
    - Kinematics Unit position
        - translation axis
        - rotation axis
    - load sensor (dynamometer)
        - top and bottom interface between REPA and Kinematics Unit (for both REPAs)

Chapter 5

Design

Having the boundary conditions for the REPA Test Rig specified in chapter 4, the subsequent chapter contributes to the technical implementation of those. An externally designed Kinematics Unit serves to enable realistic rotation and expansion motion of the test components. Based on the Kinematics Unit's geometric presets, an HTF cycle is connected to it. In doing so, the fluid's properties must be adjustable in terms of mass flow (pump, see chapter 5.1.2), temperature (heater, see chapter 5.1.3) and pressure (expansion vessel, see chapter 5.1.4). Afterwards, the main focus will be on the implementation of load sensors (dynamometers) which carry and measure the forces and torques stemming from the REPAs. Providing a first impression, figure 5.1 presents the CAD model of the test rig with its Kinematics Unit (left) and the attached HTF cycle (right).

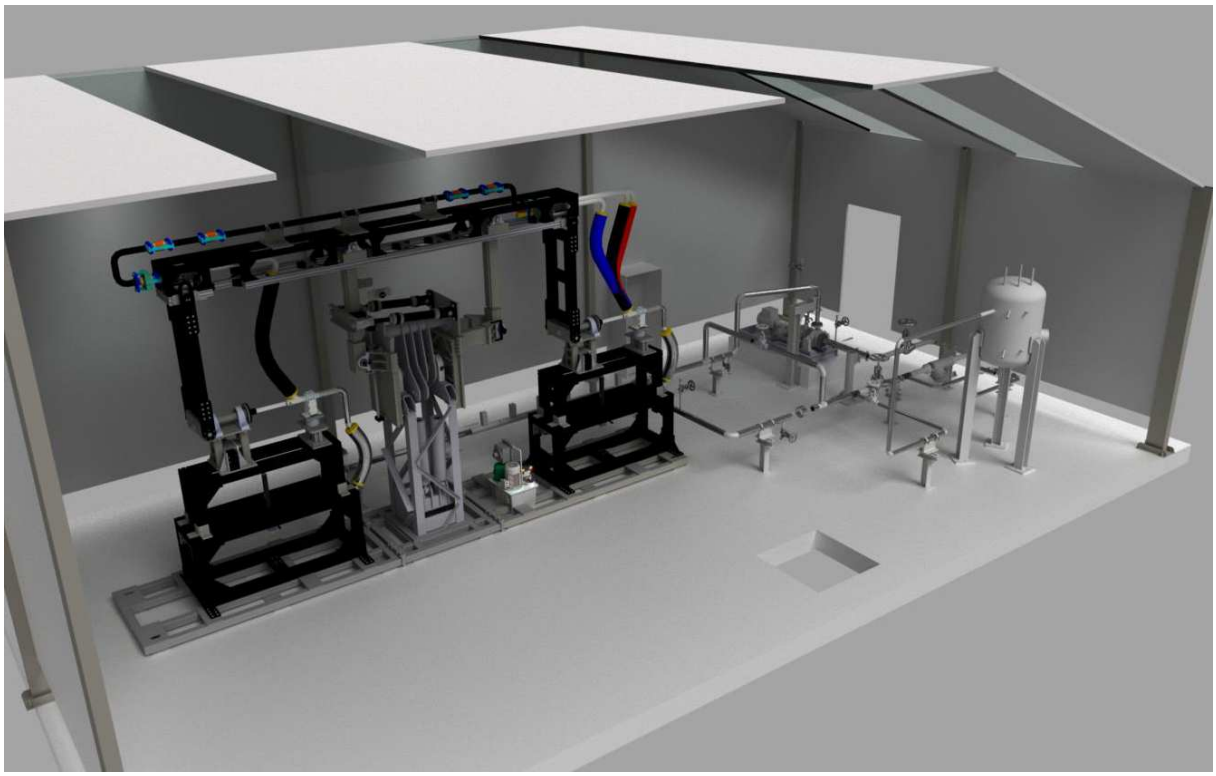

Figure 5.1: CAD model of the REPA Test Rig

5.1 HTF Cycle

The HTF cycle design is split in different sections: At first, the general structure and all relevant components are depicted. Then, special attention is given to the design of the pump, the heater and the expansion vessel.

5.1.1 HTF Cycle Structure

The HTF cycle serves to carry HTF through the test objects. The present design respects the components for commissioning the test rig. Later on, a comprehensive upgrade – e.g. including actuated valves – is planned.

Figure 5.2 depicts the Piping and Instrumentation Diagram (P & ID) with superimposed labels. Starting at the discharge side of the pump, the HTF is conveyed and heated up in a straight pipe by band heaters (see chapter 5.1.3). A flow meter is used to monitor and control the volume flow. The connection to the Kinematics Unit (see chapter 5.2) are two corrugated tubes which serve to compensate for the thermal expansion of the pipe system. In doing so, the axial loads on the anchor points are diminished. After passing the Kinematics Unit, the HTF circulated back to the pump's suction side. On its way it passes a check valve in order to avoid counterflow in the system. A strainer is installed upstream the pump to inhibit any kind of damage on the impeller of the pump induced by possible particles inside the HTF. In addition, there are two bypasses attached. The first one serves as a "bridge" to connect the pump's discharge and suction side. Once the valve on top of it is open, it enables pumping the fluid in a closed circuit without impinging the Kinematics Unit (for testing purposes). The second bypass is the conjunction with the expansion vessel having a top inlet and a bottom outlet connection. There are two hand valves in the bypass in order to disconnect it from the main cycle. Another hand valve is installed in the main circuit to allow pumping through the vessel. The expansion vessel is connected to a nitrogen assembly. It serves to both maintain a constant pressure in the HTF cycle and to prevent oxidation of the fluid (cf. chapter 5.1.4).

In the course of the above mentioned comprehensive upgrade, the installation of an additional, actuated valve is planned for security matters. It will be located upstream the Kinematics Unit and controlled by the pressure sensor downstream the Kinematics Unit. In case of any failure in regard to the HTF conveying the Kinematics Unit, the fluid pressure drops and the actuated valve is closed.

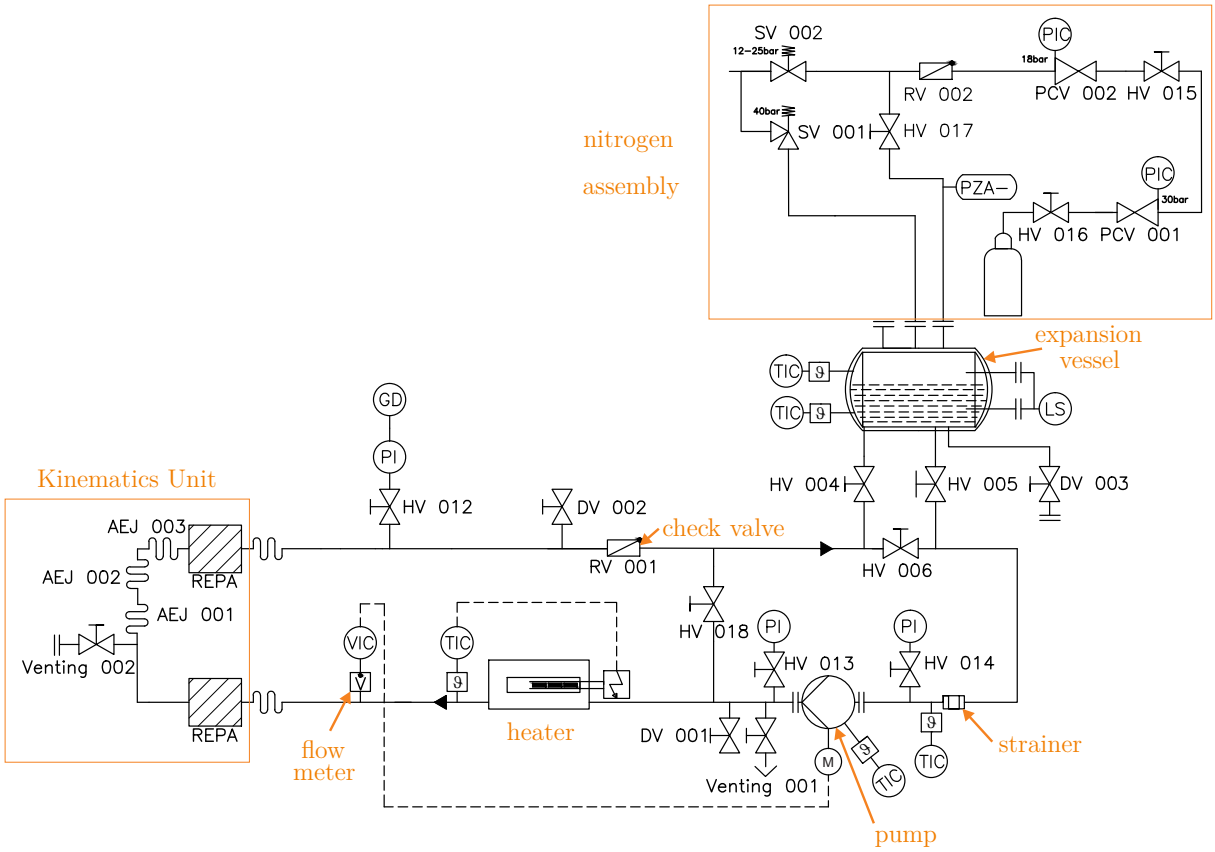

Figure 5.2: Piping and Instrumentation Diagram (P & ID) of the commissioning status

Based on the P & ID, the design of a functional pipe system and its components is carried out in consideration of the position and the functionalities of each part. In doing so, the spatial arrangement of all pipe sections and the accompanied components must be designed in respect of a "compact" shape, yet taking into account possible restrictions of the components. Those are, for instance, run-in distances (straight pipe sections) of the pump and the flow meter. Within the framework of this thesis, the implemented arrangement and connection of all elements (excluding the Kinematics Unit) is reproduced within the simulation software *ROHR2* made by *SIGMA Ingenieurgesellschaft mbH*. Since the system must cope with HTF at maximum operation conditions of 450 $°C$ and 40 bars, a stress analysis is carried out. The final result is presented in figure 5.3. The isometric view depicts the consequent realization of the specifications and arrangements given in the P & ID, see figure 5.2. The pump is modelled as a fix point both at the suction and the discharge side. However, given the manufacturer's datasheet, the piping close to the pump must be supported by additional anchors and connected "stress-free". Therefore, two additional anchor points are designed; their technical drawings can be found in appendices D.1 (suction side) and D.2 (discharge side); above that, a photo is presented in appendix E.2. The interface between the HTF cycle and the Kinematics Unit is realized using corrugated tubes made by *Senior Flexonics GmbH*. Their implementation

in *ROHR2* is achieved with lateral expansion joints (see figure 5.16), since they have the same mode of action. Appendix E.1 presents a photo of the HTF cycle in a first erection phase; compared to figure 5.3, however, the corrugated tubes are not yet mounted.

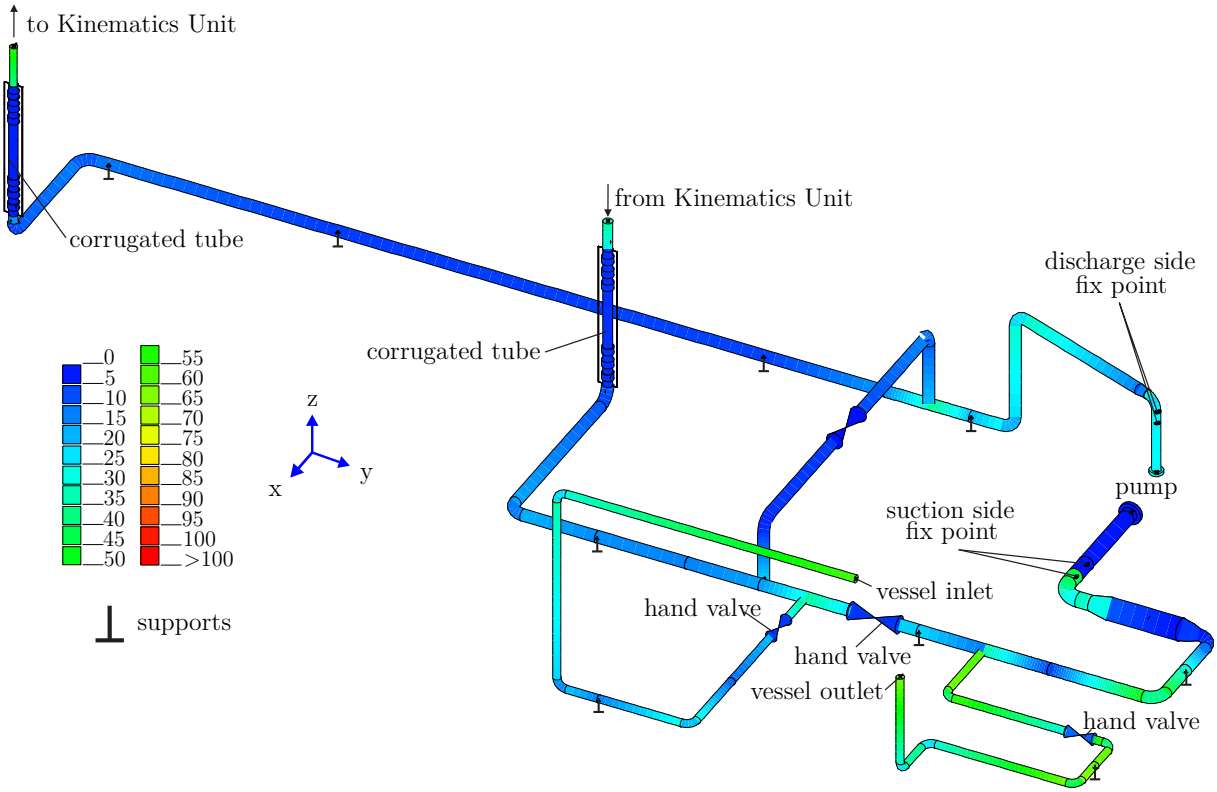

Figure 5.3: Stress analysis according to ASME B31.1; Utilization Analysis (Secondary Loads due to temperature and pressure)

5.1.2 Pressure Loss Estimation and Characteristic Curves

In order to select a suitable pump configuration, it is necessary to calculate its operation conditions. The most important design parameter is the pressure drop / increase of the piping system the pump has to overcome / provide. In closed loop systems – such as the HTF cycle of the REPA Test Rig – pressure losses are solely caused by friction between the fluid and the system's components. Further, this energy loss is highly dependent on the load case (temperature, mass flow) and the type of HTF (density). This is why the pressure drop calculation is carried out for every possible scenario. The resulting dissipation leads to an increase of the HTF temperature. All equations used in the following section are derived from *Tabellenbuch für den Rohrleitungsbau* (2012) [42].

The pressure drop in closed-loop pipe systems is given by

$$\Delta p = \sum \zeta_i \cdot \frac{\rho \cdot w^2}{2} \tag{5.1}$$

$\sum \zeta_i$ is the sum of all resistance coefficients of each type of pressure loss, w is the fluid velocity and ρ is the HTF density. The pressure loss is caused by

- **friction between fluid and pipe walls**

$$\zeta_{fr} = \lambda \cdot \frac{L}{d_i} \tag{5.2}$$

  - λ = pipe friction coefficient
  - d_i = pipe inner diameter
  - L = pipe length

  Since the HTF cycle contains different pipe sections with varying pipe nominal diameters, the calculations have to be carried out for each section and diameter. Values for λ in steel pipes are:

Table 5.1: Pipe friction coefficients for steel pipes [42]

d_i [mm]	50	200	1000
λ [-]	0.02	0.015	0.012

Based on these reference values, a power trendline is calculated:

$$\lambda = 0.0381 \cdot {d_i}^{-0.17} \tag{5.3}$$

- **change of cross section**

  Regarding pressure losses due to change of the pipe inner diameter, a distinction is made between diameter *enlargement* and *reduction*. The resistance coefficients depend on the cone angle δ of the cross section's change, which is 30°. The enlargements of cross-section can be calculated using

$$\zeta_{cs} = \xi \cdot \left(\frac{d_{i,out}^2}{d_{i,in}^2} - 1 \right)^2 \tag{5.4}$$

  with

$$\xi = tanh\left(1.41 \cdot \frac{\delta}{100}\right) + 522 \cdot \left(\frac{\delta}{100}\right)^{4.365} \cdot e^{(-8\delta/100)} = 0.6466 \tag{5.5}$$

  For cone angles which are smaller than 40° the resistance coefficient for reductions is

$$\zeta_{cs} = 0.04 \tag{5.6}$$

- **pipe bends**

  The resistance coefficients ζ_b for 90° pipe bends are dependent on the ratio of bend radius r and pipe nominal diameter d. They are listed in tabular form:

Table 5.2: Resistance coefficients for 90°-pipe bends [42]

r/d	1	2	4	6	10
ζ_b	0.29	0.18	0.14	0.12	0.11

  The pipe bends are designed according to type *3D* (cf. [43]). By means of assigning every possible continuous value of $\frac{r}{d}$, a power trendline is created:

$$\zeta_b = 0.2639 \cdot \left(\frac{r}{d}\right)^{-0.419} \tag{5.7}$$

- **intersections**

  In regard to intersections (T-junctions), the flow direction must be respected. A derivation is made between *coalition*

$$\zeta_{is} = 2 \cdot \Big(-0.871 \cdot x^2 + 1.494 \cdot x + 0.019 \Big) - \Big(1 - (1 - x^2) \Big) \tag{5.8}$$

  and *separation*

$$\zeta_{is} = 2 \cdot \Big(1.00888 \cdot x^2 - 1.24 \cdot x + 0.02 \Big) - \Big((1 - x^2) - 1 \Big) \tag{5.9}$$

of flow. Figure 5.4 illustrates both situations. In this case – the calculation of the maximum pressure drop of the HTF cycle – the fluid only circulates through the main cycle, i.e. neither coalition nor separation of mass flow in the T-Junction. Hence, there is no fluid conveying the bypasses and the velocities w_3 are always zero. As a result of this, the resistance for each T-junction ζ_{is} is 0.04 both for coalition and separation.

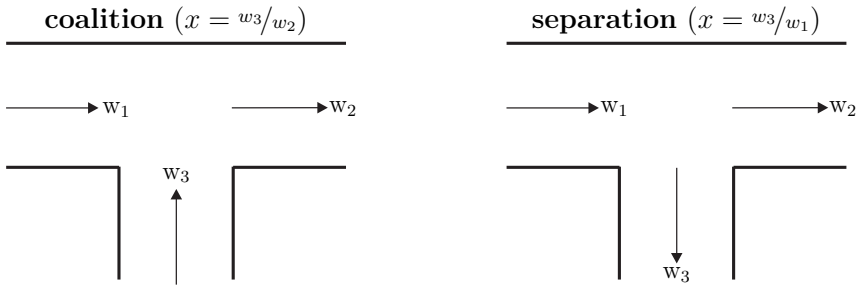

Figure 5.4: T-Junction; coalition (left) and separation (right)

- **valves**
  Every valve can be characterized by the K_v-value (flow coefficient). This value describes the maximum possible amount of flow in a fully-open valve causing a differential pressure (pressure loss) of 1 bar. Substituting DN with the nominal diameter of the valve, the resistance coefficient is individually calculated as

$$\zeta_v = \frac{1}{626.3} \cdot \left(\frac{DN^2}{K_v} \right)^2 \tag{5.10}$$

  for every valve that is part of the closed-loop HTF cycle.

- **miscellaneous installations**
  The HTF cycle contains additional installations which have to be taken into account. The accompanied maximum pressure of those components drops are:

  - strainer = 0.012 bar
  - throttel plate = 0.183 bar

  The manufacturers only provide these maximum values, thus they are estimated to be constant. Since the heating system (cf. chapter 5.1.3) is non invasive, no further pressure drop is added in this section.

All resistance coefficients ζ_i (equations (5.2) - (5.10)) are only dependent on the components' geometry. Thus, once they are calculated (see appendices B.1 - B.4), the pressure drop can be obtained easily for every possible operation point and for each HTF (see

appendices B.5 - B.7). Said operation point is defined by the operation temperature (affecting the density ρ) and the volume flow (affecting the fluid's velocity w). The pump can operate with a speed of up to 2900 min^{-1}. However, since the pump's discharge head is oversized, an operation point with lower speed needs to be found. In order to ensure validity of these curves for all fluids, the pressure drop is converted into water differential head H:

$$H = \frac{\Delta p}{\rho \cdot g} \tag{5.11}$$

- H = differential head
- Δp = pressure drop
- ρ = water density (= 999 $^{kg}/_{m^3}$)
- g = gravity (= 9.81 $^{m}/_{s^2}$)

Having the above calculations done[13], system characteristic curves can be obtained for each HTF and temperature. Pumps are always adjusted for the operation point where the pump characteristic curve and the system characteristic curve converge. Consequently, given the pump characteristic curve by the manufacturer, the point of intersection of both curves represents the resulting operation point. The pump for the REPA Test Rig is made by *Dickow Pumpen KG*; the datasheet can be found in appendix A.1. Figure 5.5 depicts the system characteristic curves for different operation temperatures when using *Therminol® VP-1* as HTF. Moreover, the pump characteristic curves for different pump speeds are depicted. Both system and pump characteristic curves describe the relation between the flow rate (x-axis) and the water differential head (y-axis). First of all, it is apparent that increasing the pump speed (or rather the power input) increases the differential head. Likewise, decreasing the HTF temperature increases the differential head, i.e. the pressure drop.

The characteristic diagram serves to identify possible operation points of the system. It has to be kept in mind that pump and system characteristic curve will intersect, since the conversation of energy has to be taken into account. Consequently, the system will always maintain a steady-state flow depending on the given power input. When, for instance, the pump is operating with 2100 min^{-1} and *Therminol® VP-1* at 300 $°C$, a volume flow of approx. 59 m^3/h will result.

Additionally, the same characteristic diagrams are illustrated in figure 5.6 for *Syltherm 800* and in figure 5.7 for *HELISOL® 5A*. Comparing the three diagrams, *Therminol® VP-1* turns out to cause the highest pressure losses. This is derived from its density, which

[13]The numerical results can be found in appendices B.5, B.6 and B.7

is, compared to the silicone oils, the highest in the whole temperature range. A maximum pressure drop of approx. 2.95 bars, which equals 30.1 m of water differential head, can be obtained when operating the REPA Test Rig with *Therminol® VP-1* conveying with 60 $^{m^3}/_h$ and ambient temperature (25 $°C$). However, this operation point will not occur, thus the value only serves to determine the installed power input of the pump. Finally, it can be concluded that the pump is capable to convey each of the three HTFs in the whole operation range which was determined in chapter 4.3.

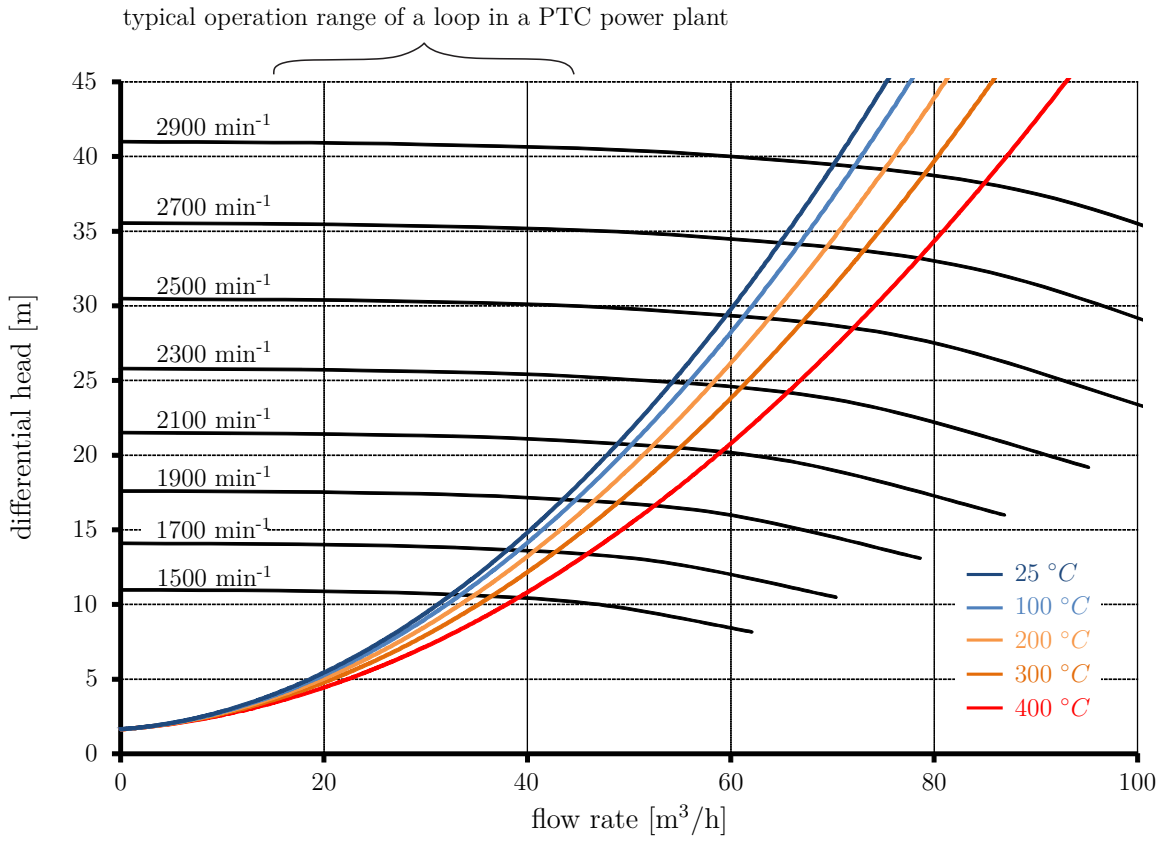

Figure 5.5: Pump characteristic curves for varying speeds and system characteristic curves of *Therminol® VP-1* for varying temperatures

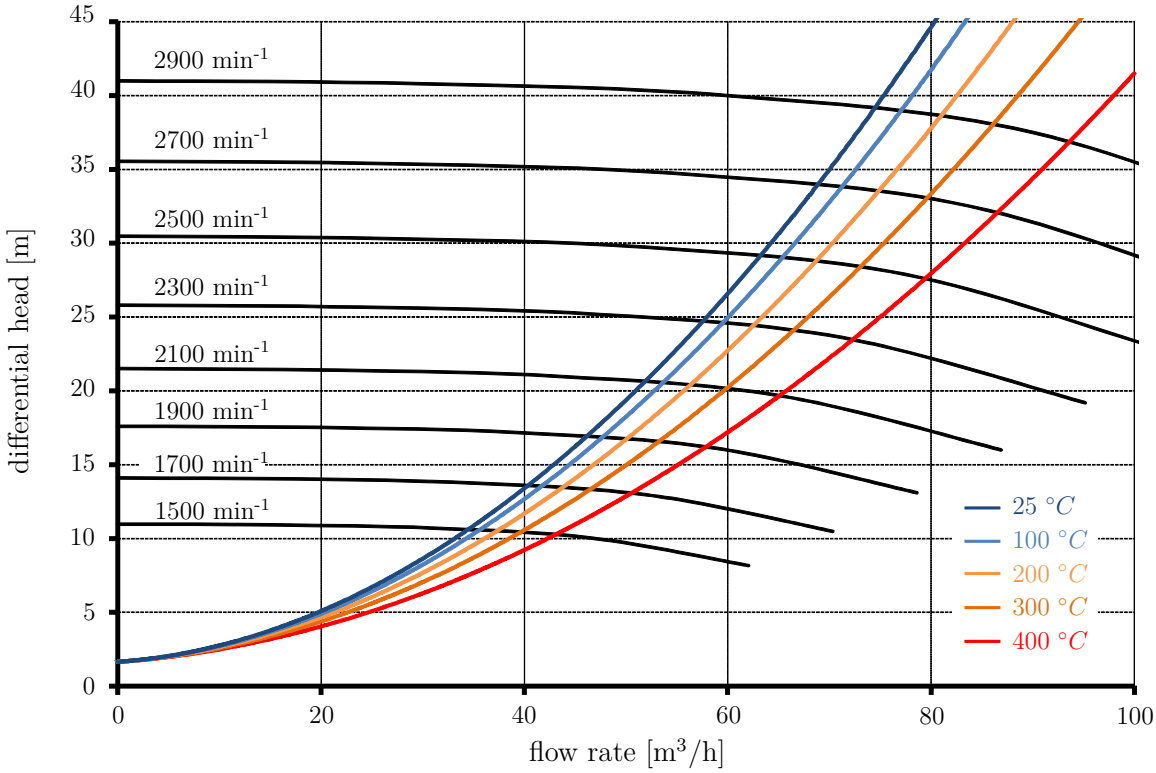

Figure 5.6: Pump characteristic curves for varying speeds and system characteristic curves of *Syltherm 800* for varying temperatures

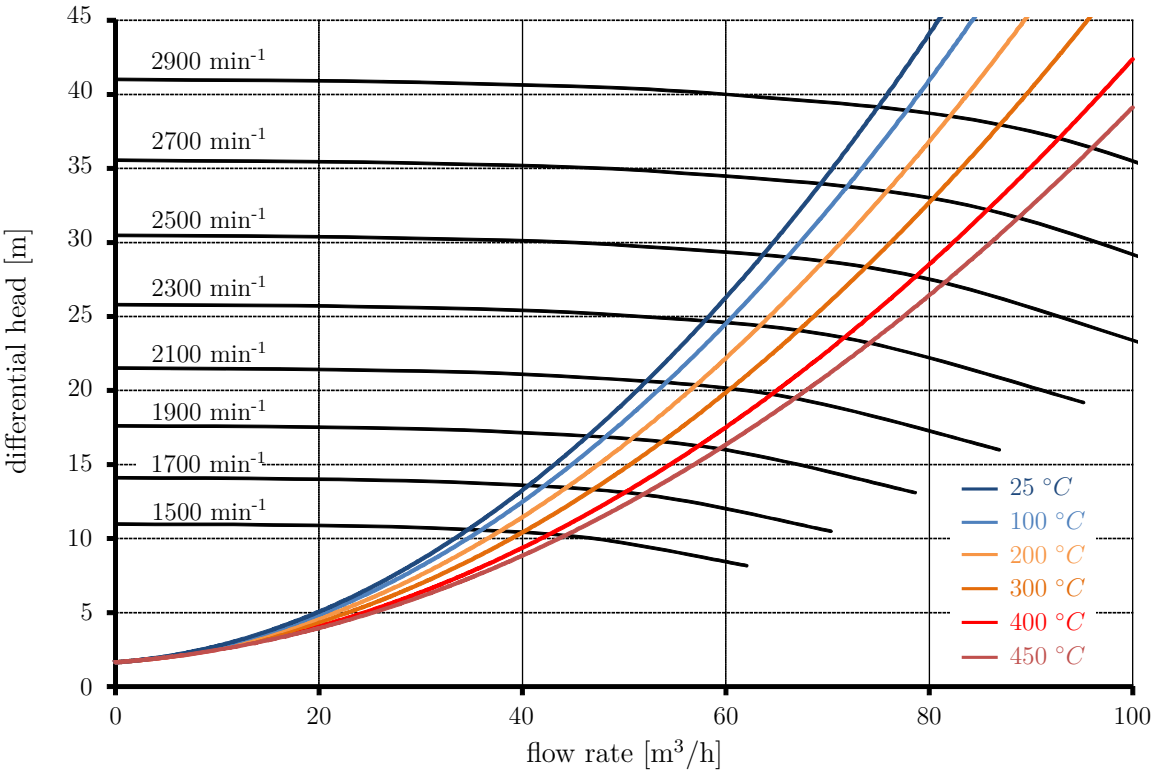

Figure 5.7: Pump characteristic curves for varying speeds and system characteristic curves of *HELISOL® 5A* for varying temperatures

5.1.3 Thermal Losses and Selection of Heater

Owing to the fact that the HTF cycle requires operation with a maximum bulk temperature of 450 $°C$ (see chapter 4.3), a suitable heating system must be designed. Therefore, an accurate calculation of the estimated thermal losses along with the necessary insulation thickness is required. Knowing the test rig's peak heat loss (at maximum temperature) is the basis for selecting a qualified electrical heater, since it describes the minimum effective power input of the latter. All formulas used in the following section derive from *Wagner* (2008) [43].

The heat loss of a pipe system (length L) is defined as

$$\dot{Q}_L = k_L \cdot \Delta\vartheta \cdot L \tag{5.12}$$

$\Delta\vartheta$ is the difference between fluid operation temperature and ambient temperature

$$\Delta\vartheta = \vartheta_{HTF} - \vartheta_{amb} \tag{5.13}$$

Based on a negligible heat resistance of the steel pipes ($\vartheta_{HTF} \approx \vartheta_{i,p} \approx \vartheta_{o,p}$), the thermal transmission coefficient k_L of a pipe can be written as

$$\begin{aligned} k_L &= \frac{\pi}{\underbrace{\frac{1}{\alpha_i \cdot d_i}}_{\approx 0} + \underbrace{\frac{1}{2\lambda_p} \cdot ln\frac{d_{o,p}}{d_{i,p}}}_{\approx 0} + \frac{1}{2\lambda_{ins}} \cdot ln\frac{d_{o,ins}}{d_{i,ins}} + \frac{1}{\alpha_o \cdot d_{o,ins}}} \\ &= \frac{\pi}{\frac{1}{2\lambda_{ins}} \cdot ln\frac{d_{o,ins}}{d_{i,ins}} + \frac{1}{\alpha_o \cdot d_{o,D}}} \end{aligned} \tag{5.14}$$

The heat transfer coefficient between insulation and environment α_o consist of a radiational and a convective proportion

$$\alpha_o = \alpha_{o,rad} + \alpha_{o,conv}$$

According to Wagner (cf. [43]), the convective proportion for pipes outside of buildings is

$$\alpha_{o,conv} = 8.9 \cdot \frac{w^{0.9}}{d_o^{0.1}}{}^{14} \tag{5.15}$$

Assuming a wind velocity w in Tabernas (location of the test rig) of 2 $^m/_s$, a pipe outer diameter of 88.9 mm and an insulation thickness of 120 mm, the convective heat transfer

[14] This equation is valid for $w \cdot d_o > 0.00855$ $^{m^2}/_s$.

coefficient at the outer surface of the insulation is

$$\alpha_{o,conv} = 18.56\ {}^{W}/_{m^2K} \tag{5.16}$$

The proportion of radiational heat losses is given by

$$\alpha_{o,rad} = \epsilon \cdot \sigma \cdot \frac{(\vartheta_{ins,o} + 273.15K)^4 - (\vartheta_{amb} + 273.15K)^4}{\vartheta_{ins,o} - \vartheta_{amb}} \tag{5.17}$$

- $\sigma = 5.67 \cdot 10^{-8}\ {}^{W}/_{m^2K^4}$ (Stefan-Boltzmann constant)
- $\epsilon = 0.05$ (polished aluminium sheet) [44]
- $\vartheta_{ins,a} \approx 50\ °C$ (permitted surface temperature)
- $\vartheta_{amb} = 25\ °C$

$$\alpha_{a,rad} = 0.34\ {}^{W}/_{m^2K} \tag{5.18}$$

The thermal conductivity λ_{ins} of the insulation material (*ROCKWOOL ProRox PS 960*) can be extrapolated from the data sheet and is 0.151 ${}^{W}/_{mK}$ at the maximum operation temperature of 450 $°C$ [45]. Based on a insulation thickness of 120 mm, the result is inserted in equation (5.14) and equation (5.12). Heat losses for different diameters are calculated and presented in table 5.3 for the regular piping:

Table 5.3: Heat losses for different pipe diameters at 450 $°C$

	unit	DN50	DN65	DN80	DN100
outer diameter	mm	60.3	73	88.9	114.3
wall thickness[15]	mm	5.54	7.01	7.62	8.56
inner diameter	mm	49.2	59.0	73.7	97.2
k_L	${}^{W}/_{mK}$	0.574	0.632	0.701	0.809
$\dot{q}'_L$	${}^{W}/_{m}$	243.8	268.4	298.1	343.8
L	m	10.0	15.1	21.2	1.3
$\dot{Q}_L$	kW	2.43	4.04	6.32	0.44

Considering all pipes and diameters, the total heat loss of insulated pipe sections adds up to

$$\dot{Q}_{L,piping} = 13.23\ kW \tag{5.19}$$

[15] According to ASME B36.10 (Schedule 80) [46]

Concerning the flexible pipe sections, e.g. REPAs, a different type of insulation is installed. During commissioning, the test rig is equipped with *RotationFlex®* Rotary Flex Hose Assemblies manufactured by *Senior Flexonics GmbH*. Furthermore, the linear thermal expansion in the HTF cycle is carried by *Tuboflex®* corrugated tubes made by *Senior Flexonics GmbH*. Given the manufacturer data, the thermal transmission coefficient is $k_{L,flex} = 0.748\ {}^{W}/_{mK}$, thus the heat loss of all flexible pipes (length 7.1 m) can be calculated and is

$$\dot{Q}_{L,flex} = 2.26\ kW \tag{5.20}$$

Taking into account additional heat losses (e.g. valves, pump, supports) of 2 kW (estimated) as well as a security factor of 1.1, a total peak heat loss of the REPA Test Rig of

$$\dot{Q}_L = \sum \dot{Q}_i \cdot 110\% = 19.24\ kW \tag{5.21}$$

is obtained.

The thermal energy is provided by customized band heaters from *LCS IsoTherm GmbH & Co. KG*. Band heaters benefit from being non-invasive, by which means additional pressure losses are avoided and no additional volume is required. They are installed around the piping and surrounded with additional insulation. Each module has an installed power of 3.5 kW. Thus, six units are mounted having a total power input of 21 kW. The modularity is, above that, advantageous in regard to further installations, which might increase the thermal losses of the REPA Test Rig. Additional modules can be installed easily. An adverse effect of this solution is the increased heat loss compared to invasive elements which penetrate the tube wall and thus are surrounded by the fluid directly. Six band heaters are installed on the discharge side of the pump – upstream the Kinematics Unit. The technical drawing can be found in D.7.

5.1.4 Expansion Vessel

Expansion vessels are fundamental components in order to guarantee safe operation of closed HTF cycles. Owing to the characteristic of fluids of varying their density under the influence of temperature changes, the integration of a expansion vessel into the HTF cycle is mandatory in order to avoid unacceptable system pressures. This applies in particular to those oils which are intended to be used at the REPA Test Rig. For instance, the density of *Syltherm 800* varies between 930 ${}^{kg}/_{m^3}$ at ambient temperature (25 $°C$) and 547 ${}^{kg}/_{m^3}$ at maximum operation temperature (400 $°C$).

Above that, there are some general rules for designing expansion vessels for HTF circuits. At first, it should be sized in a way that the HTF consumes 25% of its volume at ambient

temperature and 75% at nominal operating temperature, respectively [24] [47]. Moreover, all organic HTFs undergo oxidation when exposed to air, which causes accelerated ageing of the product and hence a loss of heat transfer efficiency. At elevated temperatures ($> 200°C$) the oxidation of all three HTFs must be prevented in any case by means of an inert gas supply, e.g. nitrogen. Thus, a nitrogen assembly is connected to the expansion vessel. Thereby, a non-reactive atmosphere in the expansion vessel's head space is ensured. Additionally, the expansion vessel is equipped with an electronic level gauge, two thermocouples Type K (one in the liquid and one in the head space), a level switch and a pressure indicator [47]. For filling and venting purposes it is useful if the vessel is located higher than the pump and all other HTF cycle components, but not higher than the highest point of the pipe section of the Kinematics Unit. Thus, the expansion vessel serves as the main venting point of the HTF cycle for ageing components of the fluid.

According to *DIN 4754* expansion vessels *"shall be designed to accommodate at least 1.3 times the increase of the filling volume occurring at temperatures between the filling temperature and the permissible operating temperature above the minimum filling level"* [48]; in mathematical terms, this leads to

$$V_{vessel} \overset{!}{\geq} V_{HTF,vessel,min} + \Delta V_{HTF} \cdot 1.3 \tag{5.22}$$

Since *HELISOL® 5A* does not only have the highest operating temperature, but hence also the highest volumetric expansion when heated up, the calculations will be based on its data. The total volume of HTF in the cycle at ambient temperature (20 $°C$) is

$$V_{HTF,\vartheta_{amb}} = V_{piping} + V_{HTF,vessel,min} \tag{5.23}$$

The total volume of the pipe system is derived from the CAD drawing and is 225 l. Yet, since the minimum filling level $V_{HTF,vessel,min}$ is a fractional amount of the vessel volume and therefore hinges on knowing this volume, a circular reference problem has to be solved. To accomplish this, an iterative approach was chosen by estimating the vessel volume. The iterations will not be subject in this work. Based on a vessel volume of $V_{vessel} = 450\ l$ (last iteration), the minimum HTF volume in the vessel can be obtained as

$$V_{HTF,vessel,min} = \frac{V_{vessel}}{4} = 112.5\ l \tag{5.24}$$

It is said in advance that the HTF temperature inside the expansion vessel will be sig-

nificantly lower than of the HTF inside the piping. This is due to the fact that the band heaters only heat circulating HTF. Thus, the "hot" expanded volume, that enters the vessel, will mix with the "cold" minimum level volume inside the vessel. Therefore the HTF temperature inside the vessel will be conservatively presumed 350 $°C$[16]. Nevertheless, the expansion vessel must be designed to withstand temperatures up to 500 $°C$ and pressures up to 50 bars, although it is very unlikely to "see" such high temperatures during operation. When being heated up, the volumetric increase of HTF in the system is

$$\begin{aligned} \Delta V_{HTF} &= V_{piping} \cdot \left(\frac{\rho_{HTF,\vartheta_{amb}}}{\rho_{HTF,\vartheta_{max}}} - 1 \right) \cdot \frac{\rho_{HTF,\vartheta_{max}}}{\rho_{HTF,\vartheta_{vessel}}} \\ &\quad + V_{HTF,vessel,min} \cdot \frac{\rho_{HTF,\vartheta_{amb}}}{\rho_{HTF,\vartheta_{vessel}}} \\ &= 215\ l \end{aligned} \tag{5.25}$$

Now, the maximum amount of HTF that will penetrate the expansion vessel can be obtained as

$$V_{HTF,vessel,max} = V_{HTF,vessel,min} + \Delta V_{HTF} = 327.5\ l \tag{5.26}$$

The resulting minimum required vessel volume – taking into account the above mentioned safety factor of 1.3 – is

$$V_{vessel,min} = V_{HTF,vessel,max} \cdot 1.3 = 427\ l \tag{5.27}$$

which is lower than the volume of 450 l. Consequently, the estimated volume is sufficient and the expansion vessel is designed to contain up to 450 l. A photo of the vessel, manufactured by *IMETAL*, can be found in appendix E.3.

5.1.5 Hydraulics Measurement

To monitor and control the operation of the HTF cycle, the installation of a variety of sensors is crucial. Those can be derived from the specification sheet (cf. chapter 4.3) and its implementation into the Piping and Instrumentation Diagram, see figure 5.2.

The HTF unit contains three pressure transducers, four thermocouples, a differential pressure sensor, which is connected to an orifice plate assembly to measure the volume flow, and two[17] level switches mounted on the expansion vessel – one each for the top and bottom level. The functionalities of those sensors will be outlined in the following.

[16] This temperature will lower during steady-state operation, as the vessel is not heated.
[17] During commissioning only one level switch at the bottom is installed.

- **Pressure Sensors**
  In total, there are four pressure sensors required in the HTF cycle: one upstream and one downstream the pump (monitoring the pressure drop of the pump), one after the Kinematics Unit (for security matters, see chapter 5.1.1)and one measuring the pressure inside the expansion vessel (in order to monitor the system pressure). Due to their simple construction accompanied by high accuracy, *S-20* pressure transmitters are supplied by *WIKA* using diaphragm seals. The measuring range was set to 0-60 bars. Since those sensors can only withstand temperatures up to 200 $°C$, a cooling tower as well as a capillary hose is included.

- **Temperature Sensors**
  So as to protect the HTF cycle from excessive temperatures, the implementation of temperature sensors is crucial. There is one thermocouple in the pump's suction side (close to the pump inlet), one resistance thermometer inside the pump, one thermocouple after the heating elements and two thermocouples inside the expansion vessel (liquid and head phase for redundancy). Since the geometric design of the expansion vessel includes two thermowells, the thermocouples must be designed accordingly. *TC10-B* thermocouples, supplied by *WIKA*, with a measuring range of $0 - 500$ $°C$ were chosen.

- **Flow Measurement**
  A volume flow measurement is crucial to control this boundary condition in between the pump's range ($6 - 60$ $^{m^3}/_h$). To ensure a measurement at low pressure drop, a combination of an orifice plate, which is mounted in between two flanges, and a differential pressure transmitter was chosen. The assembly is made by *WIKA* and installed upstream the Kinematics Unit. A technical drawing can be found in D.6.

- **Expansion Vessel Fluid Level**
  The avoidance of draining the expansion vessel during operation is mandatory with respect to the occurrence of gas in the circuit – induced by possible leakage. Since the latter must be avoided in any case, a level switch is mounted at its low level height. A *VEGASWING 66* supplied by *VEGA* was chosen, ensuring operation under said process temperatures and pressures which also apply to the expansion vessel. A inductive drive energizes a tuning fork to vibrate at its resonance frequency. When the expansion vessel falls below its minimum level, the cease of the medium covering the fork leads to a change of frequency which is converted into a switching command.

5.2 Kinematics Unit

The Kinematics Unit is a custom-made machine which serves to realize sophisticated movements in terms of force, speed and motion cycles in order to simulate an accelerated endurance test of two serially connected REPAs. It is connected to the piping of the adjacent *HTF cycle* and thus is wetted with HTF at adjustable temperature, mass flow and pressure conditions. These circumstances place special demands on its design, which is why it was designed to meet the requirements specified in chapter 4.2 by *IW Maschinenbau GmbH* (IW). Yet, there was a close collaboration between DLR and IW in order to assure the realization of all technical demands. The specifications mentioned in chapter 4.2.2 have been implemented. All technical functionalities of the Kinematics Unit design are described below.

5.2.1 Configuration

Figure 5.8 depicts the technical drawing of the Kinematics Unit. A base frame forms the foundation of the machine, on which a drive pylon and two frames are mounted. The drive pylon is adapted to a *EuroTrough* application. It serves to generate the rotational movement. Therefore, it includes two drive pistons. Moreover, there are two drive pistons attached on top of the drive pylon to realize the translational motion. Each piston is supplied by a central hydraulics unit, which is installed at the bottom of the drive pylon.

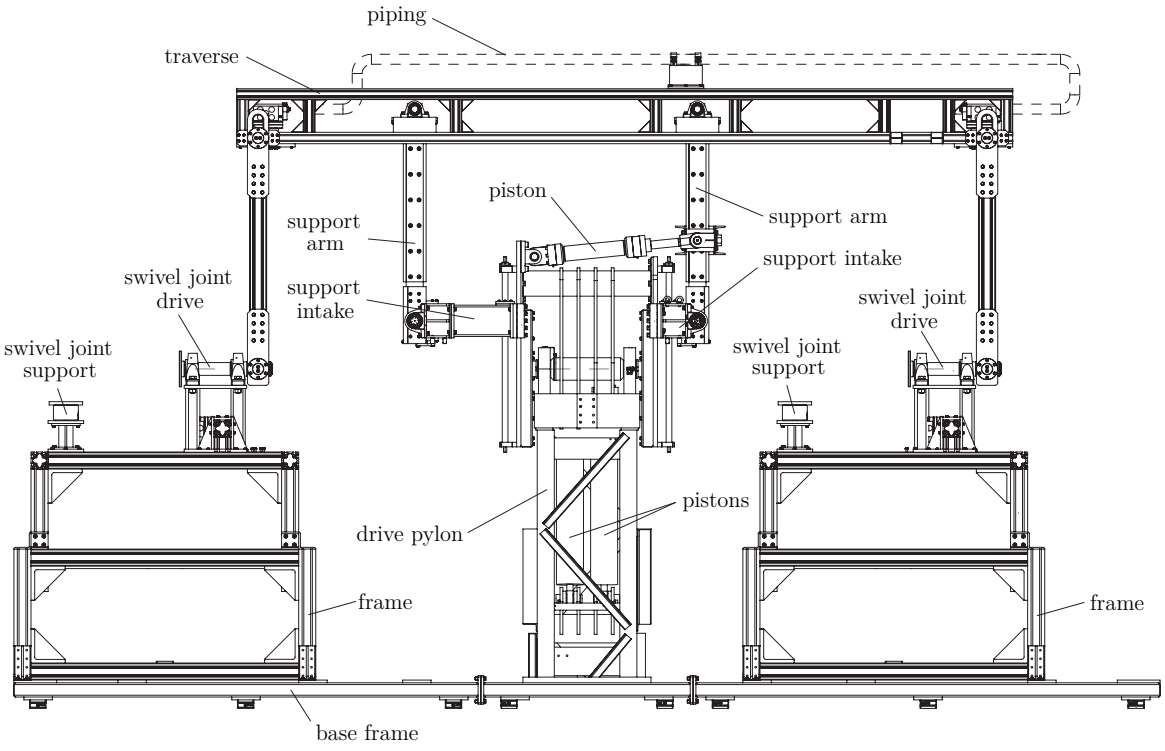

Figure 5.8: Technical drawing of the Kinematics Unit (configuration for testing RFHA)

The two support arms are the connection link between the drive pylon's transmission plates and the top part, the so called traverse. Beyond their bearing role, they transmit the forces from the drive unit to the traverse. The latter comprises an assembly of aluminium beams. It conduces to maintain the top connection to the REPAs; consequently, it conducts the motion to the test specimens. In doing so, it also carries the piping connection between the serially connected REPAs. A detailed description of the traverse including the design of both force measuring points – where the HCE-end of the REPA is mounted – is given in chapter 5.3.

The two frames support the bottom connection point of the test objects. Since testing of REPAs for different collector types will be enabled, which requires the adjustability of distinct focal lengths (see table 2.1), the frames are vertically adjustable. Additionally, the connection point can be shifted horizontally to enable the installation of different REPA configurations representing all kind of collector configurations and geometries: Figure 5.9 shows a possible interface for Rotary Flex Hose Assemblies (left) and Ball Joint Assemblies (right). The configuration for RFHAs is equipped with an anchor point at the outside of the frame and an additional support for the swivel joint, in between which a dynamometer is installed. Due to their distinct kinematics properties, the bottom connection for BJAs is mounted on top of the frames. The swivel joint drive – including its support arm to the traverse – can be omitted for testing BJAs, since forces are applied by the HCE, which is here represented by the top connection point at the traverse.

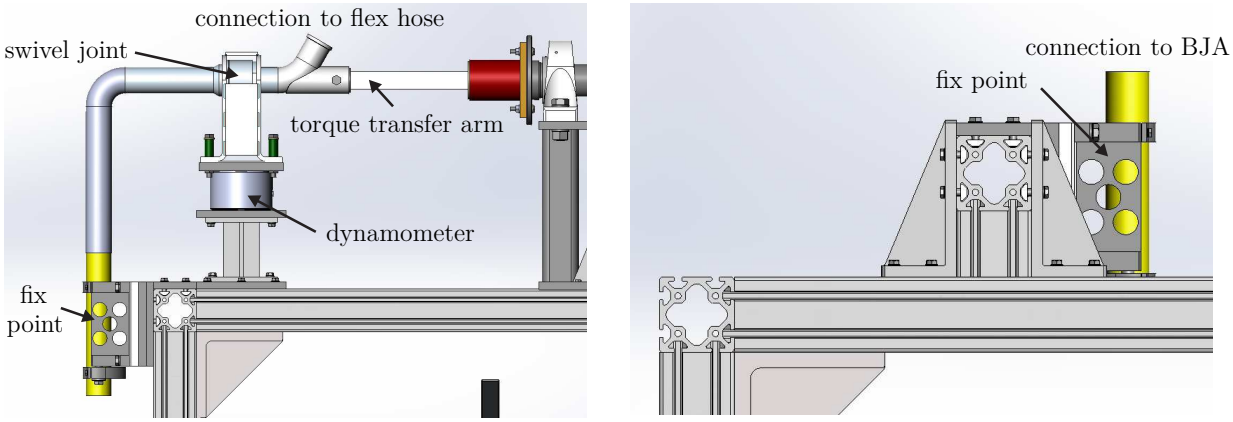

Figure 5.9: Frame; Interface for Rotary Flex Hose Assemblies (left) and Ball Joint Assemblies (right)

The fact that the Kinematics Unit is designed having two REPAs serially connected, not parallel, is not a coincidence but rather designed deliberately. This alignment is aimed at both test objects to perform an identical motion. The duplication / redundancy of identical measurements increases the significance. Despite its increased complexity in design – especially regarding the pipe routing on the traverse, see chapter 5.3 – the comparison of two test object under identical conditions increases the reliability of the

testing method.

In order to illustrate the kinematics of the machine, figure 5.10 shows a Computer-Aided Design (CAD) model with superimposed translation and rotation axes. The Kinematics Unit is capable of performing +45° in its translation axis. In its perpendicular rotation axis, an angle from -120° (stow position) to +90° (horizontal position) is feasible.

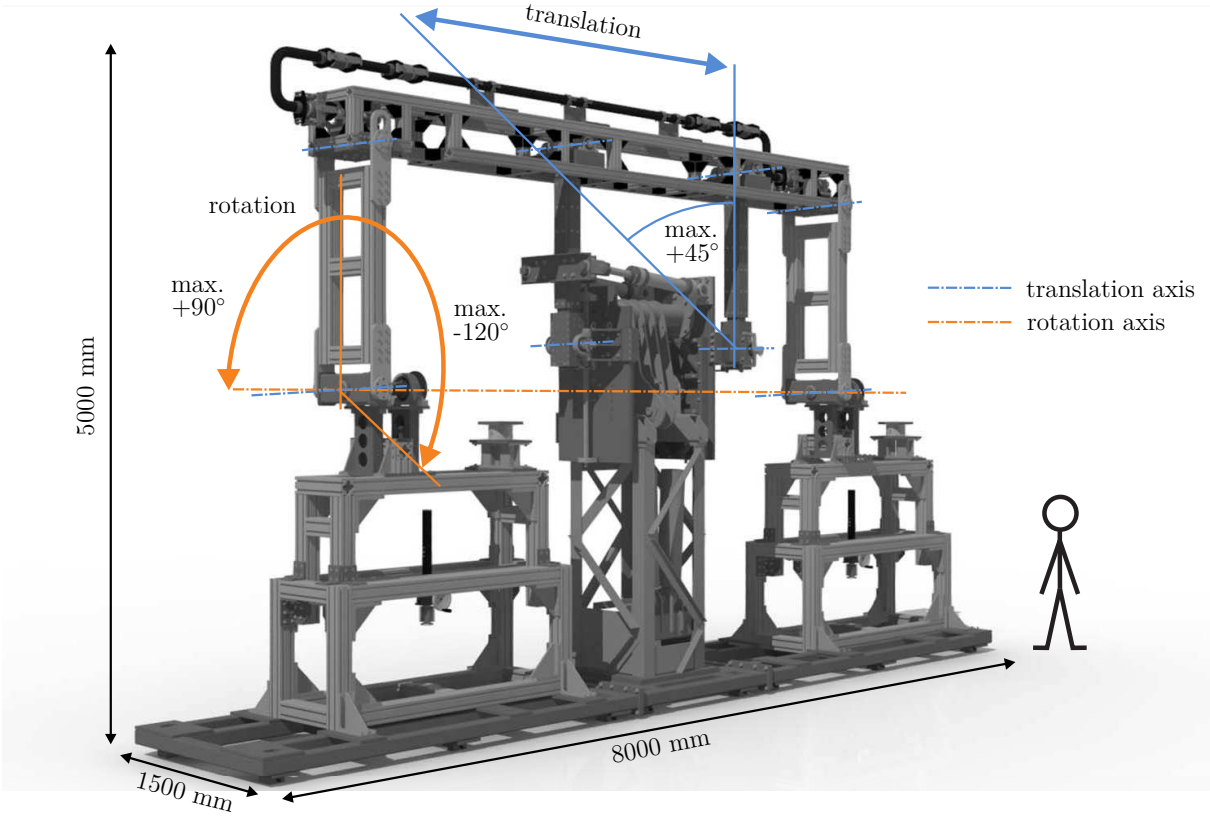

Figure 5.10: CAD model of the Kinematics Unit (no REPAs installed; configuration for testing RFHA)

5.2.2 Measurement of Kinematics

As mentioned above, the rotation range can be adjusted between -120° and +90° and must not be exceeded in both directions. This is ensured by two switch flags – one for each limit – which are installed on the shaft of the drive pylon, see figure 5.11 (right). Once the rotation approaches its peak, an inductive sensor detects the switch flag and sends a signal to the control unit to stop the rotation. In addition, the shaft is covered with a magnetic tape to monitor the position using a position sensor, see figure 5.11 (left).

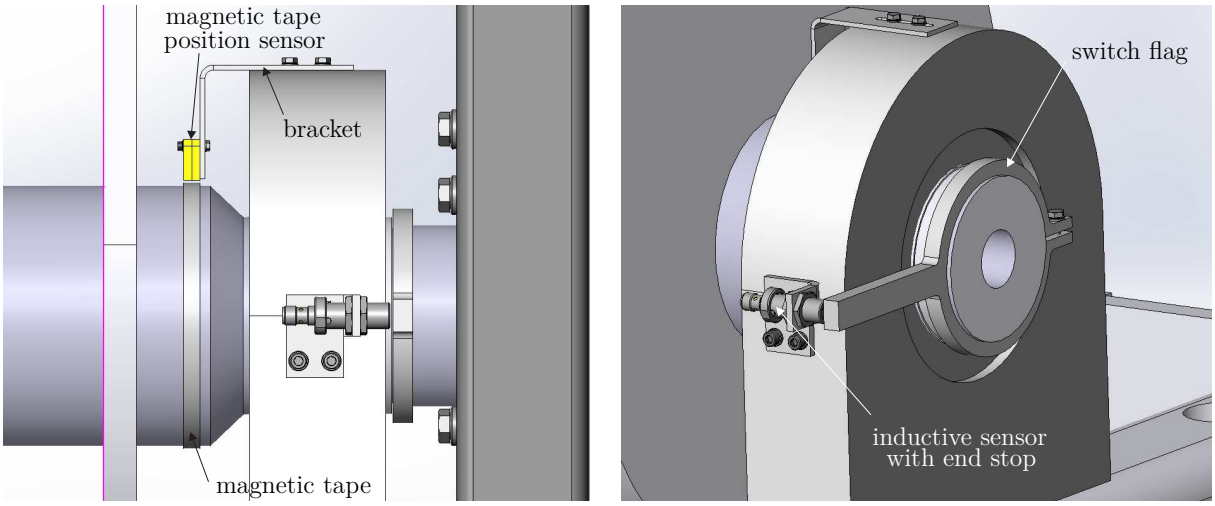

Figure 5.11: Measurement of rotational position

For measuring the translational displacement of the test rig, a rotary position transducer is coupled to the pedestal bearing at the left support intake, see figure 5.12. Furthermore, the shaft of the right support intake is equipped with a switch flag on each side. Just like described above, inductive sensors detect the flag's appearance to prevent the translational motion to exceed its mechanical limits (0° - 45°).

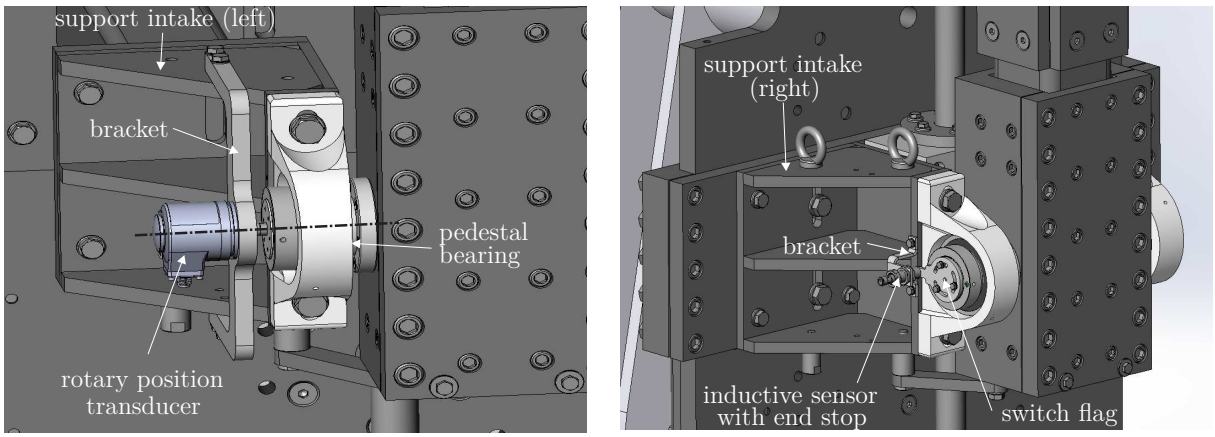

Figure 5.12: Measurement of translational position

The most important measurement task of the REPA Test Rig is the measurement of forces induced by the test object. Therefore, the REPAs will be equipped with dynamometers in both the bottom and the top connection to the Kinematics Unit. Owed to the complexity of enabling realistic measurements whilst eliminating disturbance variables, an individual section is dedicated to the implementation of the dynamometers, see chapter 5.3.

5.3 REPA Load Measurement

As mentioned in chapter 4.3, there are two dynamometers for each REPA, one on the traverse ("top" of the REPA) and one at the bottom connection ("top" of the frame) to the adjacent piping of the HTF cycle. The loads carried by the REPAs are at the heart of understanding possible wearing and failure mechanisms. A transgression of the manufacturer's design specifications may cause critical malfunction and can be identified via the sensor (dynamometer) reaching beforehand. To enable a precise and representative measurement of the dynamometers, a carefully considered implementation of these instruments into the Kinematics Unit is crucial. The present thesis will only describe the setting on top of the Kinematics Unit.

The major challenge in design is the "force-free cutting" of each dynamometer towards the pipe connection side in order to avoid external influences. Those influences are forces introduced by the adjacent piping at both the top and the bottom connection of the REPA. However, a rigid connection between these elements is unavoidable, since the HTF must stream in a closed circuit. As the dynamometers are connected to said rigid pipe sections close to the objects of interest – the REPAs – it must be ensured that the majority of forces and torques transmitted to the dynamometers are actually "emitted" by the REPA. This fact requires the incorporation of flexible elements in order to lower the above mentioned forces. Thus, in an idealized situation the dynamometers are only going to be stressed by REPA-induced forces, whilst "external" forces are negligible. Yet, it should be mentioned that this ideal setting can only be obtained to some extent due to imprecision of simulation and limitations regarding the technical setup. Owing to the Kinematics Unit's design specification having two REPAs not symmetrically, but serially connected, the compensation of said forces turns out to be rather complicated. As a consequence of this, particular attention is paid to the the following chapter.

In order to facilitate the calculations, the CAE[18] system *ROHR2* from *SIGMA Ingenieurgesellschaft mbH* is used. It enables pipe stress analysis and is a standard tool for pipe static and structural framework analysis. The stress calculation will be carried out according to ASME B31.1, since the pipe system is designed with respect to this standard [49]. The rigidity of pipe bearings is, according to *VDI 3842* (2004), dependent on the nominal pipe diameter [50]. The database is implemented in *ROHR2* and distinguished in a nominal scale: *soft*, *medium* and *hard*. For the subsequent calculations a *medium* rigidity will be used which conforms to a translatory stiffness of 1 kN/mm and torsion stiffness of 630 kNm/°.

[18] Computer-Aided Engineering

5.3.1 Initial Setup and Task

Prior to choosing an appropriate and suitable technology for the compensation, it is indispensable to clarify the system's geometry and to calculate the resulting thermal displacements that have to be carried. Figure 5.13 (top) depicts an isometric view of the pipe system (dashed) that is mounted to the traverse (cf. figure 5.8). Additionally, a side view including the pipe dimensions is shown. There are location bearings both at the inlet (right) and the outlet (left) as well as in the center. The latter can be considered to split up the thermal dilatation on both sides. Consequently, it is distributed halfway on each side at the center bearing and two subsystems are considered. Each of these subsystems contains a vertical offset which is geometrically realized by an S-bend and a U-bend on the left and on the right, respectively.

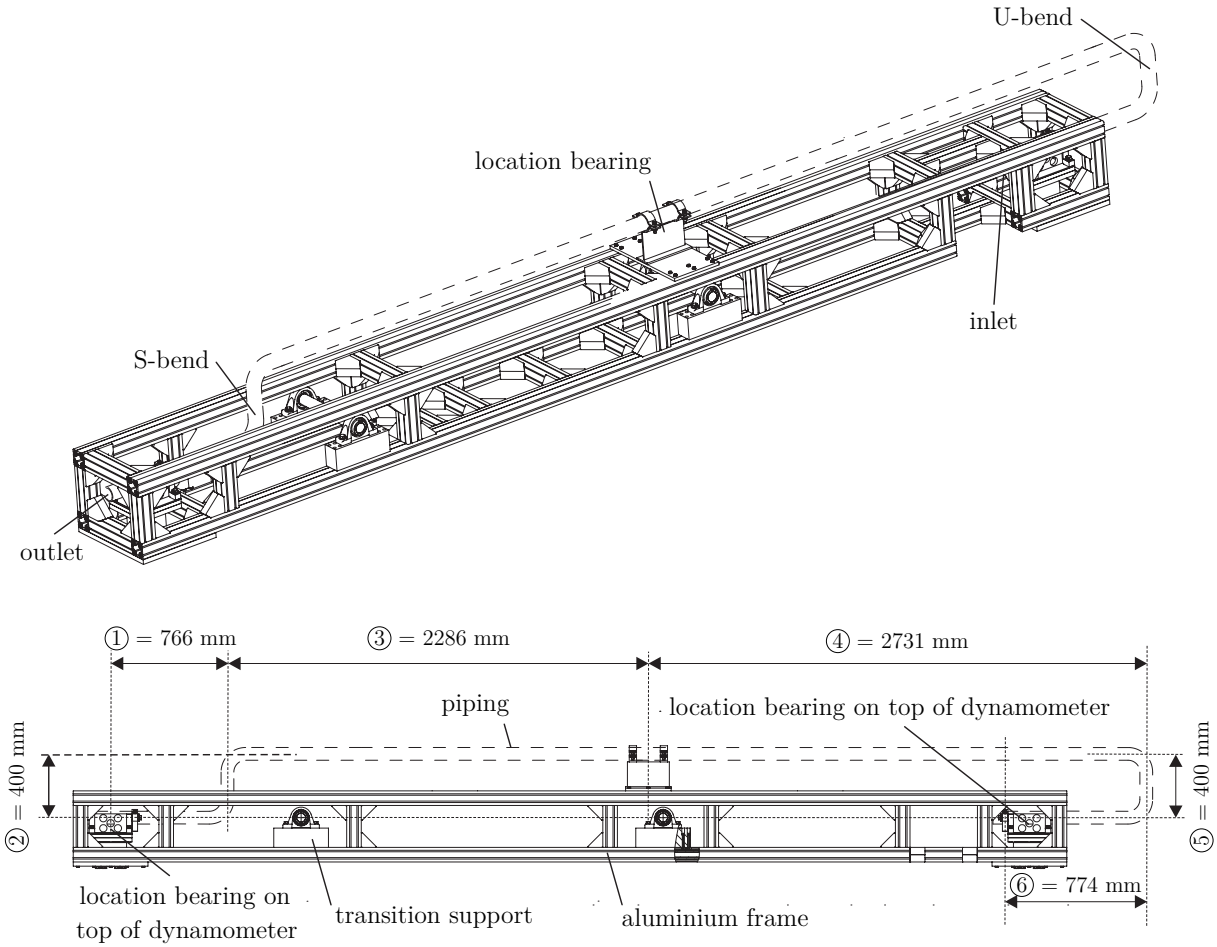

Figure 5.13: Technical drawing of the traverse; isometric view (top) and side view (bottom)

The thermal expansion of steel pipes can be calculated according to

$$\Delta L = \alpha \cdot L_{cold} \cdot \Delta\vartheta \tag{5.28}$$

Given the piping dimensions derived from figure 5.13, a maximum temperature difference of $\Delta\vartheta = (450 - 20)K = 430K$ and a thermal expansion coefficient α of $13.7 \cdot 10^{-6}\ {}^{1}/_{K}$ [19], the maximum thermal dilatation for each pipe section is presented in table 5.4:

Table 5.4: Thermal expansion between 20 $°C$ and 450 $°C$ for different pipe sections (numbered) on the traverse

No.	L_{cold} [mm]	ΔL [mm]	L_{hot} [mm]
①	766	4.51	770.51
②	400	2.36	402.36
③	2286	13.50	2299.50
④	2731	16.09	2747.09
⑤	400	2.36	402.36
⑥	774	4.56	778.56

The *K6D175* dynamometers, manufactured by *ME Meßsysteme GmbH*, are capable of measuring forces as well as torques in all spatial directions. The two dynamometers serve as supports of location bearings, hence they measure the restraint force of the bearings. The sensors are bolted to connection plates, see figure 5.14. The bottom connection plate serves as a joint attaching the dynamometer to the traverse. The two top plates depict the connection to the anchors: Each assembly consists a location bearing at the left (REPA junction) and a floating bearing at the right (piping on top of the traverse). The axial clearance of the floating bearing is ensured by the axial clearance of the bush.

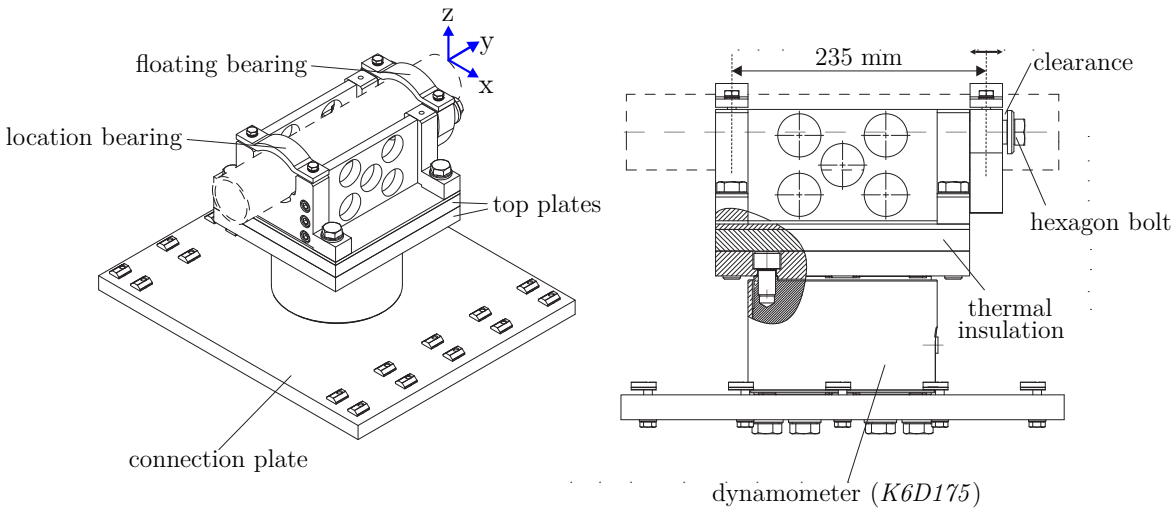

Figure 5.14: Isometric view (left) and side view (right) of the dynamometer and the pipe bearing assembly

[19] Valid between 20 $°C$ and 450 $°C$ for 13CrMo4-5 (interpolated) [51]

For commissioning the test rig only one dynamometer is installed (outlet). Its nominal loads as well as the measuring uncertainties of the dynamometers (according to the calibration report) are depicted in table 5.5:

Table 5.5: Nominal load and measuring uncertainty of the *K6D175* dynamometers (coordinate system see figure 5.14)

	F_x	F_y	F_z	M_x	M_y	M_z
nominal load	10 kN	10 kN	20 kN	1 kNm	1 kNm	2 kNm
uncertainty	±30 N	±70 N	±80N	±8 Nm	±6 Nm	±16 Nm

If these dynamometer and pipe bearing assemblies constrain the system from free expansion (hypothetically), the restraint forces will exceed: Figure 5.15 depicts an isometric view of the traverse and its bending line superimposed (not to scale) when the piping is exposed to HTF at 450 $°C$ and 40 bars – the maximum operation conditions. In addition, the stress analysis is depicted (bottom illustration). The red bending line illustrates the consequences of thermal expansion, as it can be seen that the pipe section is displaced significantly. The S-bend (left) shows both a vertical and horizontal offset, whereas the U-bend (right) is shifted to the right. One of the most important issues that emerges from these effects is the accompanied load that has to be carried by the bearings. The resulting axial forces are 12.7 kN and 8.5 kN on the left and on the right, respectively. Taking into account the limited rigidity of the restraints (approximated 1 kN/mm), their flexibility will cause a displacement. Without any type of compensation, these loads would not only distort the measurements of REPA forces, but might also lead to critical damage of the bearings.

In addition, the stress analysis reveals exceedance of the material treshold at various locations of the pipe section (marked red). These stresses are mainly bending torques about the x-axis. They are induced by thermal expansion which is blocked by the location bearings. This manifests more distinctly around the S-bend compared to the U-bend, since the latter constitutes a natural compensation (cf. chapter 5.3.2); however, just to a certain degree, since the horizontal pipe sections in between the location bearings are not symmetrical.

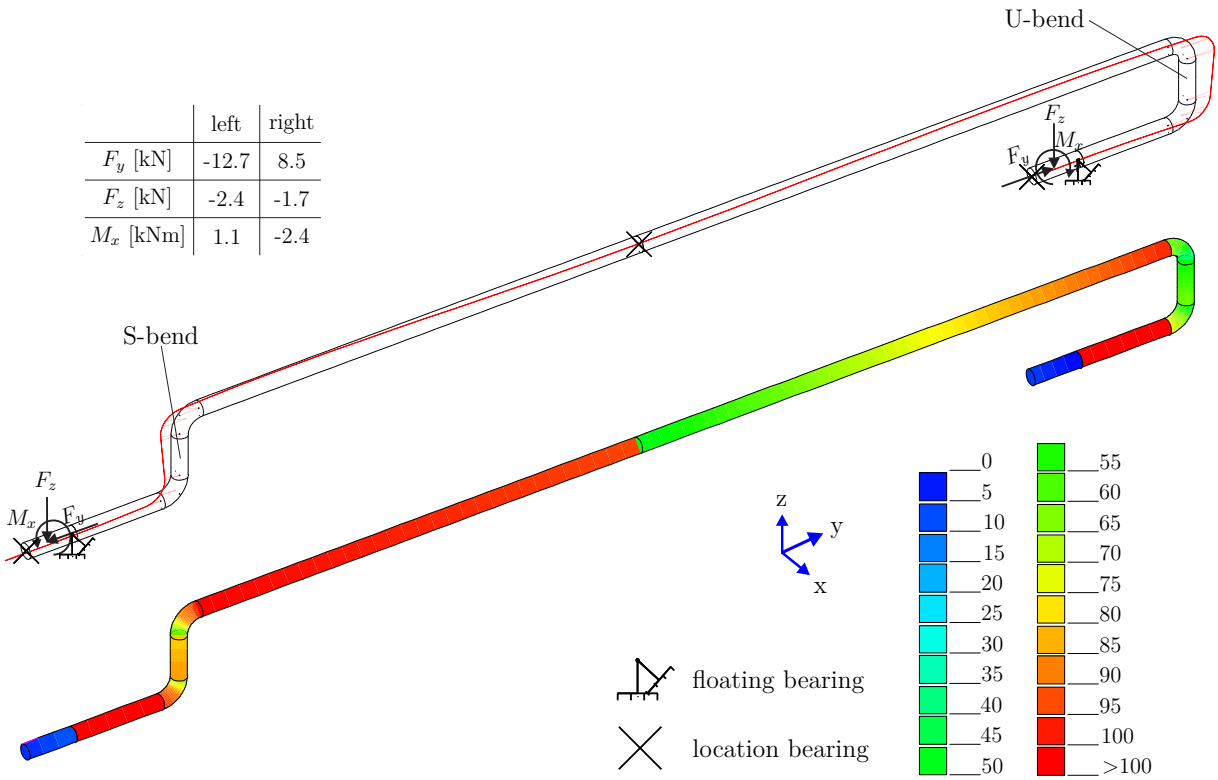

Figure 5.15: Isometric view of the traverse with superimposed thermal expansion at 450 $°C$ (red curve; top) and stress analysis (bottom) for the hypothetical case of no compensation

5.3.2 Solution Approaches

As a consequence of the above restrictions, the implementation of compensation is crucial. In general, a distinction is made between **natural compensation** by elastic bending of pipe legs and installation of **flexible metal elements**, such as corrugated tubes or expansion joints. In this particular design problem, the use of neither natural compensation nor corrugated tubes is feasible. This is due to the space and material that these kind of solutions would require; e.g. a compensation by a U-bend ("Lyra-Bogen") would significantly increase the height of the Kinematics Unit. Hence, the design is focussed on finding a solution using expansion joints.

Expansion joints consist of metal bellows, which are, due to the toroidal corrugations, flexible on all planes. This ability allows them to compensate movements in pipe systems, e.g. caused by thermal expansion [52]. There are two major types of expansion joints: axial expansion joints and hinged expansion joints. Hinged expansion joints can be distinguished between angular and lateral expansion joints. In addition, a distinction is made between single hinged (flexibility in one axis) and gimbal hinged (flexiblity in a plane) expansion joints. Figure 5.16 depicts the three types of expansion joints and their modes of action. Having a closer look at the illustration, it is apparent that each expansion

joint can, starting at the neutral position, perform movements of the same magnitude in both directions. This can be taken advantage of by pre-tensioning the components. Accordingly, it will be explained later (cf. chapter 5.3.3).

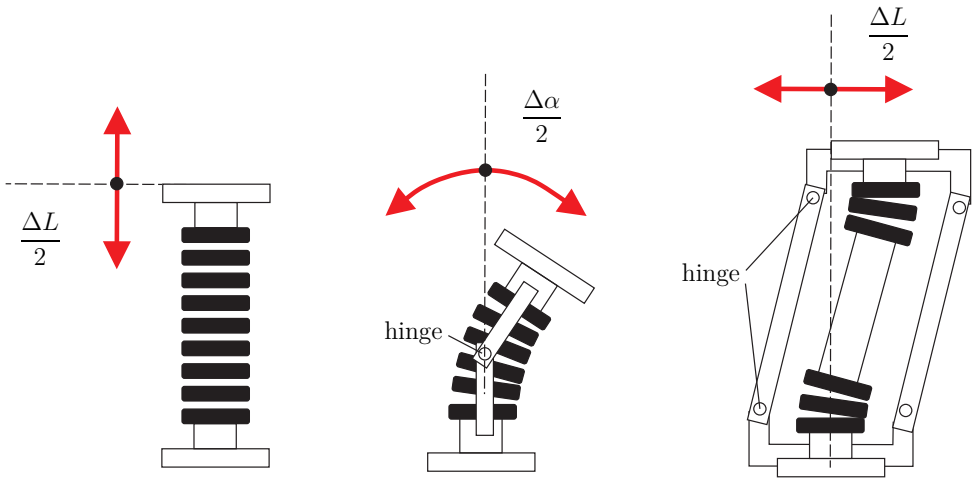

Figure 5.16: Schematic illustration of basic movements of an axial (left), angular (middle) and lateral expansion joint (right) (cf. [43])

The following subsections will set out different approaches for the compensation with regard to technical and spatial feasibility, degree of compensation and the general purpose of "force-free-cutting" of the dynamometers.

A: Axial Expansion Joints

A first attempt to compensate for the thermal dilatation is an assembly of axial expansion joints. Those components absorb axial movements caused by thermal dilatations in pipe systems. Additionally, small lateral and angular offsets are possible. They require only little space and are relatively cheap per unit. Suitable axial expansion joints for this particular problem were designed and offered by *Witzenmann GmbH*. A drawing as well as technical data, which are used in the following section, can be found in D.8. However, axial expansion joints are solely able to compensate for thermal expansion in straight pipe sections; this is why anchor points (location bearings) must be positioned at the corners of offset systems (e.g. bends). Figure 5.17 shows the arrangement using this kind of solution. The isometric view depicts the pipe section with a superimposed bending line which represents the pipe's displacement when exposed to maximum operation conditions ($450°C$ and 40 bars).

Yet, the forces introduced into the anchor points are remarkable: One the one hand, tensioning the compensator results in an axial adjusting force F_δ which is proportional to the spring rate c_δ and the compensator dilatation δ. Assuming this movement to be approx. 13 mm (cf. table 5.4), the force is

$$F_\delta = c_\delta \cdot \delta = 715 \ {}^{N}/_{mm} \cdot 13 \ mm = 9.3 \ kN \tag{5.29}$$

On the other hand, exposing the expansion joint's metal bellows to high-pressurized fluids induces an axial reaction force F_p which is proportional to the fluid pressure p and the effective cross section of the bellow A:

$$F_p = p \cdot A = 40 \cdot 10^5 \ \frac{N}{m^2} \cdot 0.00739 \ m^2 = 29.6 \ kN \tag{5.30}$$

The last mentioned effect distorts the force measurement particularly, since this force must be carried by the anchor point. The effective cross section A of 0.00739 m^2 results in a reaction force $F_{p=40bar}$ of 29.6 kN, which is distributed halfway of each side and thus stresses both anchor points with approx. 14.8 kN (provided that their rigidity is infinite). This corresponds to a weight force of approx. 1500 kg. However, the location bearings permit axial forces of only ± 5.1 kN, see appendix D.9. Thus, the axial forces are too high.

The simulation carried out by *ROHR2* reveals axial forces of -13.4 and 17.4 kN on the left and on the right location bearing (top), respectively. Additionally, there is a lack of compensation in between these location bearings and the dynamometers which results in

anchor forces on the dynamometer of -15.2 kN (left) and 10.6 kN (right). Apart from being too high, which causes critical damage, the dimension of these values is a tenfold of the anticipated REPA-induced forces. Those are rather to be expected around ± 1.5 kN [36]. Consequently, the "force-free" cutting of the dynamometers has failed.

In addition to the anchor loads, a stress analysis of the piping is carried out using *ROHR2*. Figure 5.17 illustrates the percentage utilization of the maximum pipe stress due to displacement load ranges. On the one hand, the figure reveals low stresses in between the S- and U-bend on the top part of the traverse: the utilization of maximum tolerable stresses is approx. 25%. This is stemming from the additional anchor points carrying the bending torques. On the other hand, the effect of thermal expansion in the S- and U-bend is remarkable: the resultant bending torques close to the bends show a distinct exceedance of up to 191% of the maximum allowable stress. This corresponds to 352 N/mm^2. Since it is, as mentioned above, crucial to install those fix points next to the offsets when using axial expansion joints, the approach of using those components only to compensate the thermal dilatation is discarded.

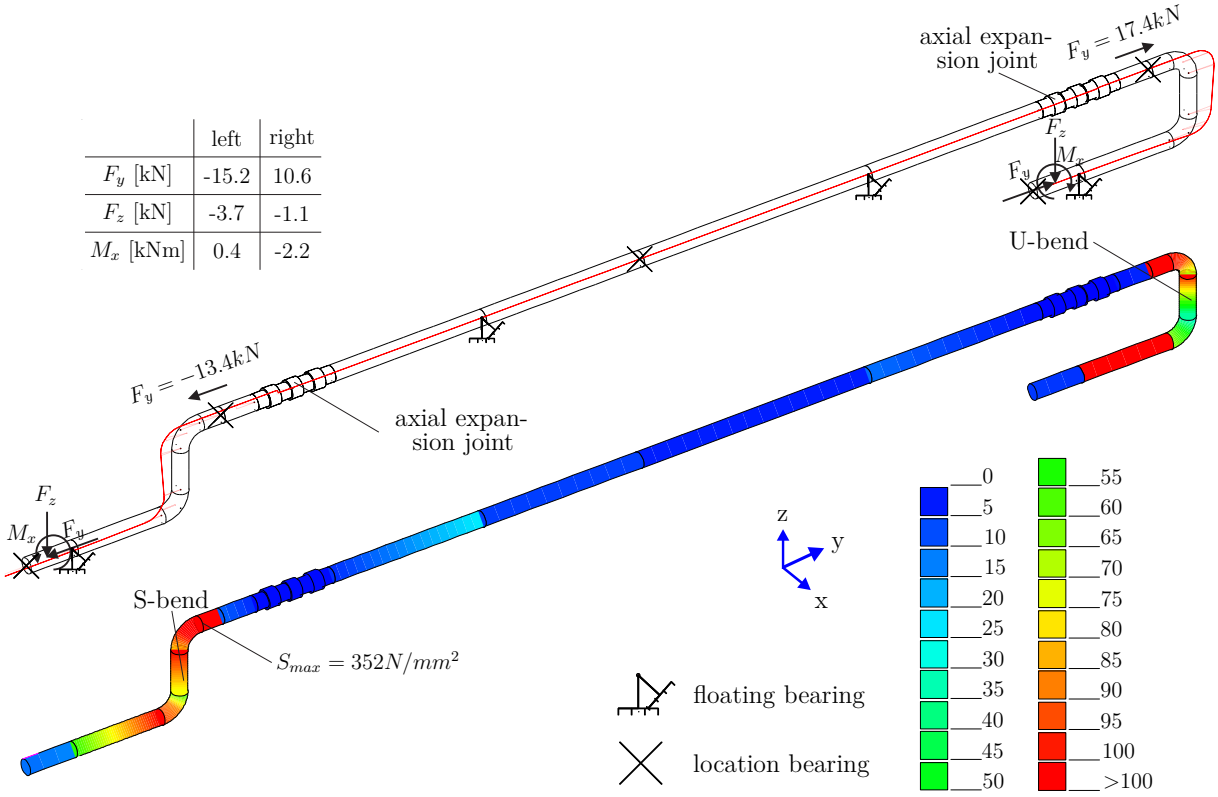

	left	right
F_y [kN]	-15.2	10.6
F_z [kN]	-3.7	-1.1
M_x [kNm]	0.4	-2.2

Figure 5.17: Isometric view of the pipe section on the traverse using axial expansion joints; bending line (top) and stress utilization [%] (bottom) at nominal operating conditions (450 °C and 40 bars)

B: Axial and Lateral Expansion Joints

The approach depicted above revealed several weak spots. Aside from the transgressed axial anchor loads – which might be fixed using more rigid bearings –, the dynamometers are strained by intolerable forces accompanied with excessive pipe stresses. This applies in particular to the pipe bends. A different attempt expands the axial expansion joints by one additional lateral expansion joint on each side. Lateral expansion joints are a combination of two hinged expansion joints. They benefit from the advantage not to place additional forces on the anchor points which are caused by axial reaction forces. This load is carried by the hinge parts instead. As a result of this, the anchor point forces are reduced drastically.

Figure 5.18 shows an isometric view of the pipe section as above. Using approach B, the lateral expansion joints are mounted in the vertical part of the S- and U-bend. They compensate thermal movements between the dynamometer anchor points and the anchor points on top (close to the bends). Owing to their minimum installation space, the vertical offset increases from 400 mm to 637 mm[20].

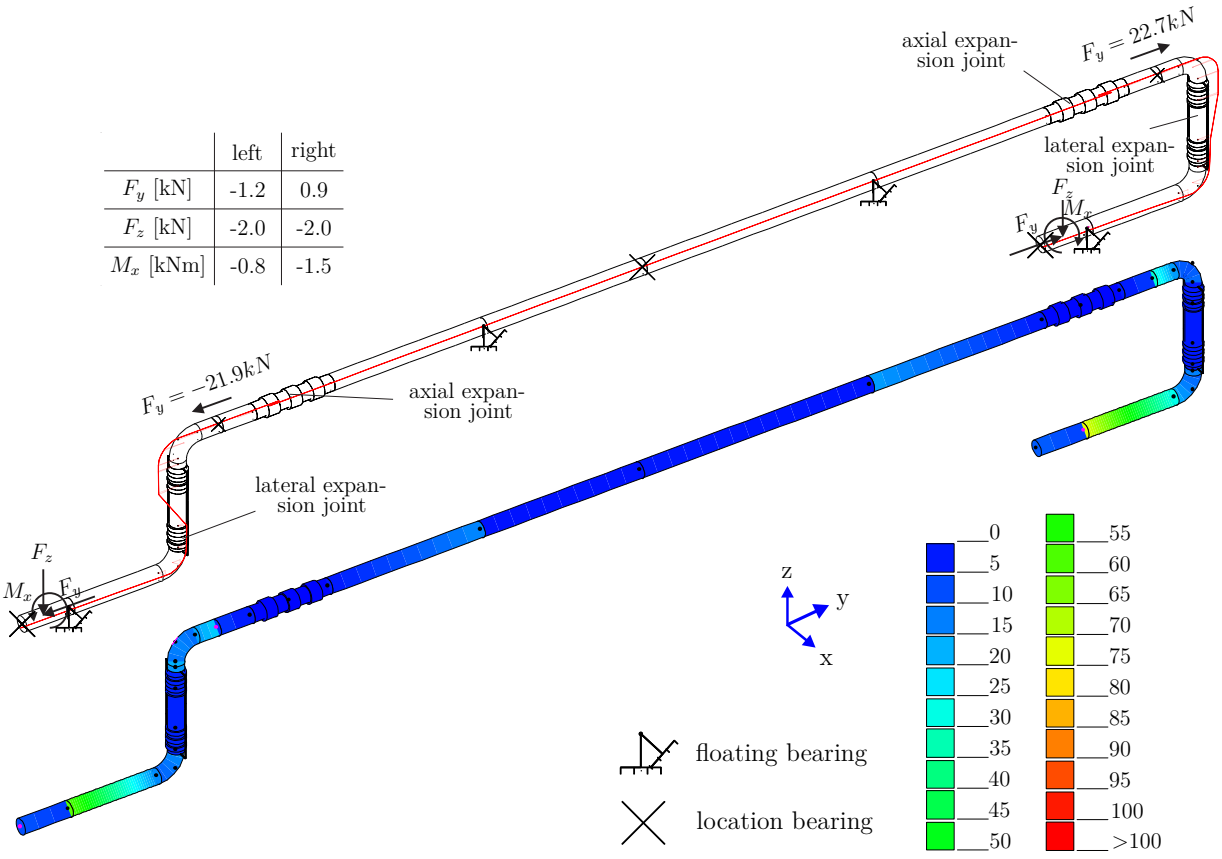

	left	right
F_y [kN]	-1.2	0.9
F_z [kN]	-2.0	-2.0
M_x [kNm]	-0.8	-1.5

Figure 5.18: Isometric view of the pipe section on the traverse using axial and lateral expansion joints; bending line and stress utilization [%] at nominal operating conditions (450 °C and 40 bars)

[20] considering a minimum installation length of 416 mm (*Witzenmann*)

The bending line reveals an effective compensation of thermal expansion around both the S- and U-bend. This is confirmed by the forces introduced into the dynamometer location bearings; they are only strained less than one-tenth compared to approach A. The axial forces are diminished to -1.2 kN (left) and 0.9 kN (right). However, the thermal expansions in the vertical sections of the S- und the U-bend are still constrained by the anchor points. This force effect even increases due to the elevated height of the system. This is why notable forces in the z-axis induce torques M_x about the x-axis (see figure 5.18, stress analysis). Those are -0.8 kNm (left) and -1.5 kNm (right) and carried by the bearings of the dynamometer anchor points. Combined with anchor forces (top) that are more than four times greater than the maximum ($\pm$ 5.1 kN are allowed), the attempt of utilizing both axial and lateral expansion joints is dismissed.

C: Lateral Expansion Joints

Accordingly, a different solution will be investigated. The major obstacles in regard to approaches A and B are the additional anchor points close to the S- and U-bend, respectively. Therefore, approach C substitutes the axial expansion joints (and their anchor points) with "large" lateral expansion joints. In contrast to approach B, they are capable of compensating the entire thermal expansion on each side. In doing so, the vertical offset increases to 800 mm.

Figure 5.19 depicts the isometric view of the pipe section using only lateral expansion joints for the compensation. The bending line shows a distinct displacement around both the S- and U-bend. The horizontal displacement is carried by the expansion joints. Consequently, the axial forces "straining" the dynamometer anchor points are reduced (-0.9 kNm and 0.6 kNm). However, there is also a vertical displacement due to thermal expansion which cannot be compensated; it is carried by the pipe system instead. Bending stresses are the result. Hence, additional torques are carried into the dynamometer anchor points distorting the measurement. Furthermore, since those types of lateral expansion joints are welded in the vertical pipe part of the traverse, the height of the piping needs to be increased leading to higher torques M_x about the x-axis in the system.

Despite its advanced reliability concerning the compensation of thermal influences, approach C still has another disadvantage in its use: Based on a limited stiffness of the dynamometer, the location bearing will bend when facing an amount of forces and torques induces by the REPA. Given the current configuration, this bending is decreased by the pipe system, since the lateral expansion joints are only capable of compensating in a horizontal plane. A vertical REPA force F_z (e.g. weight force), for instance, leads to a reaction force in the pipe distorting the measurement likewise. The target to cut the dynamometers "force-free" is failed.

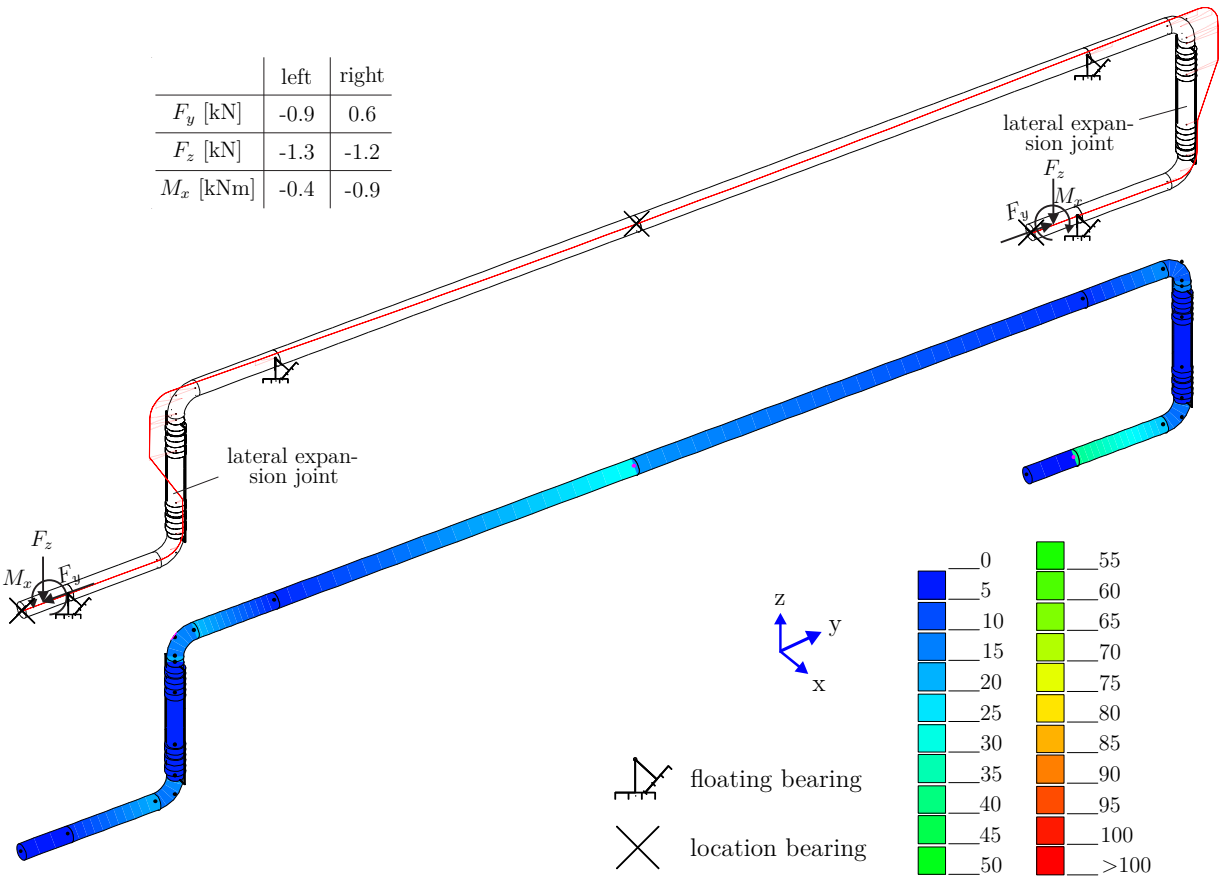

Figure 5.19: Isometric view of the pipe section on the traverse using lateral expansion joints; bending line and stress utilization [%] at nominal operating conditions (450 $°C$ and 40 bars)

D: Angular Expansion Joints

The most mature approach is the use of angular expansion joints which in their entity both compensate for the thermal expansion and enable "force-free" cutting of the dynamometer anchor points. In contrast to axial expansion joints (approach A), which are used to compensate thermal expansion independently, angular expansion joints are only suited in a combination of two or (maximum) three forming a statically determinate system. Just like lateral expansion joints, angular expansion joints do not strain anchor points by means of axial reaction forces. Instead, they transmit those forces through their hinges (cf. figure 5.16).

Figure 5.20 shows the implementation of three angular expansion joints on each side with superimposed bending line (top) and stress analysis (bottom). The bending line reveals a distinct vertical offset around the S-bend. This effect illustrates the kinematics of the angular expansion joint system carrying the axial expansion by a vertical displacement. In doing so, the centrally arranged expansion joint will always perform the sum of both other's angular displacement. Due to the system's flexibility both in the y- and z-axis, there are only low vertical forces and consequently only low bending torques about the x-

axis. This can be manifested in the stress analysis, since the utilization does not transcend 7.1 % of the maximum value (184.4 N/mm^2).

The expansion joints in the top part of the pipe section are single hinged (see appendix figure D.10), whilst both bottom expansion joints close to the dynamometers are gimbal hinged (see appendix figure D.11). The latter offers an additional degree of freedom perpendicular to the longitudinal axis of the piping. By this means, both systems in between the anchor points maintain their elasticity in regard to translation in all spatial directions. Thus, the location bearing carries approx. all forces and torques induced by the REPA.

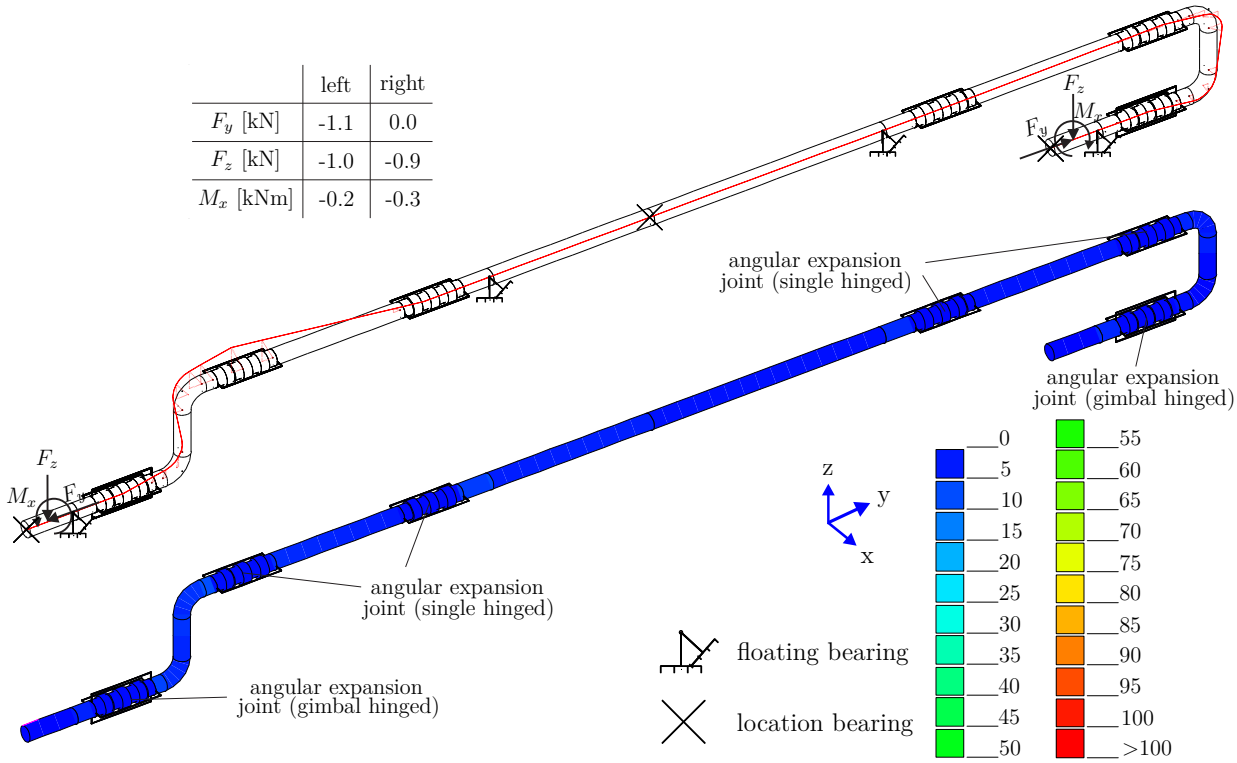

Figure 5.20: Isometric view of the pipe section on the traverse using angular expansion joints; bending line and stress utilization [%] at nominal operating conditions (450 °C and 40 bars)

Compared to the approaches A, B and C, the use of angular expansion joints is the most sophisticated. This can be manifested in the greatest reduction of loads on the dynamometers compared to the initial setup. The gimbal hinged design of both bottom angular expansion joints allows flexibility in all spatial directions. The REPA forces will not by constrained significantly and a basis for realizing accurate measurements is created. Consequently, the implementation of angular expansion joints is selected. Figure 5.21 offers the technical drawing of the traverse (cf. figure 5.13), but having angular expansion joints installed.

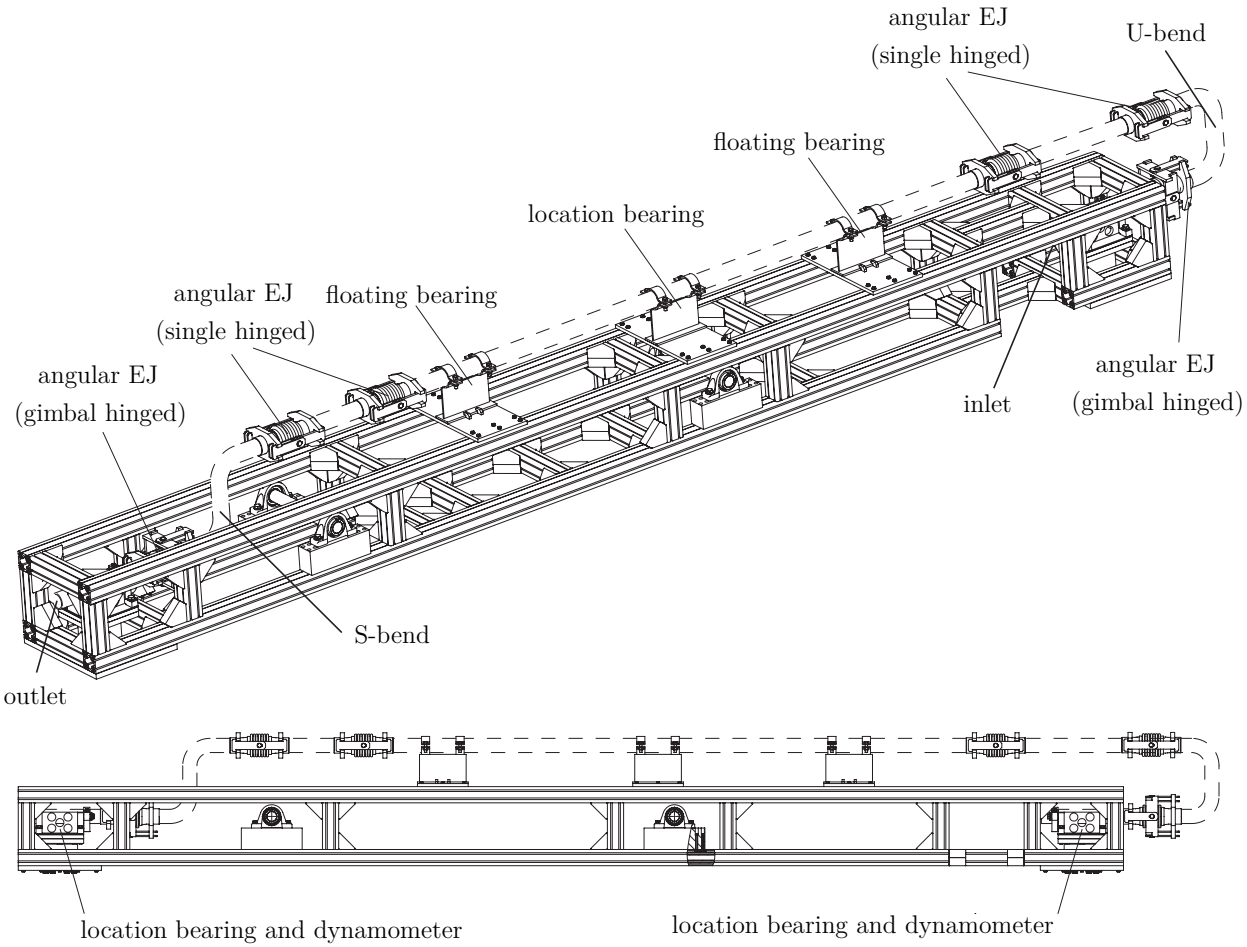

Figure 5.21: Technical drawing of the traverse with assembled angular expansion joints; isometric view (top) and side view (bottom)

5.3.3 Pre-Tensioning of the Pipe System

The above section served to find an applicable solution minimizing the loads carried by the location bearing. Yet, in order to optimize the angular expansion joint's lifetime and to exploit the full movement capability, it is crucial to pre-tension the pipe system on the traverse. Therefore, the geometry of the pipe system is intentionally changed during assembly to produce a desired initial displacement and stress [49]. In doing so, the assembly attains its most favourable position when heated up. Another effect that is accompanied with pre-tensioning is of no less importance in this particular problem: When the system is operating in the desired temperature range, the thermal expansion moves the pipe system close to its "neutral position" (c.f. the dashed pipe section in figure 5.21). Thus, the reaction forces of the angular expansion joints are minimized and the dynamometers are barely stressed by unintended axial forces (F_y) and torques about the x-axis (M_x).

From their neutral position, expansion joints can perform movements of the same magnitude in both directions. The expansion joints that are chosen for the REPA Test Rig are capable of performing 1000 cycles of angular motion with a magnitude of 11° in both directions, i.e. 22° in total. However, if only 5.5° in each direction is exploited, the number of life cycles increases to 10.000, see appendix D.10 and D.11. Hence, it is expedient to install the expansion joints under pre-tension, since the thermal dilatation of the piping will be only in one direction (expansion). The amount of pre-tensioning can be chosen in between two extremes:

- 50% pre-tensioning: the expansion joint is deflected 50% of its total movement (see figure 5.22, left)
- 100% pre-tensioning: the expansion joint is deflected 100% of its total movement; it moves to its neutral position under maximum temperature (see figure 5.22, right)

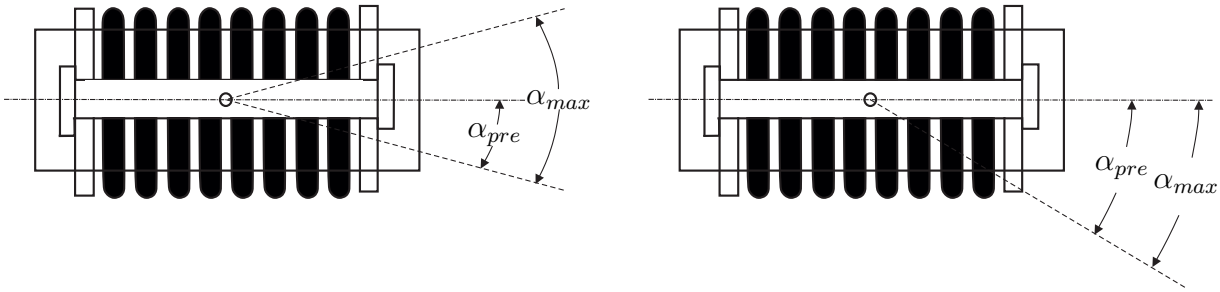

Figure 5.22: Angular Expansion Joint with 50% pre-tensioning (left) and 100% pre-tensioning (right) (cf. [52])

Since it is desirable that the system is as close as possible to its neutral position when heated up, a *Design Point* for the angular expansion joints has to be found. This *Design Point* is defined by the operation temperature, at which the system is in its neutral position (geometrically). Based on a temperature difference of 430 $°C$ between ambient (20 $°C$) and the maximum operation temperature (450 $°C$), it seems reasonable to specify a design point of 235 $°C$ in respect to the angular expansion joints. This complies with 50% pre-tensioning and would minimize the total magnitude of the angular expansion joints. However, this approach interferes with the effort to operate the system as close to its neutral position as possible, since a temperature of 235 $°C$ is not to be expected in PTC loops. Those temperatures are rather in a range between approx. 300 $°C$ and 400$°C$, cf. chapter 3.1, 3.2 and 4.1.4. Consequently, the design point is chosen to have a temperature of 350$°C$. This is equivalent to 77% pre-tensioning[21]. In this configuration, the system will only perform little deflections in both directions during operation, which are corresponding to $\pm 50°C$.

[21] $330K/430K \approx 77\%$

The implementation of the pre-tension is accomplished by means of taking up table 5.4 again. For each of the six mentioned pipe sections the thermal expansion is re-calculated in regard to the design point of 350°C, see table 5.6. The thermal expansion coefficient must be adapted to $13.2 \cdot 10^{-6}$ $^1/_K$ with respect to its validity in the given temperature range. The quantity of thermal expansion is conform to the length the pipe sections have to be "cut", i.e. they are installed with a shorter length:

Table 5.6: Thermal expansion between 20 °C and 350 °C for different pipe sections on the traverse and resulting pre-tensioning condition

No.	L_{cold} [mm]	ΔL [mm]	$L_{pre\text{-}tension}$ [mm]
①	766	-3.35	762.65
②	400	-1.74	398.26
③	2286	-9.96	2276.04
④	2731	-11.90	2719.10
⑤	400	-1.74	398.26
⑥	774	-3.37	770.63

Figure 5.23 illustrates a side view of the pipe section on the traverse with installed angular expansion joints. Implementing the above calculated pre-tension leads to a bending line (red) of the assembly situation. The neutral position is obtained when the pipe system is exposed to fluid at 25 bars and 350 °C, cf. table 5.7.

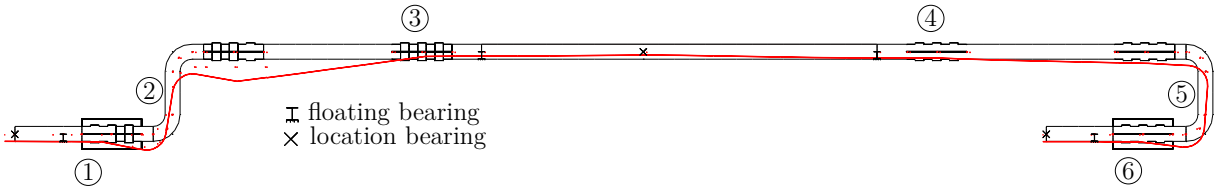

Figure 5.23: Side view of the pipe section on the traverse with superimposed bending line (red) under pre-tensioning condition (not to scale)

5.3.4 Load Cases

So as to simulate the kinematics of the angular expansion joints when exposed HTF at typical PTC operating conditions, suitable load cases need to be defined. Based on the findings given in chapter 3, the *Design Point* is determined at 350 °C and 25 bars, since it is conform to the mean conditions that are to be expected in a commercial PTC loop. Accordingly, – given a temperature increase inside a PTC loop of 100 °C – the *Inlet* temperature is 50 °C lower and the *Outlet* temperature is 50 °C higher, respectively. The additional load case *Maximum* takes future operation conditions into consideration using innovative HTFs, e.g. *HELISOL® 5A*. The HTF pressure and density are adapted likewise. Table 5.7 provides an overview of the load cases used in the *ROHR2* simulation.

Table 5.7: Load cases for *Therminol® VP-1*

	pressure [bar]	temperature [°C]	HTF density [kg/m^3]
Idle[22]	1	20	1
Inlet	30	300	817
Design Point	25	350	760
Outlet	20	400	694
Maximum[23]	20	450	512

This data is implemented in *ROHR2*. The results obtained from this analysis are presented in figure 5.24. The figure illustrates an isometric detail view and distinguishes between the inlet (right bottom) and outlet (left top) pipe section on the traverse. The bending lines for the above defined load cases are superimposed on top of each other.

Outlet section

Having a closer look to the outlet section, there is a clear trend to be seen: Beginning with the pre-tensioned *Idle* condition (no HTF, only pre-tensioned pipe), the pipe section lifts when increasing the temperature step by step. This applies in particular to the expansion joint in the center (O2) which performs the largest deflection both rotationally and translationally. In the *Idle* load case it is 3.43° pre-tensioned. When the system is exposed to HTF at *Inlet* conditions, it lifts and the angular deflection decreases to 0.63°. A further rise in temperature to *Outlet* conditions causes a deflection of -0.37°. Consequently, the centrally arranged angular expansion joint (O2) performs an angular deflection of 1.00° between *Inlet* and *Outlet* condition, which is a satisfying result with respect to the lifetime of the expansion joints (cf. chapter 5.3.3). Moreover, it has to be mentioned that the deflection between the *Design Point* and the *Inlet* and *Outlet* condition is not distributed symmetrically. This asymmetry is the result of weight forces (pipe, expansion joints and HTF) and is even enhanced by the temperature dependence of the fluid in respect to its density. The maximum deflection between *Idle* and *Maximum* is 4.38° (3.43° to -0.95°). This amount of deflection is always corresponding to the sum of deflection the other two expansion joints (O2 and O3) perform due to their geometrical arrangement. Thus, they will always carry smaller angular deflections.

[23] density for air
[24] density for *HELISOL® 5A*

Inlet section

The inlet section shows, owing to its distinct geometry, a different behaviour. In the *Idle* load case, the U-bend is slightly lifted and shifted leftwards, see figure 5.24. In doing so, the centrally arranged expansion joint (I2) is deflected 1.28°. Conveying the system with hot HTF deflects the pipe towards its neutral position (*Design Point*). A further increase lowers the U-bend, whilst the thermal expansion moves it more and more to the right. The angular deflection of the centrally arranged expansion joint (I2) between *Inlet* and *Outlet* condition is 0.41° (0.15° to -0.26°).

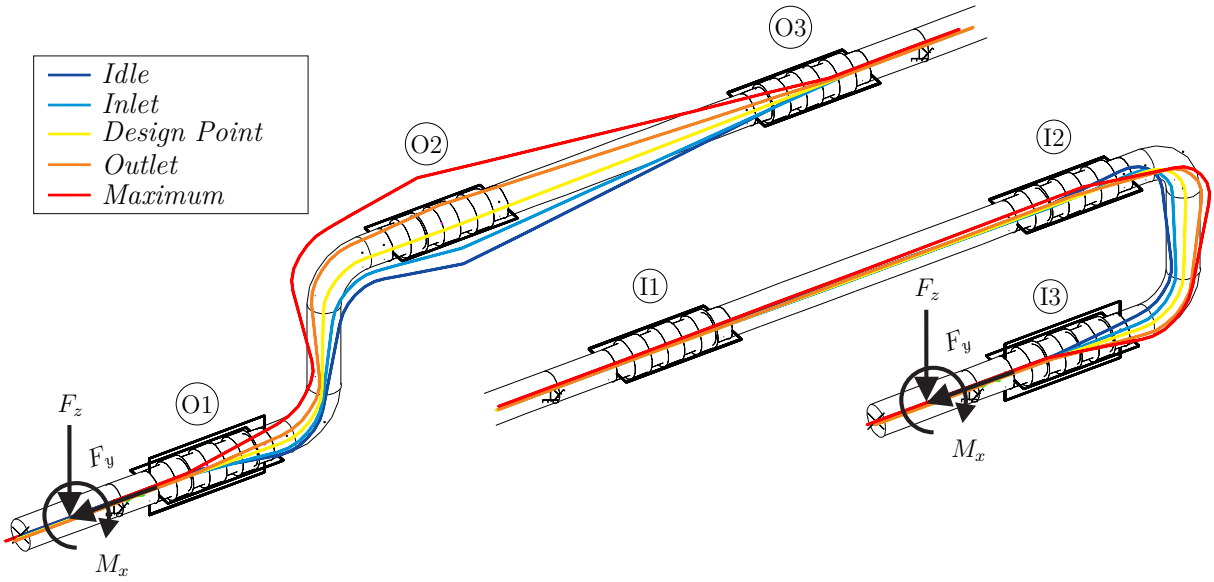

Figure 5.24: Isometric detail view of the outlet (left) and inlet (right) pipe section on the traverse with superimposed bending lines of different load cases (not to scale)

5.3.5 Assembling and Validation of the Simulation Setup

The present thesis addresses the design, but is written prior to the final assembly of the Kinematics Unit including the implementation of the REPA force measurement. Thus, the following section conduces to give advises for the assembly to be as accurate as possible.

An overview of the resultant forces and torques on both dynamometers according to the *ROHR2* simulation is given in table 5.8 for each load case. Taking into account the nominal loads of the dynamometers (cf. table 5.5), the torque about the x-axis M_x amounts to approx. 30 % of the maximum value (1 kNm). The axial (F_y) and vertical forces (F_z) amount to 7.5 % and 4.5 %, respectively. Consequently, it can be stated that these loads do not exceed the nominal load range of the dynamometers. However, they distort the REPA force measurement, as they interfere with the loads "emitted" by the REPA.

Table 5.8: *ROHR2* Simulation; forces and torques on both dynamometers for different load cases

	outlet			inlet		
	F_y [N]	F_z [N]	M_x [Nm]	F_y [N]	F_z [N]	M_x [Nm]
Idle	-515	-803	-247	-199	-832	-248
Inlet	-399	-805	-264	-300	-867	-240
Design Point	-482	-835	-268	-101	-904	-293
Outlet	-730	-887	-253	-111	-902	-290
Maximum	-749	-889	-252	-103	-898	-290

In order two diminish said interference of unintended loads with the relevant parameters, either a calibration of the sensor or the installation of additional supports is feasible. The latter can be spring or constant supports that carry the remaining loads. A first draft is presented in appendix B. However, their implementation into the system is associated with additional expenses, which cannot be procured in the erection phase of the test rig. As a result of this, an accurate calibration of the dynamometers must be carried out. Therefore, the Kinematics Units including traverse must be erected as depicted in figure 5.21 using the pre-tension measures given in table 5.6.

It is anticipated that the dimensions – particularity in terms of pre-tensioning – cannot be satisfied in regard to an accuracy that was defined in table 5.6. The pre-tension was calculated with an accuracy of 10 μm; however, it has to be expected that manufacturing accuracies of the pipe section will be significantly lower. This applies particularly to the welding of the pipe section. Therefore, and in order to still ensure a maximum accuracy, the following advises must be observed during assembly:

1. The complete section must be welded in the workshop taking into account the measures given in table 5.6. In doing so, a sufficient clearance at both pipe ends must be taken into account for posterior adjusting.

2. Once the welding process is finished, all relevant dimensions have to be measured and compared to the specification given in table 5.6.

3. Possible deviations must be documented and the required pre-tension must be re-calculated.

4. The *ROHR2* simulation must be updated calculating the updated loads.

5. The recalculated pre-tension (horizontal) must be implemented by fastening one of the location bearings at the dynamometers whilst displacing the pipe on the other side. The vertical pre-tension cannot be adapted afterwards, since the height of all supports is fixed, i.e. not adjustable.

6. Once the system is erected, the actual values of the pipe section must be once again entered in the *ROHR2* simulation calculating the resultant loads according to table 5.8

7. Comparison between the simulation and the measured forces by the dynamometer; if the values correspond, the dynamometer(s) must be calibrated.

5.4 Drafts for Testing Procedures

So as to give a rough indication for following works at the REPA Test rig, this section serves to define drafts for possible REPA testing scenarios regarding the Kinematics Unit.

- **Maximum Acceleration of REPA ageing**
  This methods depicts the first possible extreme. The machine – the hydraulic pistons in the Kinematics Unit – are driven with maximum velocity enabling REPA endurance test using the most accelerated way. The Kinematics Unit performs superimposed rotational and translational movements. However, several drawbacks in regard to precision of the simulation must be accepted.

- **Step by Step Rotation**
  SCAs do not move continuously, but rather incrementally (cf. figure 4.2). This can be taken into account, yet causing an extension of the test duration.

- **Implementation of Additional Cycles**
  Taking into consideration additional cycles, e.g. tracking errors and dumping of collectors, this methods approaches a realistic REPA testing scenario. However, the duration increases, as the drive pylon must perform backward rotation.

- **Real Simulation**
  The seconds extreme presents a testing method that is adapted to real PTC power plant conditions moving the REPAs in daily cycles. In order to reproduce the entire lifetime of the components, this procedure would take up to 30 years.

As the REPA Test Rig lacks a cooling unit, it is not possible to implement thermal cycles with regard to a similar acceleration of the Kinematics Unit. Therefore, it is recommended to perform tests at steady-state, yet specific, pressures and temperatures. They can, for instance, be adapted to the load cases that are defined in chapter 5.3.4.

Chapter 6

Summary and Outlook

Flexible pipe connections, so called Rotation and Expansion Performing Assemblies (REPAs), are essential components in Parabolic Trough Collector power plants. They compensate for both the daily rotation of the receiver's focal line relative to the fixed piping and for linear expansion and contraction due to thermal cycling of the absorber tubes. Thus, REPAs are highly stressed key components. Durability and reliability of these pipe connections are crucial aspects for proper functioning of a solar field with respect to 30 years of operation.

Within the scope of the present thesis, a new test rig for investigating the durability of REPAs is designed. First, a literature research is carried out examining and assessing already existing test rigs (cf. chapter 3). In doing so, a range of drawbacks is revealed in view of realistic operation conditions – such as pressure, temperature and mass flow – and necessary test time for durability tests. It is stated that none of the existing test facilities is capable to both reproduce the hydraulic conditions of a commercial solar field and enable accelerated motion cycles of the test specimens. Afterwards, the requirements for REPAs are investigated so as to be proficient to derive requirements for the new test rig being able to simulate all possible impacts (cf. chapter 4). Those are, for instance, the occurrence of discontinuous rotational collector motion induced by the hydraulic drive unit of a Solar Collector Assembly. Furthermore, the necessity of an HTF cycle which exposes the test objects not only to typical operation temperatures and pressures (up to 450 $°C$ and 40 bars), but also to exact flow conditions of a solar field, is clarified.

Chapter 5 comprises the design of the *HTF cycle* and its integration into an externally designed *Kinematics Unit*. Based on a Piping and Instrumentation Diagram, a compact design is created whilst taking into account a stress analysis using the CAE software *ROHR2*. All relevant component's dimensions, e.g. a pump, a heater and an expansion vessel, are calculated and incorporated.

Special emphasis is given on developing measurement assemblies which monitor the forces and torques that are "emitted" by the test specimens. Approaches are presented using different types of expansion joints that avoid unintended loads derived by thermal expansion of the adjacent pipe section. Employing assemblies of three angular expansion joints for each REPA diminishes these loads to a minimum (cf. chapter 5.3).

A facility is commissioned enabling realistic endurance tests (about 10.000 cycles) of two serially connected REPAs in less than three months. Choosing between three different HTFs (*Therminol® VP-1*, *Syltherm 800* and *HELISOL® 5A*), the hydraulic properties are adjustable in terms of mass flow ($6-60\ ^{m^3}/_h$), pressure (up to 40 bars) and temperature (up to 450 $°C$), cf. chapter 5.1. The investigations can be tailored to customized applications of the REPA concept (Ball Joint Assemblies or Rotary Flex Hose Assemblies) and the collector geometry, i.e. distinct focal lengths. Using a *EuroTrough* drive pylon with modified hydraulics, discontinuous motions (cf. chapter 4.1.1) are considered.

The design presented in this master's thesis employs all relevant components for commissioning the test rig. Further improvements, however, are crucial. The implementation of expansion joints into the Kinematics Unit is a first step towards an accurate and precise acquisition of the mechanical loads. First drafts using additional spring and / or constant supports on the traverse's pipe section revealed the potential in view of the reduction of adjacent forces below the uncertainty range of the dynamometers. In the course of a comprehensive upgrade of the test rig, additional dynamometers will be installed below the swivel joints of RFHAs. The design of these assemblies at the bottom connections of the test specimens still remains to be done. So as to introduce loads derived by adjacent pipe sections (cf. chapter 4.1.3), additional instruments which expose the swivel joint to adjustable forces may be incorporated.

References

[1] G. Knies: *Red Paper - An overview of the Desertec concept*. Desertec Foundation.

[2] R. Kneer: *University Lecture "Heat and Mass Transfer I"*. Institute of Heat and Mass Transfer, RWTH Aachen University, 2011.

[3] J. A. Duffie, W. A. Beckman: *Solar Engineering of Thermal Processes*. John Wiley & Sons, Inc., 2013.

[4] R. Stieglitz, V. Heinzel: *Thermische Solarenergie*. Springer Vieweg, 2012.

[5] C. Márquez Salazar: *CSP today - An Overview of CSP in Europe, North Africa and the Middle East*, 2008.

[6] *Direct Normal Irradiation (DNI)*. http://solargis.info/doc/free-solar-radiation-maps-DNI. `http://solargis.info/doc/free-solar-radiation-maps-DNI` Accessed: 2016-01-21.

[7] A. Fernández-García, M.E. Cantos-Soto, M. Röger, C. Wieckert, C. Hutter, L. Martínez-Arcos: *Durability of solar reflector materials for secondary concentrators used in CSP systems*. Solar Energy Materials and Solar Cells, 130:51 – 63, 2014.

[8] R. Pitz-Paal: *University Lecture "Solar Technology"*. Institute of Solar Research, RWTH Aachen University, 2014.

[9] B. Hoffschmidt: *University Lecture "Solar Components"*. Institute of Solar Research, RWTH Aachen University, 2014.

[10] D. Kearney, B. Kelly, R. Cable, N. Potrovitza, U. Herrmann, P. Nava, R. Mahoney, J. Pacheco, D. Blake, H. Price: *Overview on use of a Molten Salt HTF in a Trough Solar Field*. NREL Parabolic Trough Thermal Energy Storage Workshop, 2003.

[11] D. Laing, W. Schiel, P. Heller: *Dish-Stirling-Systeme - Eine Technologie zur dezentralen solaren Stromerzeugung*. FVS Themen, 2002.

[12] R. Pitz-Paal: *Parabolic Trough, Linear Fresnel, Power Tower - A Technology Comparison*. Institute for Advanced Sustainability Studies e.V.

[13] B. Hoffschmidt, S. Alexopoulos: *Überblick über solarthermische Kraftwerke*.

DPG AKE-Tagungsband, 2009.

[14] Environment, Nature Conservation Federal Ministry for the and Nuclear Safety (BMU): *Solar thermal power plants - Utilising concentrated sunlight for generating energy*, 2013.

[15] M. Geyer, H. Lerchenmüller, V. Wittwer, A. Häberle, E. Lüpfert, K. Hennecke, W. Schiel, G. Brakmann: *Solarthermische Kraftwerke - Technologie und Perspektiven*. FVS Themen, 2002.

[16] K. Riffelmann, T. Richert, P. Nava, A. Schweitzer: *Ultimate Trough® – A Significant Step towards Cost-competitive CSP*. In *SolarPACES*, page 1831–1839, 2014.

[17] Flagsol GmbH: *Heliotrough® - Product Facts*, 2013. `http://www.heliotrough.com/facts.html` Accessed: 2016-03-13.

[18] H. Price, E. Lüpfert, D. Kearney, E. Zarza, G. Cohen, R. Gee, R. Mahoney: *Advances in parabolic trough solar power technology*. Journal of solar energy engineering, 124(2):109–125, 2002.

[19] F. Ortiz Vivez, A. Kaufung: *New Flexible Connection System for Parabolic Trough Collectors*. In *SolarPACES*, 2008.

[20] N. Janotte: *Requirements for Representative Acceptance Tests for the Prediction of the Annual Yield of Parabolic Trough Solar Fields*. PhD thesis, RWTH Aachen University, 2012.

[21] C. Jung, J. Dersch, A. Nietsch, M. Senholdt: *Technological Perspectives of Silicone Heat Transfer Fluids for Concentrated Solar Power*. Energy Procedia, 69:663 – 671, 2015. SolarPACES.

[22] National Renewable Energy Laboratory (NREL): *Concentrating Solar Power Projects*. `http://www.nrel.gov/csp/solarpaces/` Accessed: 2016-02-17.

[23] Solutia: *Therminol VP-1 Vapour Phase Liquid Phase Heat Transfer Fluid*.

[24] Solutia Inc.: *Therminol Information Bulletin No. 4: "Heat Transfer System Expansion Tank Design"*, 1999.

[25] D. W. Kearney, U. Herrmann: *Engineering Evaluation of a Molten Salt HTF in a Parabolic Trough Solar Field*, 2004.

[26] A.T. Kearney GmbH: *Solar Thermal Electricity 2025*, 2010.

[27] J. F. Feldhoff: *Direct Steam Generation (DSG) - Technology Overview.* SFERA Summer School 2012, 2012.

[28] D. Sniderman: *Moving Hot Fluids Through Solar Troughs*, 2011. https://www.asme.org/ Accessed: 2016-02-24.

[29] Advanced Thermal Systems, Inc.: *Thermal Pak Flexible Ball Joints*, 1999.

[30] Mason-Mercer: *Stock Ball Joints, Bulletin BJ-35*, 2013.

[31] C.Prahl, T. Schapitz, R. Uhlig: *Structural optimization of a line-focussing solar collector with stationary absorber tube.* In *SolarPACES*, 2011.

[32] C. Prahl, A. Pfahl: *A new concept for line-concentrating CSP collectors.* In *SolarPACES*, 2009.

[33] *Plataforma Solar de Almería (PSA).* http://www.psa.es/en/instalaciones/ Accessed: 2016-03-20.

[34] Hyspan Precision Products, Inc.: *Summary Test Report Ball Joint Life Cycle Test Solar Plant Installations.* Technical Report, 2008.

[35] F. Ortiz Vivez, M. Meyer-Grünefeld: *Flexible Hose System - ROTATION-FLEX Connection to HCE of Parabolic Collectors.* Solarpaces, 2009.

[36] M. Saur: *Measurement of forces and torques at the Rotationflex Single System (RFS)*, 2015.

[37] D. Grogan: *Development of Molten-Salt Heat Transfer Fluid Technology for Parabolic Trough Solar Power Plants - Public Final Technical Report.* Aug 2013.

[38] D. Grogan: *Development of Molten Salt Heat Transfer Fluid Technology for Parabolic Trough Solar Power Plants.* In *Sunshot Initiative Concentrating Solar Power.* Abengoa Solar, 2013.

[39] J. J. Michalsky: *The Astronomical Almanac's algorithm for approximate solar position (1950–2050).* Solar Energy, 40:227–235, 1988.

[40] R. Pitz-Paal, J. Dersch, B. Milow, F. Téllez, A. Ferriere, U. Langnickel, A. Steinfeld, J. Karni, E. Zarza, O. Popel: *Development steps for parabolic trough solar power technologies with maximum impact on cost reduction.* Transactions of the ASME. Journal of solar energy engineering, 129(4):371–377, 2007.

[41] W. Schröder: *University Lecture "Fluid Mechanics I".* Institute of Aerodynamics,

RWTH Aachen University, 2010.

[42] ETABO Energietechnik und Anlagenservice GmbH: *Tabellenbuch für den Rohrleitungsbau*, 2012.

[43] W. Wagner: *Rohrleitungstechnik*. Vogel, 2008.

[44] *Emissivity Values for Common Materials*. `http://www.infrared-thermography.com` Accessed: 2016-02-22.

[45] ROCKWOOL® Technical Insulation: *ProRox PS 960 - Product Data Sheet*, 2012.

[46] American Society of Mechanical Engineers (ASME): *ASME B36.10-Welded and Seamless Wrought Steel*, 2004.

[47] The Dow Chemical Company: *Syltherm 800 Heat Transfer Fluid, Product Technical Data*, 1997.

[48] *DIN 4754: Heat transfer systems operating with organic heat transfer media*, September 1994.

[49] American Society of Mechanical Engineers (ASME): *Power Piping, ASME Code for Pressure Piping, B31*. pages 28–29, 2007.

[50] Association of German Engineers: *VDI 3842 - Vibrations in piping systems*, 2004.

[51] ThyssenKrupp Materials International GmbH: *Material Data Sheet - Alloy steel tubes - P12/T12 (13CrMo4-5)*.

[52] Witzenmann GmbH: *Expansion Joint Manual*, 2012.

[53] Senior Flexonics: *Reference List for Senior Flexonics CSP Products*.

[54] Advanced Thermal Systems, Inc.: *ATS Solar Ball Joint Experience List*.

Appendix A

Datasheets

Table A.1: Physical and chemical properties of the HTFs

		Therminol® VP-1	*Syltherm 800*	*HELISOL®*
composition		diphenyl/diphenyl oxide	polydimethylsyloxane	
color		clear	clear yellow	clear
max. operation temp.	$[°C]$	400	400	430
max. film temp.	$[°C]$	430	427	471
heat of combustion	$[MJ/kg]$	no info	28.7	26.3
density at 25 $°C$	$[kg/m^3]$	1061	931	918
viscosity at 25 $°C$	$[mPa \cdot s]$	3.8[24]	9.1	5

The densities for *Therminol® VP-1* and *Syltherm 800* are calculated (using the trendlines A.1 and A.2; derived from datasheets) and listed in table A.2.

$$\rho_{VP-1} = -0.90797 \cdot T + 0.00078116 \cdot T^2 - 2.367 \cdot 10^{-6} \cdot T^3 + 1083.25 \ [kg/m^3] \quad \text{(A.1)}$$

$$\rho_{Syltherm} = 953.16 - 0.91658 \cdot T + 0.42114 \cdot 10^{-3} \cdot T^2 - 1.6706 \cdot 10^{-6} \cdot T^3 \ [kg/m^3] \quad \text{(A.2)}$$

Table A.2: Densities of relevant HTFs

temperature	*Therminol® VP-1*	*Syltherm 800*	*HELISOL®*
$[°C]$	[kg/m^3]		
25	1061	930	918
50	1040	908	894
100	998	864	846
150	957	820	799
200	914	773	751
250	868	724	703
300	817	671	656
350	760	612	608
400	694	547	560
450	617	474	512

[24] linear interpolation between 20 and 30 $°C$

DICKOW PUMPEN KG / Pump Data Sheet - Magnetic Coupled Pumps

1	Order No.:	**PB15203042**	P.O. No.:	**I/348/67210595**			Date :		Week :
2	Customer :	**Deutsches Zentrum für Luft- u. Raumfahrt e.V.**					P.O.Date :	**11.02.15**	
3	Quantity :	**1**	Type :	**NMWR t huh 65/210**			Design :	**D x/1,5/40/3/1**	
4	Cust. Item No.:						Serial No.:	**PB15203042**	

Accessories

5	Motor manufacturer :	**VEM**			Delivered by :	**DICKOW**	Assembled by :	**DICKOW**	
6	Type :	**160M**	ISO-classif.:	**F**	Protection :	**IP55**	Ex - clasif.:	**nein**	
7	Output :	**11 kW**	Voltage :	**400 V**	Frequency :	**50 Hz**	Terminal box :	**manufacturers standard**	
8	Construction :	**B3**	Thermistors:	**3 pc.**	VIK :	**no**	Efficiency-class:	**IE2**	
9	**für FU-Betrieb; inkl. PT100 zur Überwachung der Wicklungstemperatur**								
10	Coupling, Manuf./Type :	**FLENDER ARPEX NAN 115-6 / 140**			Guard material :	**1.4571 perf.**	No. 50	**1148(h=210)#Z.59**	
11	Base plate/frame :	**RM8**					foundation bolts :		
12									
13	Monitoring equipment:	**Lagertemperaturüberwachung nach 84.SE.031 / Temperaturüberwachung des Schmieröles /**							
14	**PT 100 im Druckstutzen**						Name tag :	**english**	

Execution

15	Impeller diam.:	**175 mm**	Stages :	**1**	Pump flanges : Suct.:	**100**	Ratg.: **40**	Disch.: **65**	Ratg.: **40**
16	Impeller type :	**closed**			Machined acc. to :		**DIN EN 1092-1 B**		
17	Circulation :	**external**							
18	Casing mount :	**centerline**	Rotation :	**cw**			Self priming :	**no**	
19	Drain :	**DN 15 / PN 40 with counter flange**							
20	Press. gauge conn.:	**no**	Nozzle orientation :	**standard**	Painting :	**standard, RAL 9006**			
21	Heating jacket flange: Inlet DN/PN:		Outlet DN/PN:						

Materials

22	Wetted casing :		Imp. wear ring :		Rotor :	**1.4571**	Drive shaft :	**1.4021**
23	Diffuser :		Pump shaft :	**1.4021**	Rotor cover :	**1.4571**	Bearing bracket :	**GGG 40**
24	Impeller :	**1.4408**	Gasket :	**Novaph.SSTC**	Thrust bearing :	**SiC**	Support column :	
25	Side chan. imp.:		Containm. shell :	**Titan**	Radial bearing :	**SiC**	Dome cover :	
26	Wear ring :	**1.4571**	Shell flange :	**1.4571**				
27	**O-Ringe: Creaflex PFE310**							

Operating Data

28	Liquid :	**Thermalöle**					Density :	**0,512 - 0,547 kg/l**
29	Solids :	**no**	Temperature :	**450 °C**			Viscosity :	**< 10 mm2/s**
30	Flow liquid :	**60 m3/h**	Head liquid :	**40 mLC**			Power cons. liquid :	**7,5 kW**
31	Flow water :		Head water :				Power cons. water :	
32	Magnetic losses :	**1,8 kW**	Coupling power :	**21,8 kW**			max. power cons.:	
33	Vapour pressure :		Speed :	**2900 rpm**			Perf. curve :	64. **NC.56**
34	design temp.:	**450 °C**	design press. :	**40 bar**				

Tests

35	**Material**		**Hydrostatic**		**Performance**		**NPSH**	
36	Certificate:	Witnessed:	Certificate: **yes**	Witnessed:	Certificate: **yes**	Witnessed:	Certificate:	Witnessed:
37	EN 10204		Test Press. : **60 bar**		**ISO 9906-2B**	**5 point**		
38	**Balancing**		**Vibration**		**Sound power**			
39	Certificate:	Witnessed:	Certificate:	Witnessed:	Certificate:	Witnessed:		
40	DIN/ISO 1940 T1	**6.3**			ISO 9614-2			

Drawings, Build sheets, Documentation

41	Build sheet :	**23.NMWR.257**	Documentation :	No.: **1 / CD**	Language : **englisch**		EU-Language IOM: **Spanish**	
42	Comments :							
43	**Entlüftungsleitung geflanscht und geschweißt**							
44	**Entlüftungsleitung geflanscht und geschweißt**							
45	**Etagenk**							
46	**Etagenkühler**							
47	**Lagerträger: 18.1496**							
48	**Spiralgehäuse**							
49	**Rotor treibend: 43.346**							
50	**Halteschraube: 29.444**							
51	**Lagerdeckel (360.2):**							
52	**# R = 115**							
53	**Rev. C: 24.07.15 VK/OT/rf**							

Weights : net	**total**
Motor No.:	**415510/0001H**
ATEX:	

54	**Handled by**	**O. T.**	**Date**	**17.02.15**	**Techn. verified**	**Date**	**Comm. verified**	**Date**

Figure A.1: Datasheet of the magnetic coupled pump made by *Dickow Pumpen KG*

Appendix B

Calculations

Pressure Drop Calculation

Table B.1: Resistance coefficients for pipe friction

	DN65	DN80	DN100	DN150
L $[m]$	15.60	18.30	1.27	0.56
d_i $[m]$	0.0590	0.0737	0.0972	0.1464
λ [-]	0.019	0.018	0.017	0.016
ζ_{fr} [-]	5.04	4.56	0.23	0.06

Table B.2: Resistance coefficients for change of cross-section ($\xi = 0.6466$)

Inlet	DN 65	DN 80	DN 80	DN 80	DN 100	DN 150
Outlet	DN 80	DN 100	DN 150	DN 65	DN 80	DN 80
d_{in} [mm]	58.98	73.66	73.66	0.07366	97.18	0146.36
d_{out} [mm]	73.66	97.18	146.36	0.05898	73.66	73.66
qty. [-]	2	2	1	1	1	1
$\sum \zeta_{cs}$ [-]	0.41	0.71	5.61	0.04	0.04	0.04

Table B.3: Resistance coefficients for pipe bends ($3D$)

	DN 80	DN 65
ζ_b [-]	0.238	0.240
qty. [-]	9	4
$\sum \zeta_b$ [-]	2.140	0.962

Table B.4: Resistance coefficients for intersections (T-junctions)

coalition		separation	
w_2 [m/s]	>0	w_1 [m/s]	>0
w_3 [m/s]	0	w_3 [m/s]	0
$x = {}^{w_3}/_{w_2}$ [-]	0	$x = {}^{w_3}/_{w_1}$ [-]	0
qty. [-]	2	qty. [-]	2
$\sum \zeta_{is}$ [-]	0.08	$\sum \zeta_{is}$	0.08

Table B.5: Pressure drop and differential head of the HTF cycle as a function of HTF temperature and flow rate when using *Therminol® VP-1*

	$T_{HTF} = 25°C$		$T_{HTF} = 100°C$		$T_{HTF} = 200°C$		$T_{HTF} = 300°C$		$T_{HTF} = 400°C$	
$\dot{V}$	Δp	H	Δp	H	Δp	H	Δp	H	Δp	H
$[m^3/h]$	$[bar]$	$[m]$	$[bar]$	$[m]$	$[bar]$	$[m]$	$[bar]$	$[m]$	$[bar]$	$[m]$
5	0.24	2.44	0.24	2.43	0.24	2.42	0.24	2.40	0.23	2.38
10	0.30	3.04	0.29	3.00	0.29	2.94	0.28	2.88	0.27	2.79
15	0.39	3.94	0.38	3.85	0.36	3.72	0.35	3.57	0.33	3.38
20	0.52	5.28	0.50	5.11	0.48	4.88	0.45	4.62	0.42	4.29
25	0.68	6.91	0.65	6.64	0.62	6.28	0.58	5.87	0.52	5.35
30	0.90	9.17	0.86	8.79	0.81	8.28	0.75	7.68	0.68	6.93
35	1.13	11.52	1.08	10.99	1.01	10.29	0.93	9.49	0.83	8.46
40	1.44	14.68	1.37	13.99	1.28	13.08	1.18	12.03	1.05	10.68
45	1.74	17.74	1.65	16.87	1.54	15.72	1.41	14.39	1.24	12.69
50	2.14	21.85	2.04	20.78	1.90	19.35	1.74	17.71	1.53	15.61
55	2.51	25.64	2.39	24.34	2.22	22.62	2.02	20.63	1.77	18.08
60	2.95	30.13	2.80	28.58	2.60	26.53	2.37	24.16	2.07	21.14
65	3.39	34.63	3.22	32.82	2.98	30.41	2.71	27.63	2.36	24.08
70	3.87	39.50	3.67	37.40	3.39	34.60	3.08	31.38	2.67	27.26
75	4.38	44.73	4.15	42.31	3.83	39.11	3.47	35.41	3.01	30.68
80	4.93	50.31	4.66	47.57	4.30	43.92	3.89	39.71	3.36	34.33
85	5.51	56.26	5.21	53.16	4.81	49.04	4.34	44.30	3.75	38.22
90	6.13	62.57	5.79	59.10	5.34	54.48	4.82	49.15	4.15	42.35
95	6.79	69.24	6.41	65.37	5.90	60.22	5.32	54.29	4.58	46.71
100	7.47	76.27	7.05	71.98	6.50	66.28	5.85	59.71	5.03	51.30

Table B.6: Pressure drop and differential head of the HTF cycle as a function of HTF temperature and flow rate when using *Syltherm 800*

	$T_{HTF} = 25°C$		$T_{HTF} = 100°C$		$T_{HTF} = 200°C$		$T_{HTF} = 300°C$		$T_{HTF} = 400°C$	
$\dot{V}$	Δp	H	Δp	H	Δp	H	Δp	H	Δp	H
$[m^3/h]$	$[bar]$	$[m]$	$[bar]$	$[m]$	$[bar]$	$[m]$	$[bar]$	$[m]$	$[bar]$	$[m]$
5	0.24	2.42	0.24	2.41	0.23	2.39	0.23	2.38	0.23	2.36
10	0.29	2.95	0.28	2.91	0.28	2.85	0.27	2.78	0.26	2.69
15	0.37	3.74	0.36	3.64	0.34	3.50	0.33	3.35	0.31	3.16
20	0.48	4.93	0.47	4.75	0.44	4.50	0.41	4.22	0.38	3.89
25	0.62	6.35	0.59	6.07	0.56	5.68	0.51	5.25	0.46	4.72
30	0.82	8.38	0.78	7.97	0.73	7.41	0.67	6.79	0.59	6.03
35	1.02	10.43	0.97	9.88	0.89	9.12	0.81	8.27	0.71	7.24
40	1.30	13.26	1.23	12.54	1.13	11.55	1.02	10.44	0.89	9.09
45	1.56	15.95	1.47	15.03	1.35	13.78	1.21	12.38	1.05	10.67
50	1.92	19.64	1.81	18.51	1.66	16.97	1.49	15.23	1.29	13.12
55	2.25	22.95	2.12	21.59	1.93	19.72	1.73	17.62	1.48	15.07
60	2.64	26.93	2.48	25.31	2.26	23.09	2.02	20.59	1.72	17.55
65	3.03	30.89	2.84	28.98	2.58	26.37	2.30	23.43	1.95	19.88
70	3.45	35.15	3.23	32.94	2.93	29.92	2.60	26.51	2.19	22.38
75	3.89	39.74	3.65	37.20	3.31	33.73	2.92	29.82	2.46	25.08
80	4.37	44.64	4.09	41.75	3.70	37.80	3.27	33.35	2.74	27.96
85	4.89	49.85	4.57	46.59	4.13	42.14	3.64	37.11	3.04	31.03
90	5.43	55.39	5.07	51.73	4.58	46.74	4.03	41.10	3.36	34.28
95	6.00	61.24	5.60	57.16	5.06	51.60	4.44	45.32	3.70	37.72
100	6.61	67.40	6.16	62.89	5.56	56.72	4.88	49.77	4.05	41.34

Table B.7: Pressure drop and differential head of the HTF cycle as a function of HTF temperature and flow rate when using *HELISOL® 5A*

	$T_{HTF} = 25°C$		$T_{HTF} = 100°C$		$T_{HTF} = 200°C$	
$\dot{V}$	Δp	H	Δp	H	Δp	H
$[m^3/h]$	$[bar]$	$[m]$	$[bar]$	$[m]$	$[bar]$	$[m]$
5	0.24	2.42	0.24	2.41	0.23	2.39
10	0.29	2.94	0.28	2.89	0.28	2.83
15	0.36	3.72	0.35	3.61	0.34	3.47
20	0.48	4.90	0.46	4.70	0.44	4.44
25	0.62	6.30	0.59	5.99	0.55	5.59
30	0.81	8.30	0.77	7.86	0.71	7.28
35	1.01	10.33	0.95	9.73	0.88	8.94
40	1.29	13.12	1.21	12.34	1.11	11.31
45	1.55	15.77	1.45	14.78	1.32	13.48
50	1.90	19.42	1.78	18.20	1.63	16.59
55	2.22	22.70	2.08	21.22	1.89	19.27
60	2.61	26.63	2.44	24.87	2.21	22.54
65	2.99	30.53	2.79	28.46	2.52	25.73
70	3.40	34.74	3.17	32.34	2.86	29.18
75	3.85	39.26	3.58	36.51	3.22	32.88
80	4.32	44.09	4.01	40.96	3.61	36.83
85	4.83	49.24	4.48	45.71	4.02	41.04
90	5.36	54.70	4.97	50.74	4.46	45.51
95	5.93	60.47	5.49	56.05	4.92	50.23
100	6.52	66.55	6.04	61.66	5.41	55.20

	$T_{HTF} = 300°C$		$T_{HTF} = 400°C$		$T_{HTF} = 450°C$	
$\dot{V}$	Δp	H	Δp	H	Δp	H
$[m^3/h]$	$[bar]$	$[m]$	$[bar]$	$[m]$	$[bar]$	$[m]$
5	0.23	2.37	0.23	2.36	0.23	2.35
10	0.27	2.77	0.26	2.70	0.26	2.67
15	0.33	3.32	0.31	3.18	0.30	3.10
20	0.41	4.18	0.38	3.92	0.37	3.79
25	0.51	5.19	0.47	4.78	0.45	4.57
30	0.66	6.70	0.60	6.11	0.57	5.82
35	0.80	8.15	0.72	7.35	0.68	6.95
40	1.01	10.27	0.90	9.23	0.85	8.71
45	1.19	12.17	1.06	10.85	1.00	10.19
50	1.47	14.97	1.31	13.34	1.23	12.53
55	1.70	17.31	1.50	15.34	1.41	14.35
60	1.98	20.22	1.75	17.87	1.64	16.70
65	2.25	23.00	1.98	20.25	1.85	18.87
70	2.55	26.01	2.24	22.82	2.08	21.22
75	2.87	29.25	2.51	25.58	2.33	23.74
80	3.20	32.70	2.80	28.53	2.59	26.44
85	3.57	36.38	3.10	31.66	2.87	29.31
90	3.95	40.28	3.43	34.99	3.17	32.35
95	4.35	44.40	3.77	38.51	3.49	35.57
100	4.78	48.75	4.14	42.22	3.82	38.96

Additional Supports for Traverse Pipe Section

As mentioned chapter 5.3.5, the incorporation of additional supports, such as spring supports or constant supports, may be used for a further improvement in regard to a "force-free cutting" of the dynamometers. However, this section depicts only a rough draft for further improvements on the test rig. They may be located in the center of gravity, i.e. centrally between the central location bearing and each dynamometer, see figure B.1.

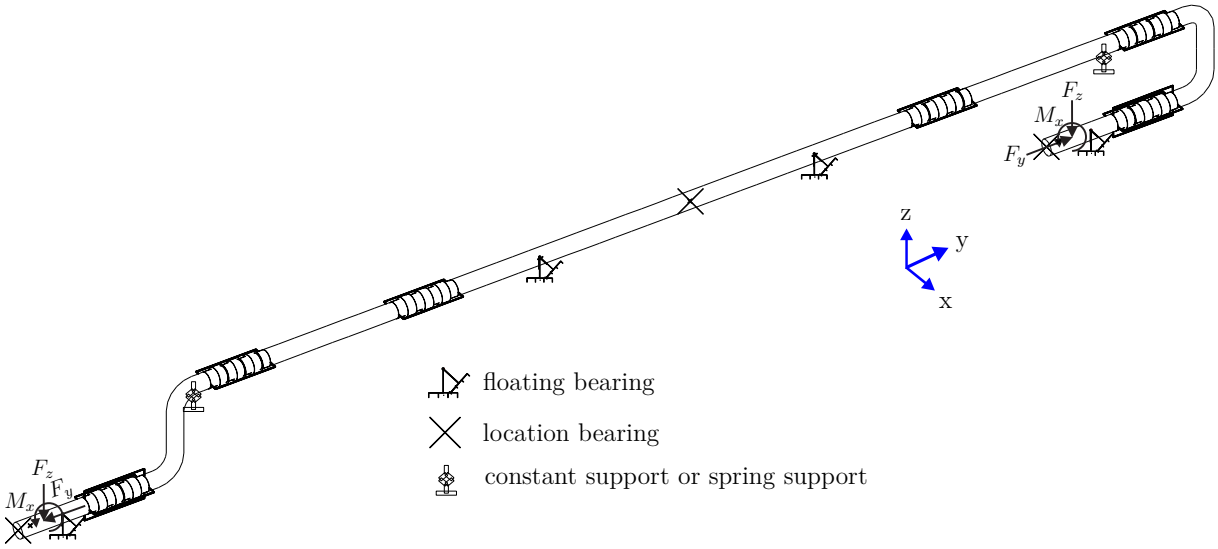

Figure B.1: Isometric view of the pipe section on the traverse using angular expansion joints and additional constant or spring supports

Table 5.8 presented the resulting forces without any type of additional support. The implementation of a spring support with a defined spring rate of 13.6 N/mm (automatically calculated by *ROHR2*) implies a reduction of both forces and torques, see table B.8. The torques about the x-axis are reduced in particular.

Table B.8: *ROHR2* Simulation; forces and torques on both dynamometers with spring support

	outlet			inlet		
	F_y [N]	F_z [N]	M_x [Nm]	F_y [N]	F_z [N]	M_x [Nm]
Idle	359	37	49	-185	-120	3
Inlet	283	-144	-29	-288	-172	4
Design Point	-69	-258	-35	-87	-211	-49
Outlet	-111	-289	-42	-97	-207	-45
Maximum	-169	-327	-53	-90	-207	-48

In contrast to spring supports, the reaction force of a constant support is – as the name already indicates – constant regardless of the stroke. *ROHR2* calculated optimized values of 0.8 kN (outlet) and 1.0 kN (outlet). It can be stated that, using this kind of solution, the loads can be reduced to a minimum.

Table B.9: *ROHR2* Simulation; forces and torques on both dynamometers with constant support

	outlet			inlet		
	F_y [N]	F_z [N]	M_x [Nm]	F_y [N]	F_z [N]	M_x [Nm]
Idle	316	-4	34	-183	-6	43
Inlet	424	-8	18	-285	-51	48
Design Point	80	-96	29	-98	-84	1
Outlet	96	-90	29	-95	-76	1
Maximum	75	-90	30	-88	-72	1

Appendix C

List of PTC Power Plants

Table C.1: List of PTC power plants and their equipment (1) [22] [53] [54]

name	country	start	P_{net} [MW]	REPA	manufacturer	SCA	HTF
SEGS I	USA	1984	14	FH[1]/BJA	SF[2]/ATS[3]	*LS-1*	no info
SEGS II	USA	1985	30	FH/BJA	SF/ATS	*LS-1*	no info
SEGS III	USA	1985	30	FH/BJA	SF/ATS	*LS-2*	no info
SEGS IV	USA	1989	30	FH/BJA	SF/ATS	*LS-2*	DP-DPO
SEGS V	USA	1989	30	FH/BJA	SF/ATS	*LS-2*	DP-DPO
SEGS VI	USA	1989	30	FH/BJA	SF/ATS	*LS-2*	DP-DPO
SEGS VII	USA	1989	30	FH/BJA	SF/ATS	*LS-3*	DP-DPO
SEGS VIII	USA	1989	80	FH/BJA	SF/ATS	*LS-3*	DP-DPO
SEGS IX	USA	1990	80	FH/BJA	SF/ATS	*LS-3*	DP-DPO
Solar One	USA	2007	72	BJA	ATS	*SGX-2*[4]	DP-DPO
Andasol I	Spain	2008	50	BJA		*EuroTrough*	DP-DPO
Andasol II	Spain	2009	50	BJA		*EuroTrough*	DP-DPO
La Risca	Spain	2009	50	BJA	ATS	*SGX-2*	DP-DPO
Solnova I	Spain	2009	50	BJA	ATS	*Astro*[5]	DP-DPO
Solnova III	Spain	2009	50	no info	no info	*Astro*	DP-DPO
Solnova IV	Spain	2009	50	BJA	ATS	*Astro*	DP-DPO
Ibersol	Spain	2009	50	no info	no info	Iberdrola	DP-DPO
Palma del Rio 2	Spain	2010	50	BJA	ATS	*SGNX-2*[4]	DP-DPO
Extresol-11	Spain	2010	50	no info	no info	*SenerTrough*	DP-DPO
Extresol-2	Spain	2010	50	no info	no info	*SenerTrough*	DP-DPO
Majadas I	Spain	2010	50	BJA	ATS	*SGNX-2*	DP-DPO
La Florida	Spain	2010	50	no info	no info	*Ingemetal*	DP-DPO
ISCC Kuraymat	Egypt	2011	20	BJA	ATS	*EuroTrough*	DP-DPO
Manchasol-1	Spain	2011	50	no info	no info	*SenerTrough*	DP-DPO
Manchasol-2	Spain	2011	50	no info	no info	*SenerTrough*	DP-DPO
Lebrija 1	Spain	2011	50	BJA	ATS	Solel	DP-DPO
Palma del Rio 1	Spain	2011	50	BJA	ATS	*SGNX-2*	DP-DPO
Helioenergy I	Spain	2011	50	BJA	ATS	*Astro*	DP-DPO
Arcosol	Spain	2011	50	BJA	ATS	*SenerTrough*	DP-DPO
Termesol 50	Spain	2011	50	BJA	ATS	*SenerTrough*	DP-DPO
Andasol III	Spain	2011	50	RFHA	SF	*EuroTrough*	DP-DPO
Megha	India	2011	50	no info	no info	*Albiasa*	DP-DPO
ISCC Hassi R'mel	Algeria	2011	20	no info	no info	*Astro*	DP-DPO
La Dehasa	Spain	2011	50	no info	no info	*Ingemetal*	DP-DPO
Termesol 50	Spain	2011	50	no info	no info	*SenerTrough*	DP-DPO
Extresol-3	Spain	2010	50	no info	no info	*SenerTrough*	DP-DPO
Martin Next Generation	USA	2010	75	no info	no info	*Gossamer*	DP-DPO
Helioenergy II	Spain	2012	50	BJA	ATS	*Astro*	DP-DPO
Morón	Spain	2012	50	no info	no info	no info	DP-DPO

[1] Flex Hose
[2] *Senior Flexonics GmbH*
[3] *Advanced Thermal Systems, Inc.*
[4] *Acciona* brand name
[5] *Abengoa* brand name

Table C.2: List of PTC power plants and their equipment (2) [22] [53] [54]

name	country	start	P_{net} [MW]	REPA	manufacturer	SCA	HTF
Solaben 2	Spain	2012	50	no info	no info	*Astro*	DP-DPO
Solaben 3	Spain	2012	50	no info	no info	*Astro*	DP-DPO
Solacor 1	Spain	2012	50	no info	no info	*Astro*	DP-DPO
Solacor 2	Spain	2012	50	no info	no info	*Astro*	DP-DPO
Orellana	Spain	2012	50	no info	no info	*SenerTrough*	DP-DPO
Guzmán	Spain	2012	50	BJA	ATS	*SenerTrough*	DP-DPO
Borges	Spain	2012	22.5	no info	no info	*SunField 6*	DP-DPO
Olivenza 1	Spain	2012	50	no info	no info	*SunField 6*[6]	DP-DPO
Astexol II	Spain	2012	50	BJA	ATS	*EuroTrough*	DP-DPO
Aste 1A	Spain	2012	50	BJA	ATS	*SenerTrough*	DP-DPO
Aste 1B	Spain	2012	50	BJA	ATS	*SenerTrough*	DP-DPO
Helios I	Spain	2012	50	no info	no info	*Astro*	DP-DPO
Helios I	Spain	2012	50	no info	no info	*Astro*	DP-DPO
Thai Solar Energy	Thailand	2012	5	BJA	no info	*Solarlite*	water/steam
Solaben 1	Spain	2013	50	no info	no info	*Astro*	DP-DPO
Solaben 6	Spain	2013	50	no info	no info	*Astro*	DP-DPO
Shams 1	UAE	2013	100	BJA	ATS	*Astro*	DP-DPO
Godawari	India	2013	50	no info	no info	*EuroTrough*	DP-DPO
Arenales	Spain	2013	50	no info	no info	*SunField 6*	DP-DPO
Enerstar (Villena)	Spain	2013	50	BJA	ATS	*SenerTrough*	DP-DPO
Solana	USA	2013	250	BJA	ATS	*Abengoa E2*	DP-DPO
Termesol 1	Spain	2011	50	no info	no info	*SenerTrough*	DP-DPO
Termesol 2	Spain	2011	50	no info	no info	*SenerTrough*	DP-DPO
Casablanca	Spain	2013	250	no info	no info	*SenerTrough*	DP-DPO
Diwakar	India	2013	100	no info	no info	*SenerTrough*	DP-DPO
KVK	India	2013	100	no info	no info	*SenerTrough*	DP-DPO
Gujarat Solar One	India	2013	25	no info	no info	*EuroTrough*	DP-DPO
Mojave Solar Project	USA	2014	250	RFHA	SF	*Abengoa*	DP-DPO
Genesis	USA	2014	250	BJA	ATS	*SenerTrough*	DP-DPO
NOOR I	Morocco	2015	143	BJA	ATS	*SenerTrough*	DP-DPO
NOOR I	Morocco	2015	143	BJA	ATS	*SenerTrough*	DP-DPO
KaXu Solar One	South Africa	2015	100	no info	no info	*Abengoa E2*	DP-DPO
Bokpoort	South Africa	2016	50	BJA	ATS	*SenerTrough*	DP-DPO
NOOR II	Morocco	2017	200	BJA	ATS	*SenerTrough*	DP-DPO
Ilanga I	South Africa	2017	100	no info	no info	no info	DP-DPO
ISCC Duba 1	Saudi Arabia	2017	43	no info	no info	no info	no info
Shagaya	Kuwait	2017	50	no info	no info	no info	DP-DPO
Ashalim	Israel	2018	110	BJA	ATS	no info	DP-DPO
Xina Solar One	South Africa	2017	100	no info	no info	no info	DP-DPO
Kathu Solar Park	South Africa	2018	100	no info	no info	no info	DP-DPO

[6] *Siemens* brand name

Appendix D

Technical Drawings and CAD Model

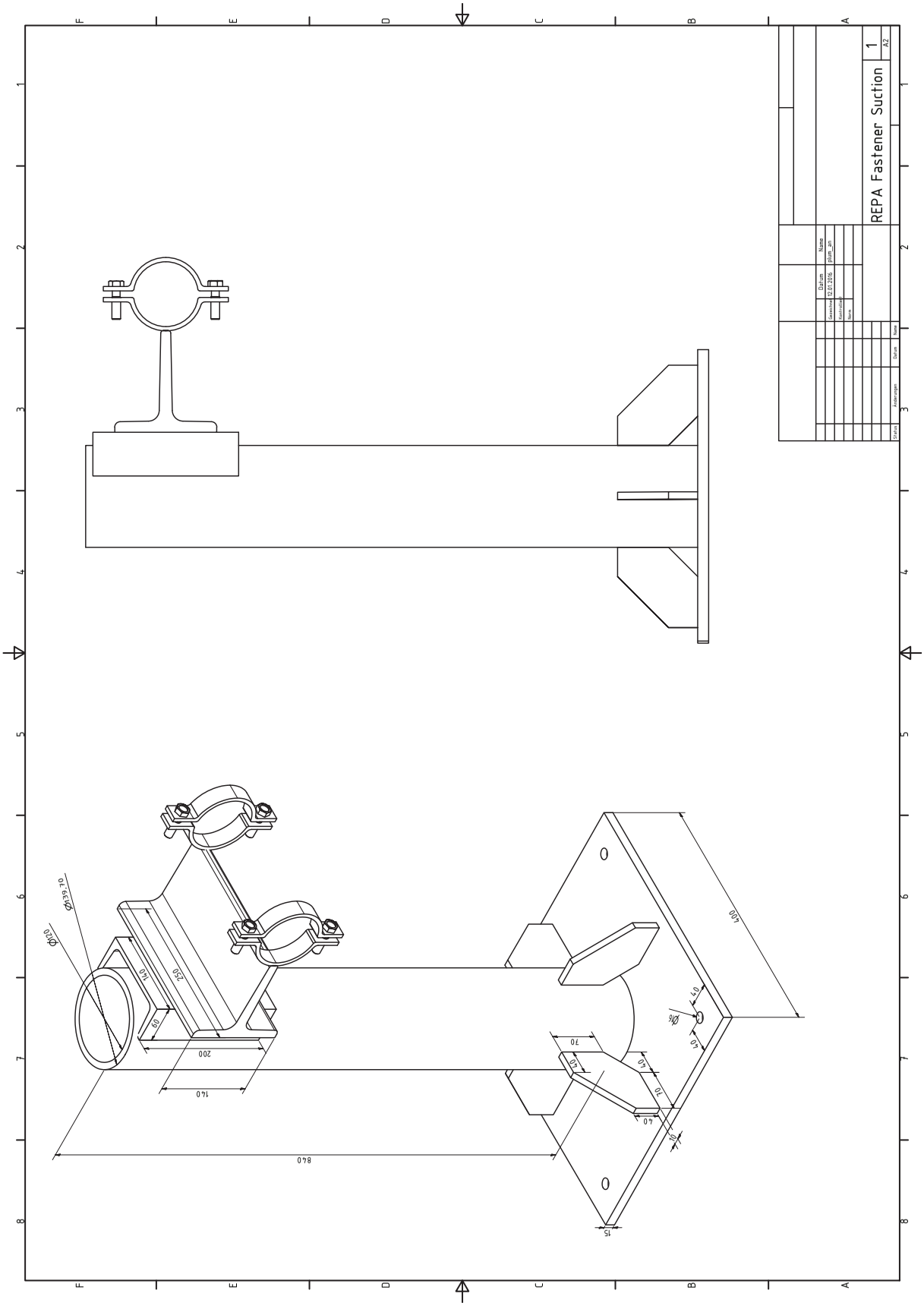

Figure D.1: Fastemer Assembly of the pump's suction side

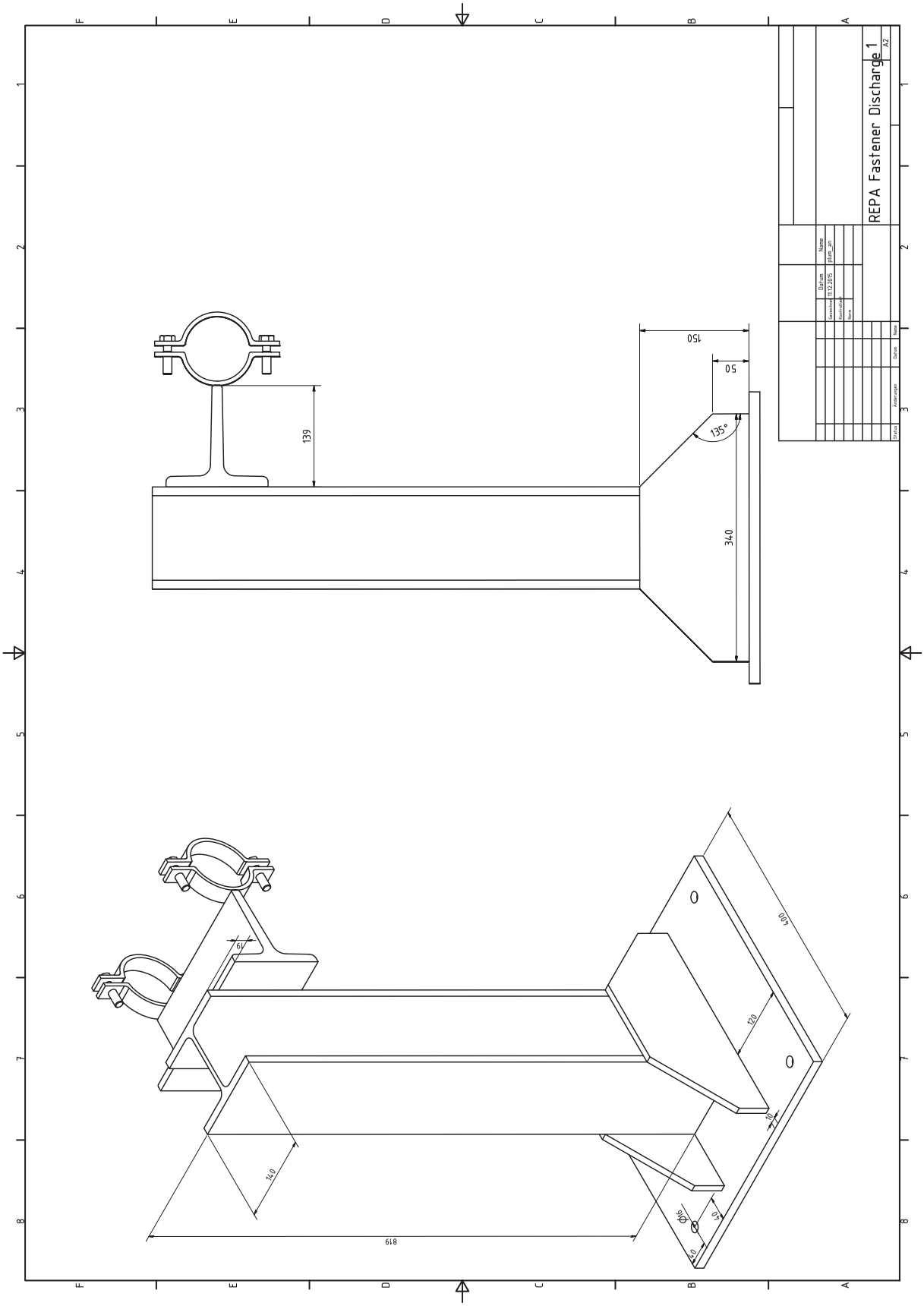

Figure D.2: Fastemer Assembly of the pump's discharge side

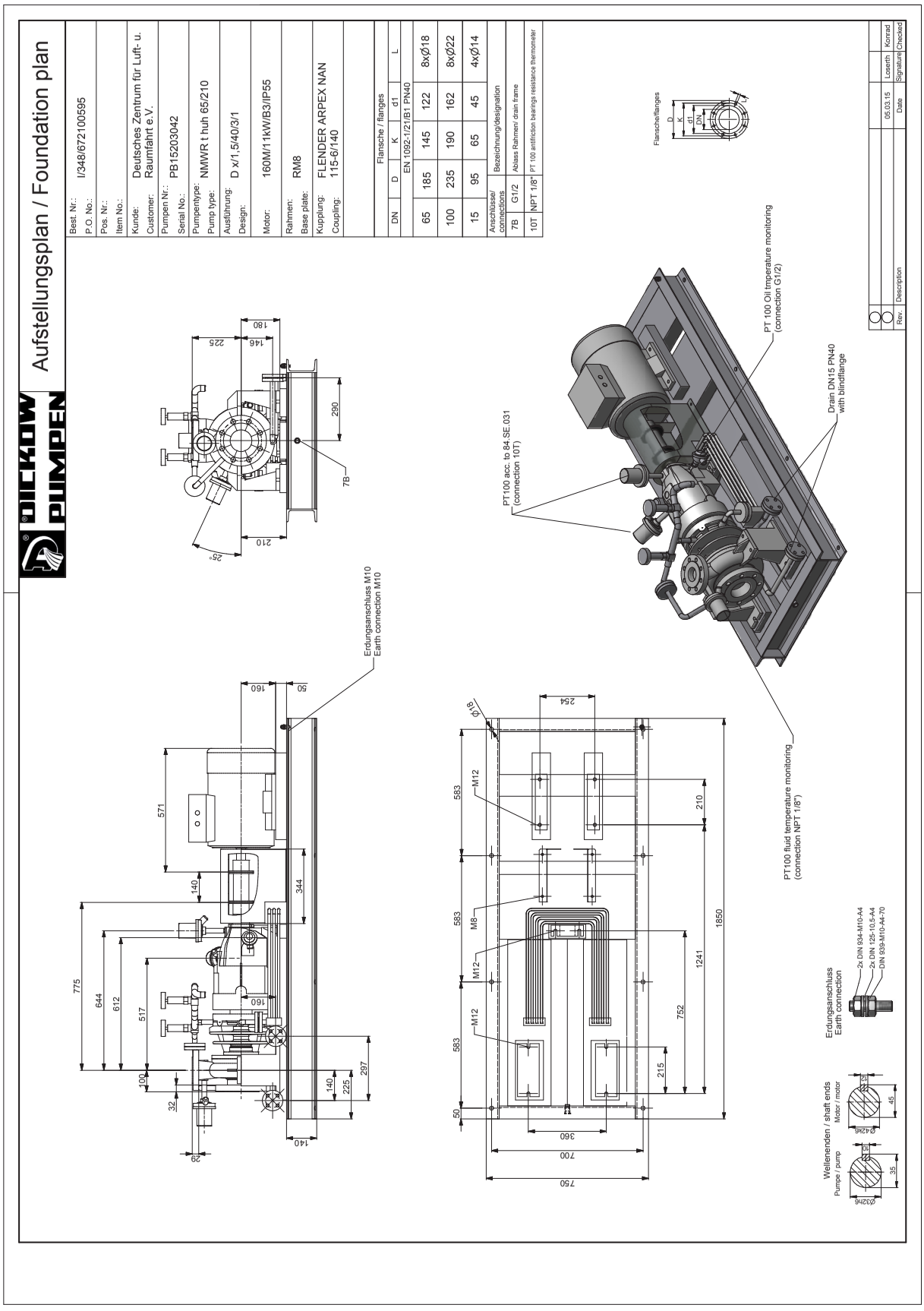

Figure D.3: Pump foundation plan DICKOW

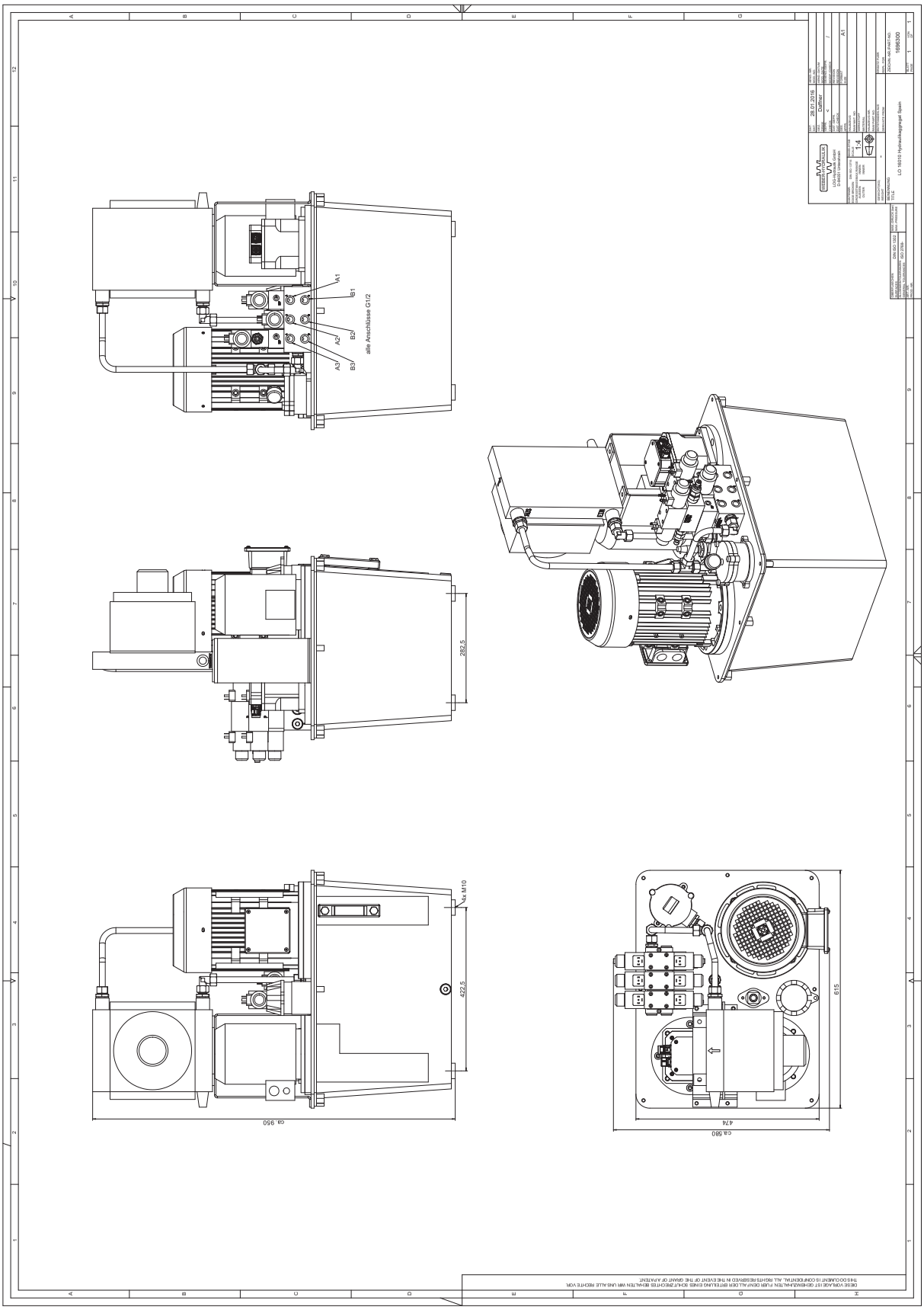

Figure D.4: Hydraulics unit

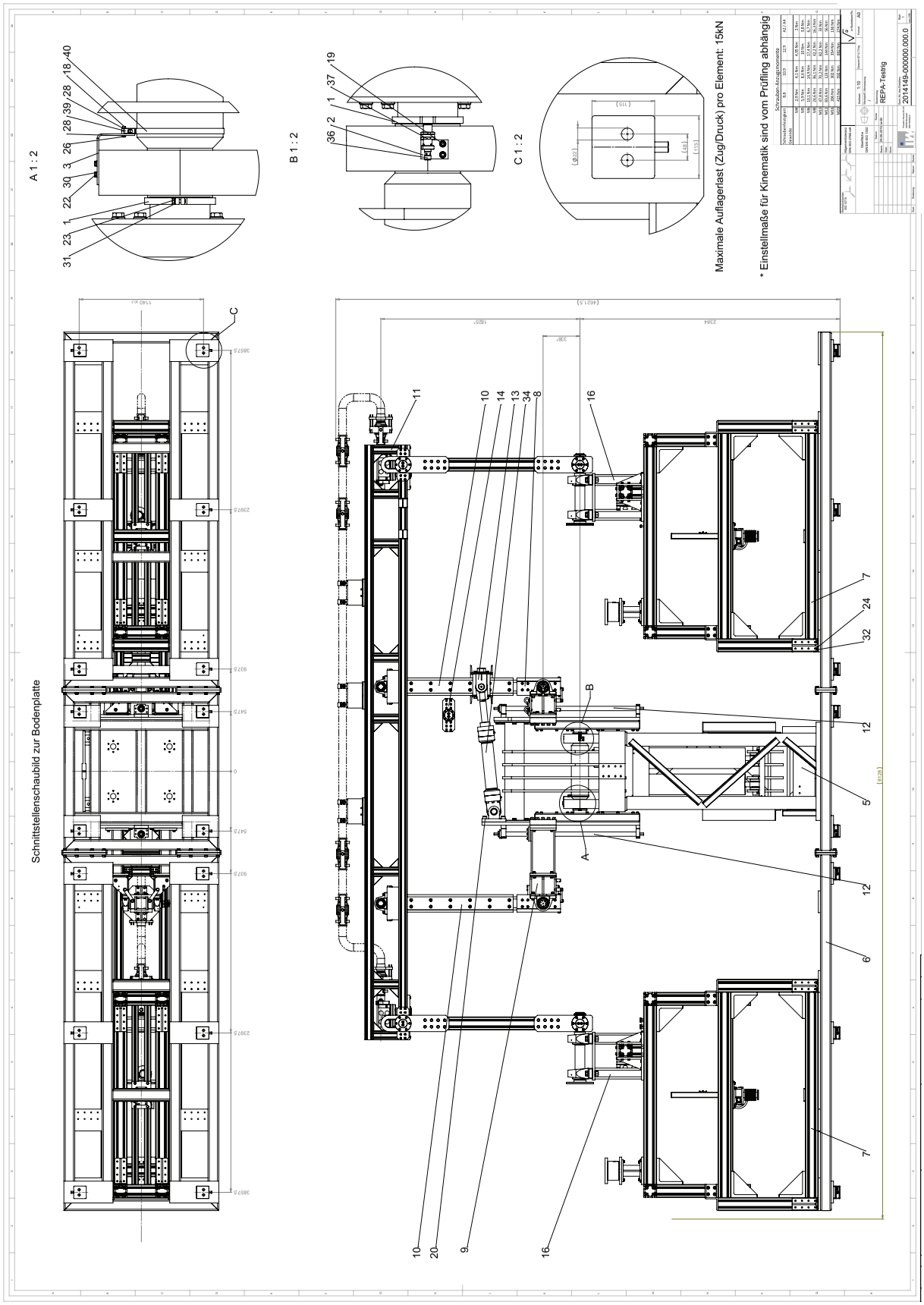

Figure D.5: Bearing Sensor

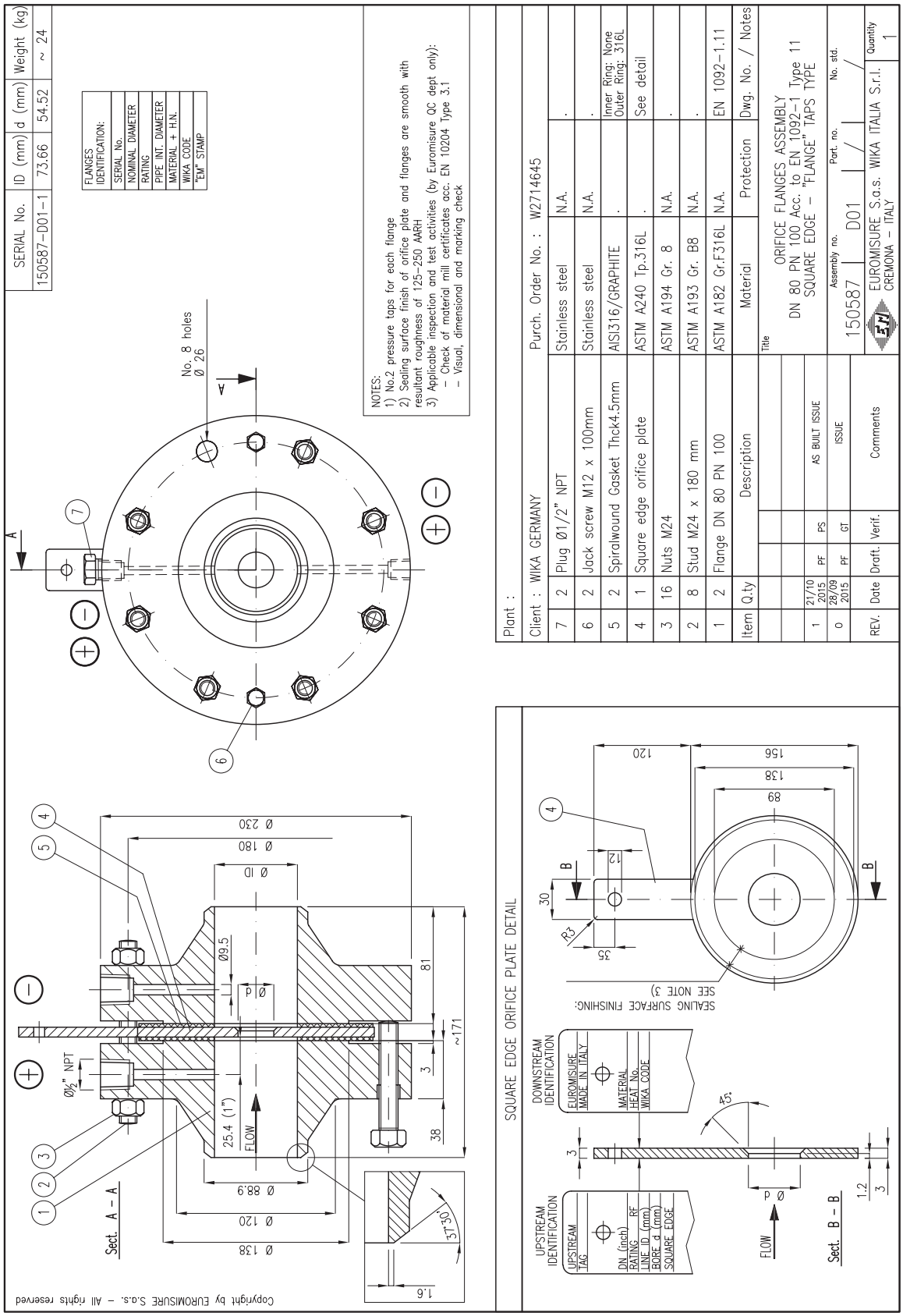

Figure D.6: Orifice plate assembly

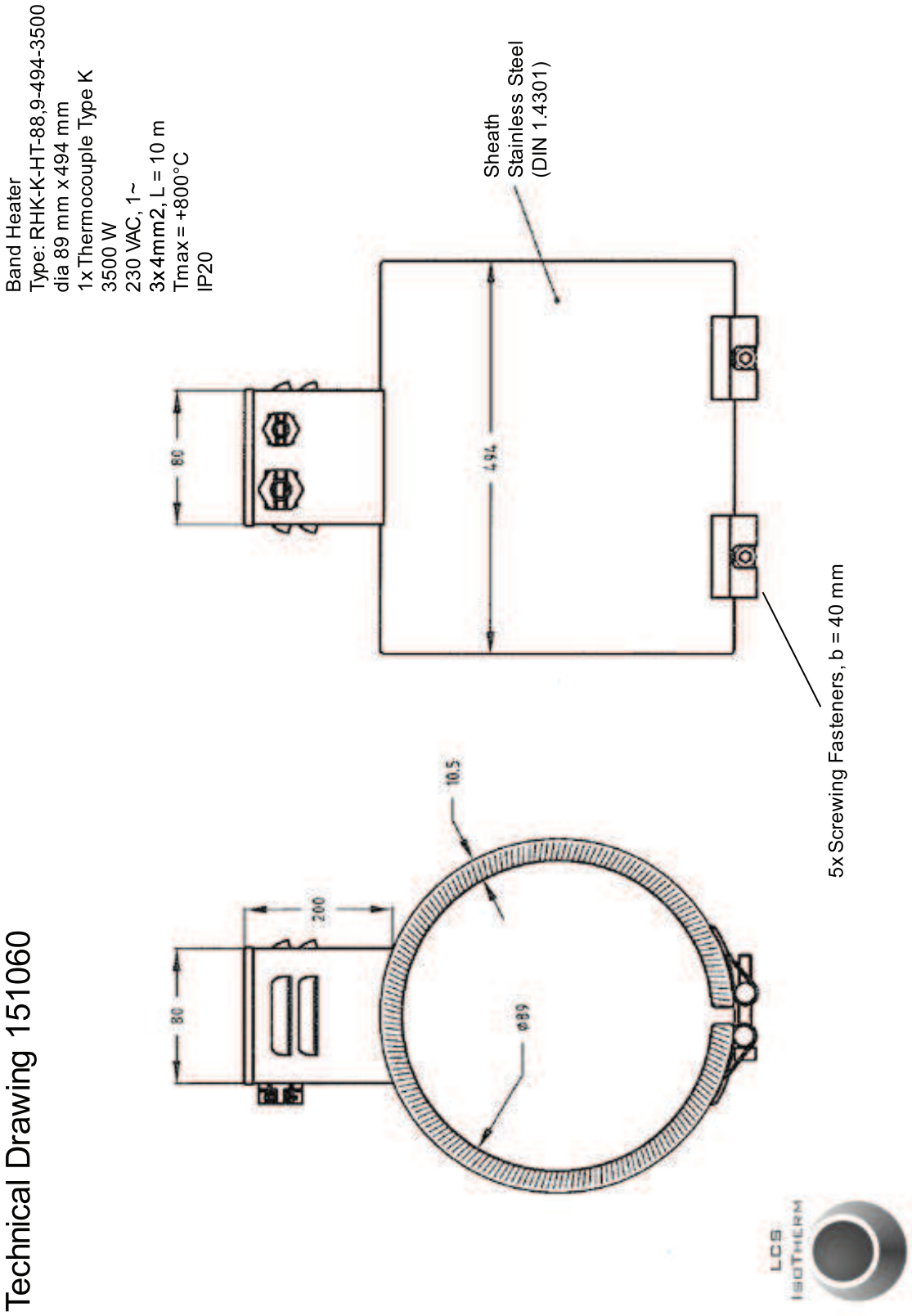

Figure D.7: Band heater element

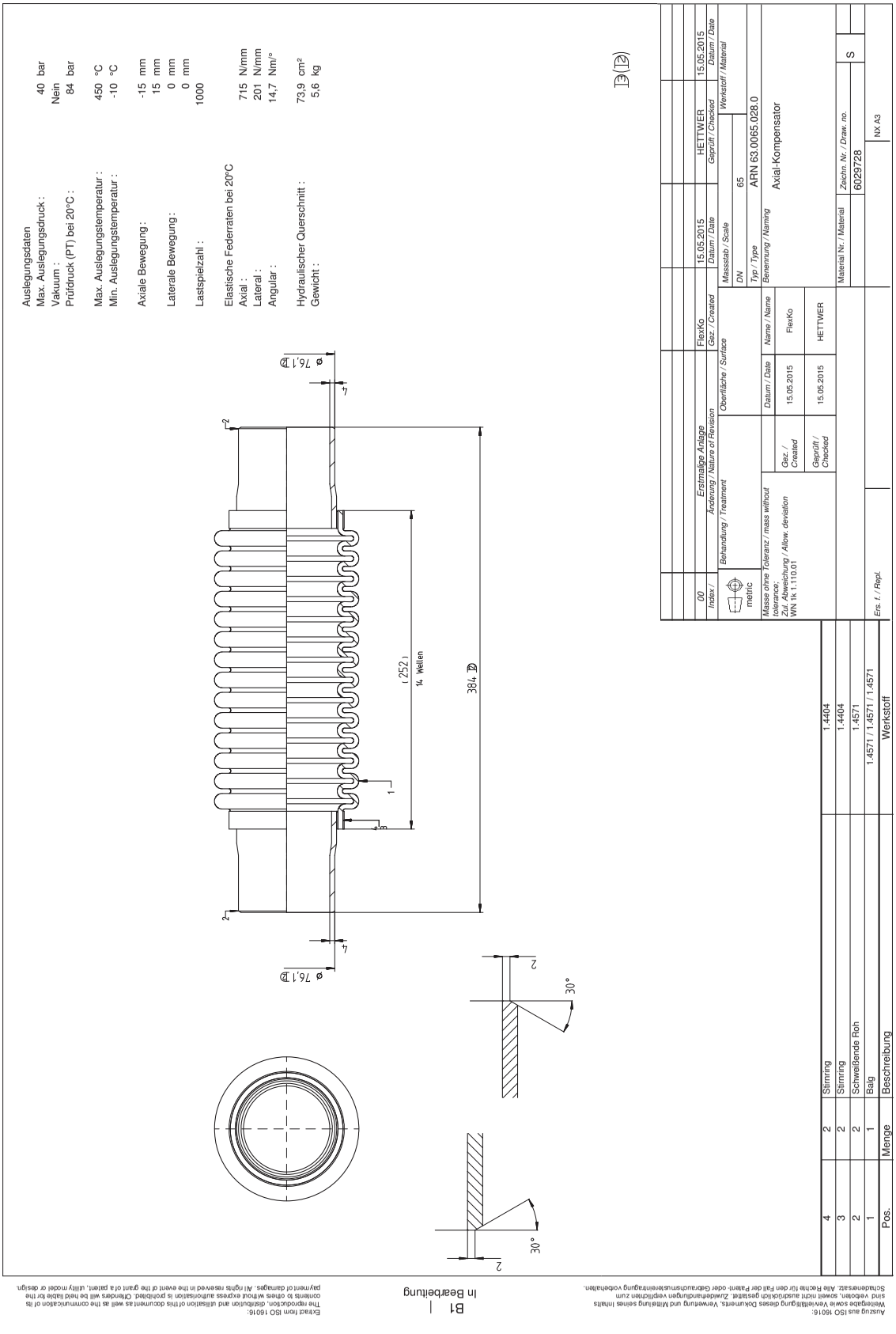

Figure D.8: Technical drawing and data sheet of the axial expansion joints

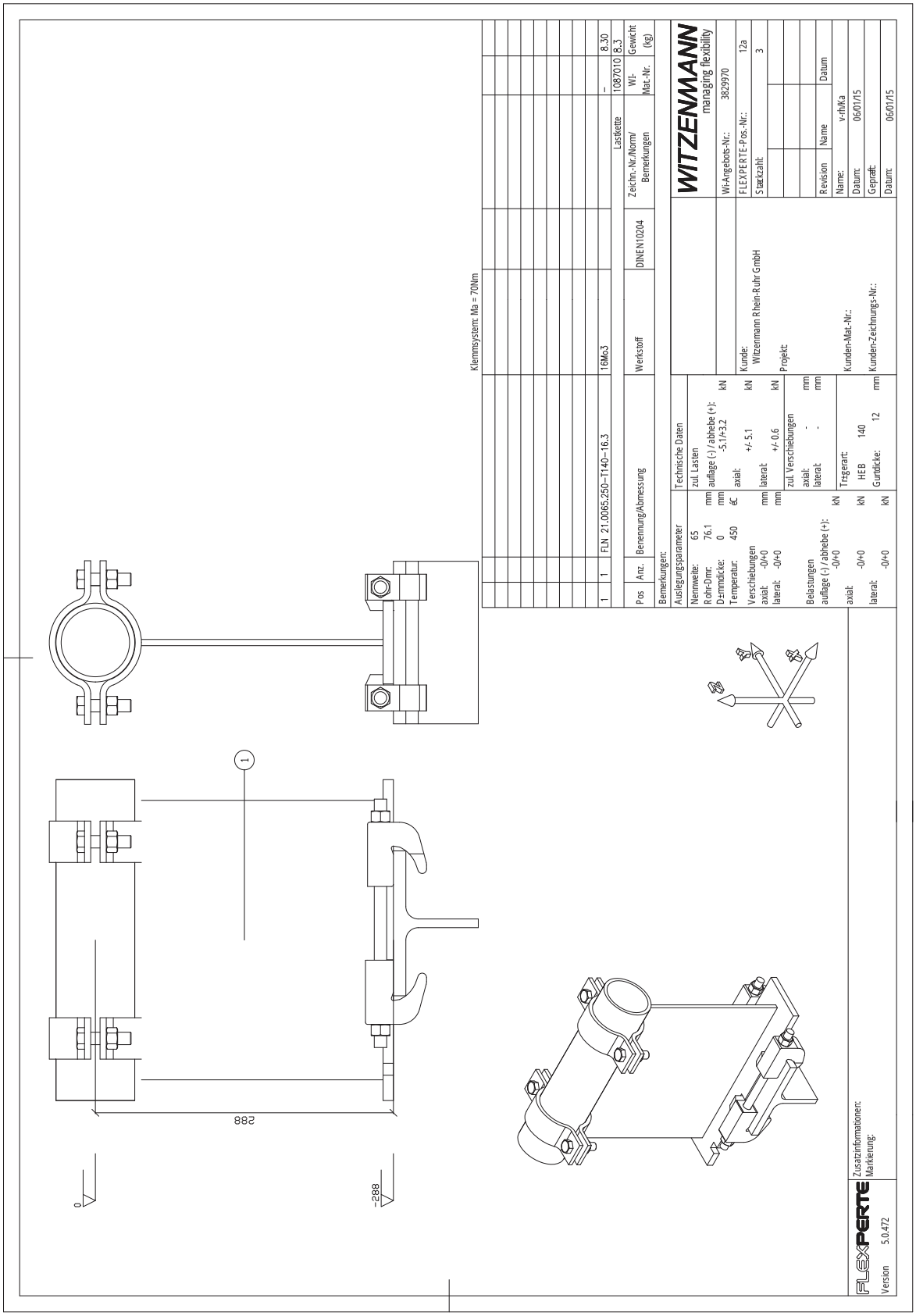

Figure D.9: Technical drawing and data sheet of the location bearing on the traverse

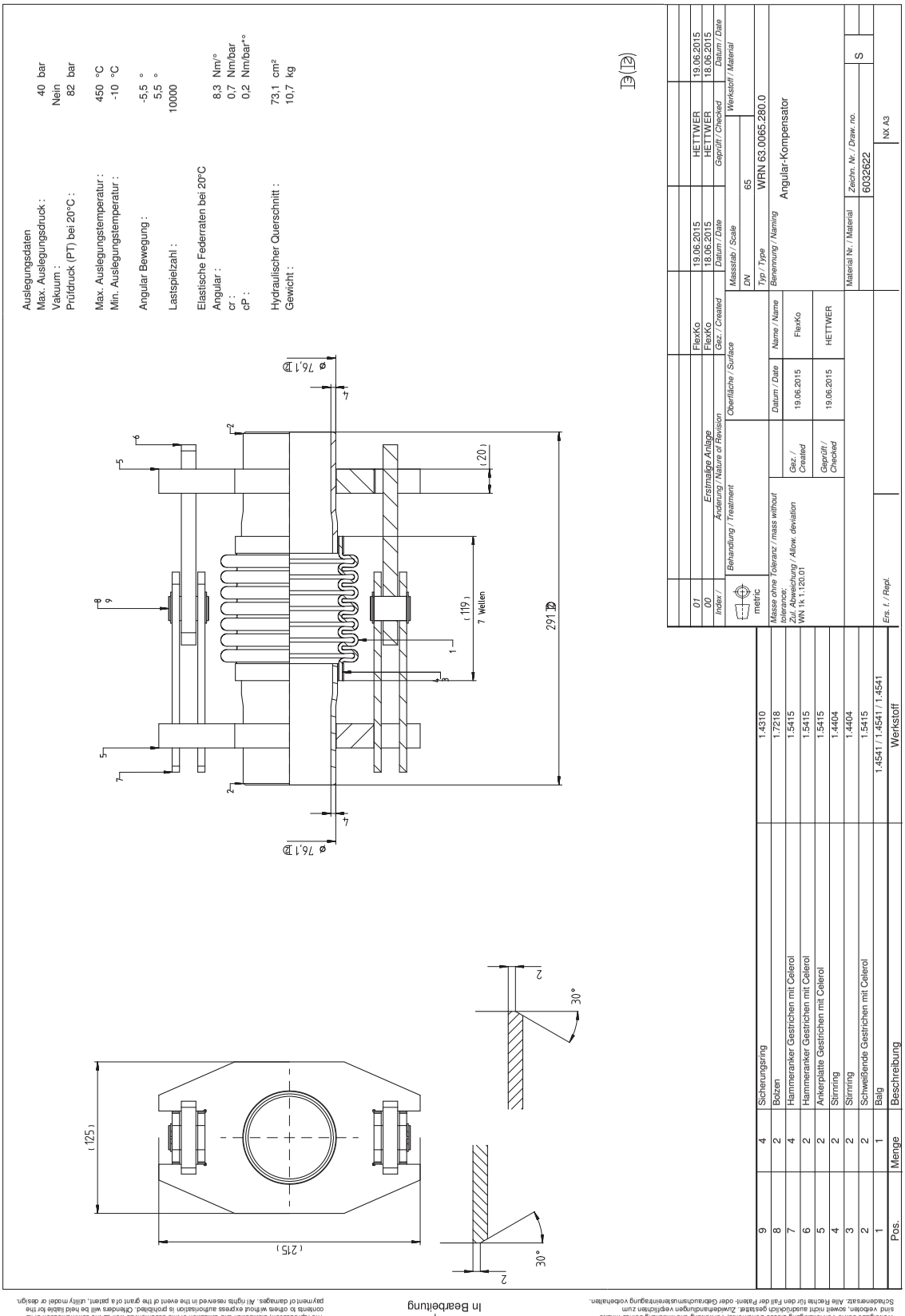

Figure D.10: Technical drawing and data sheet of the angular expansion joints (single hinged)

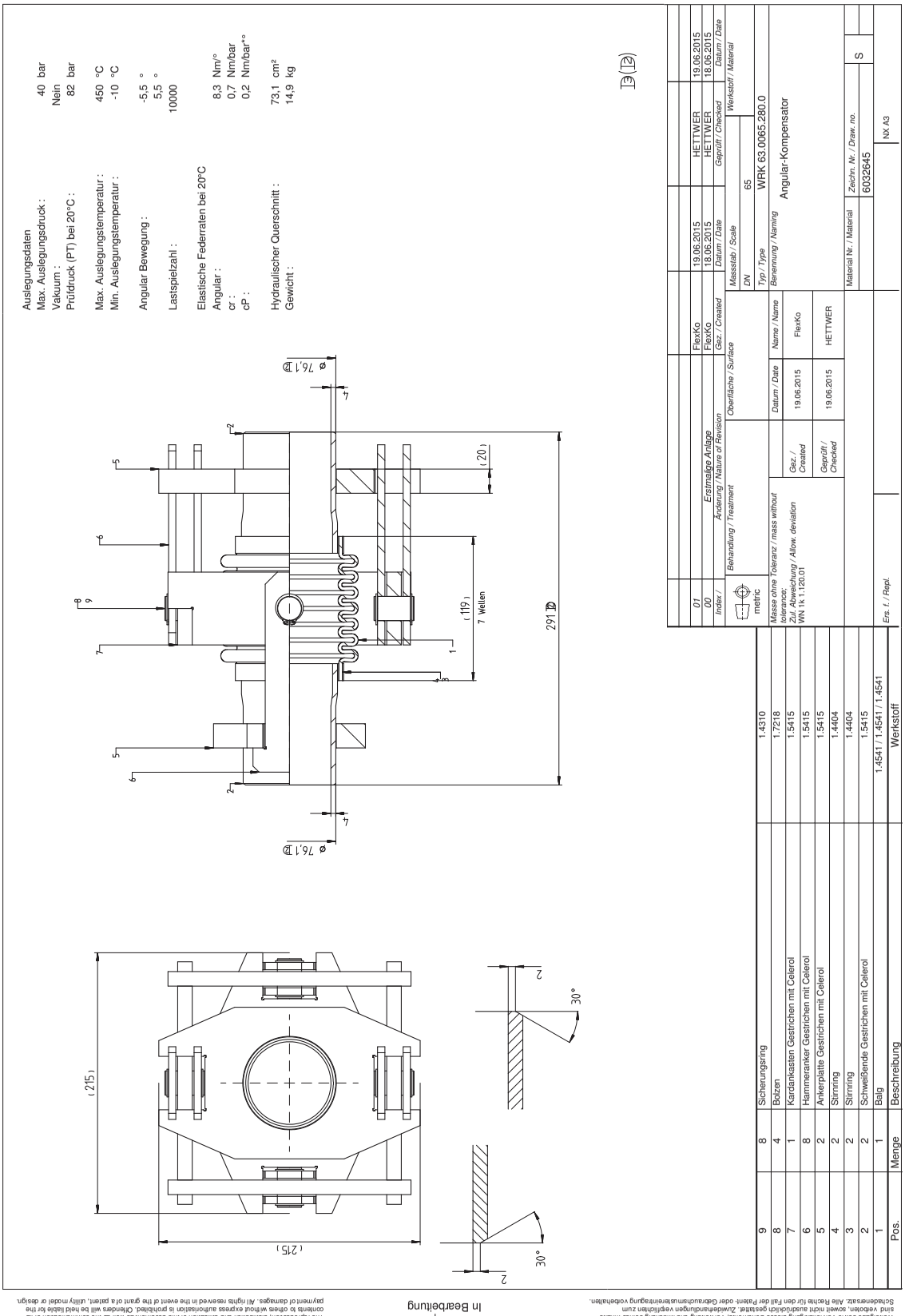

Figure D.11: Technical drawing and data sheet of the angular expansion joints (gimbal hinged)

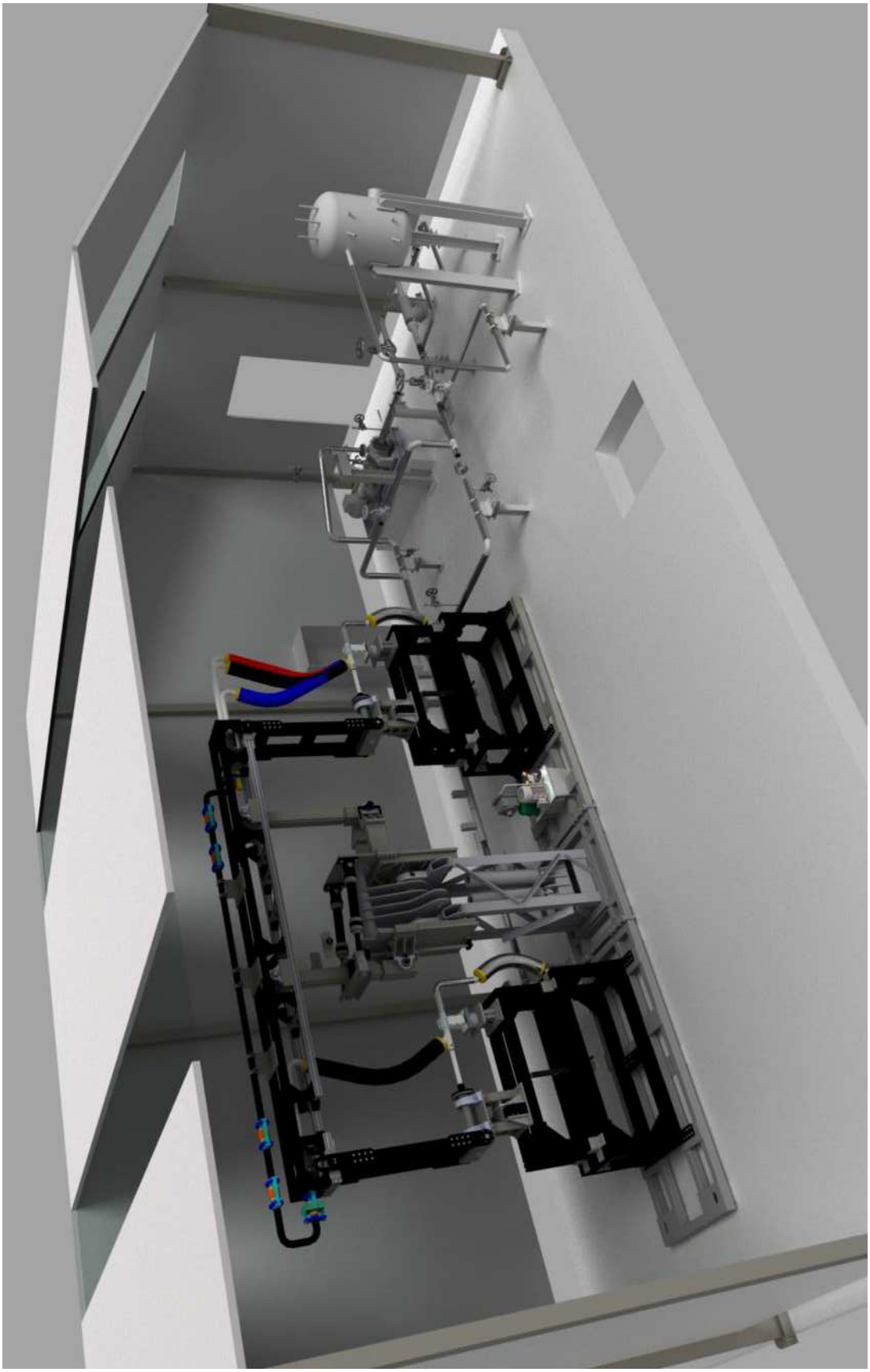

Figure D.12: CAD model of the REPA Test Rig

Appendix E

Photos of the Test Rig

All photos that are shown in the following section have been taken after a first stage erection of the HTF cycle. The Kinematics Unit is not presented.

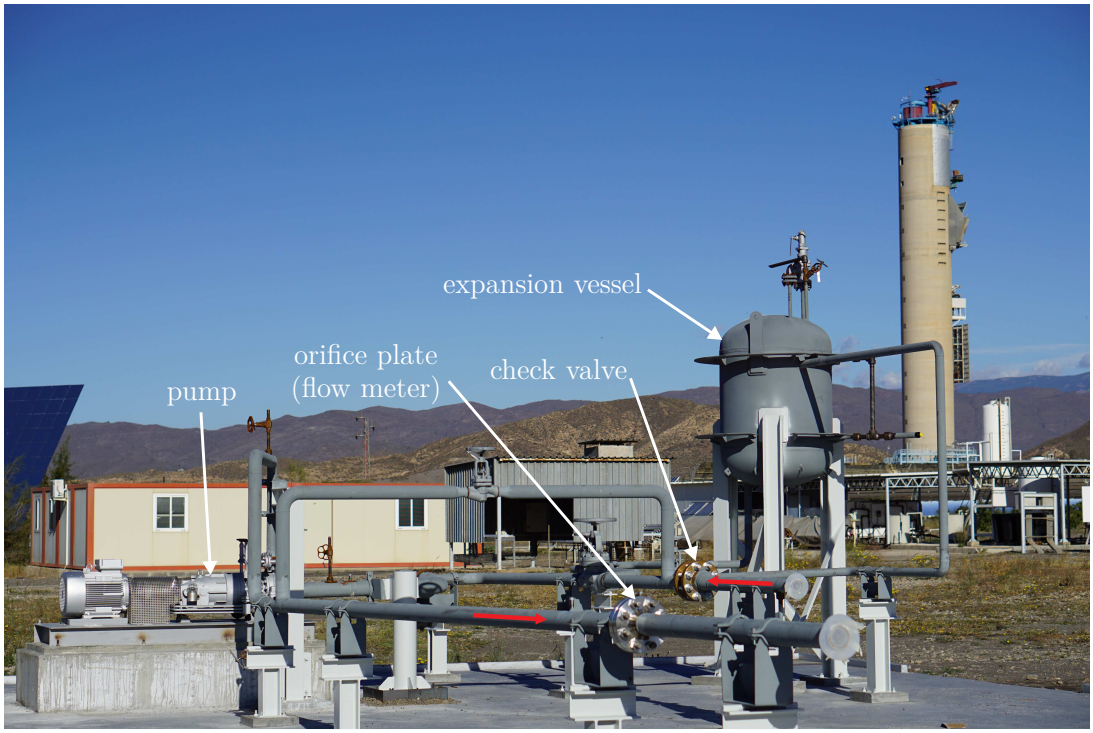

Figure E.1: Photo of the HTF cycle (first stage erection)

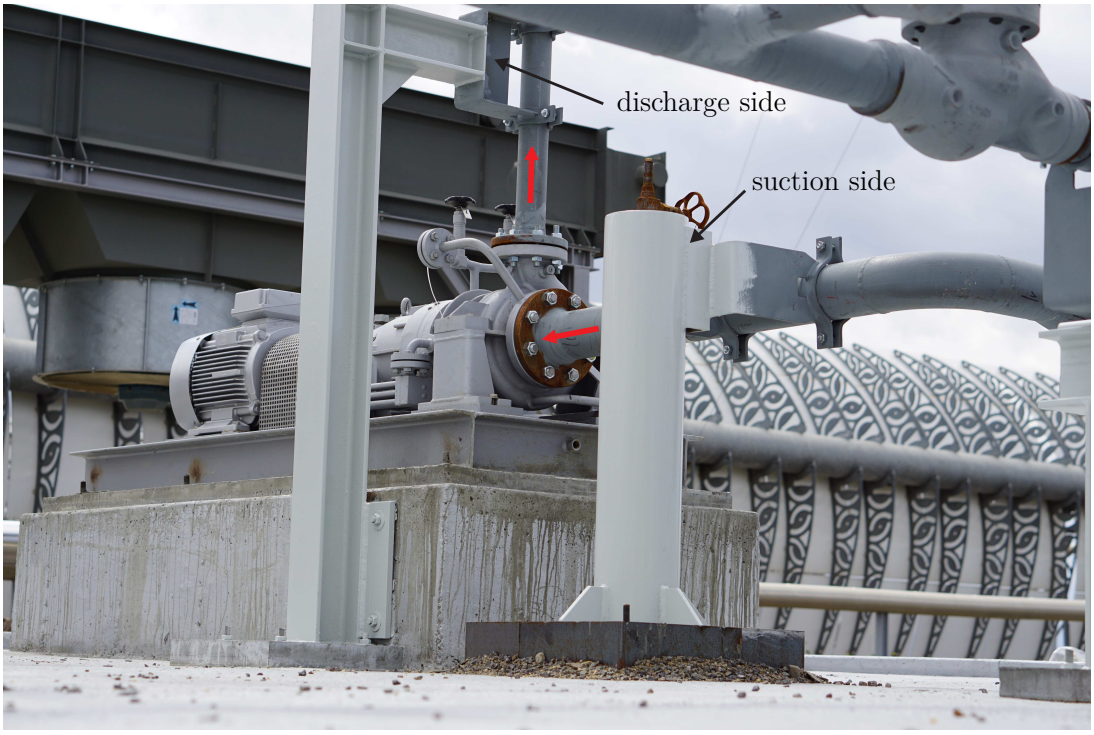

Figure E.2: Photo of the fix points up- and downstream the pump

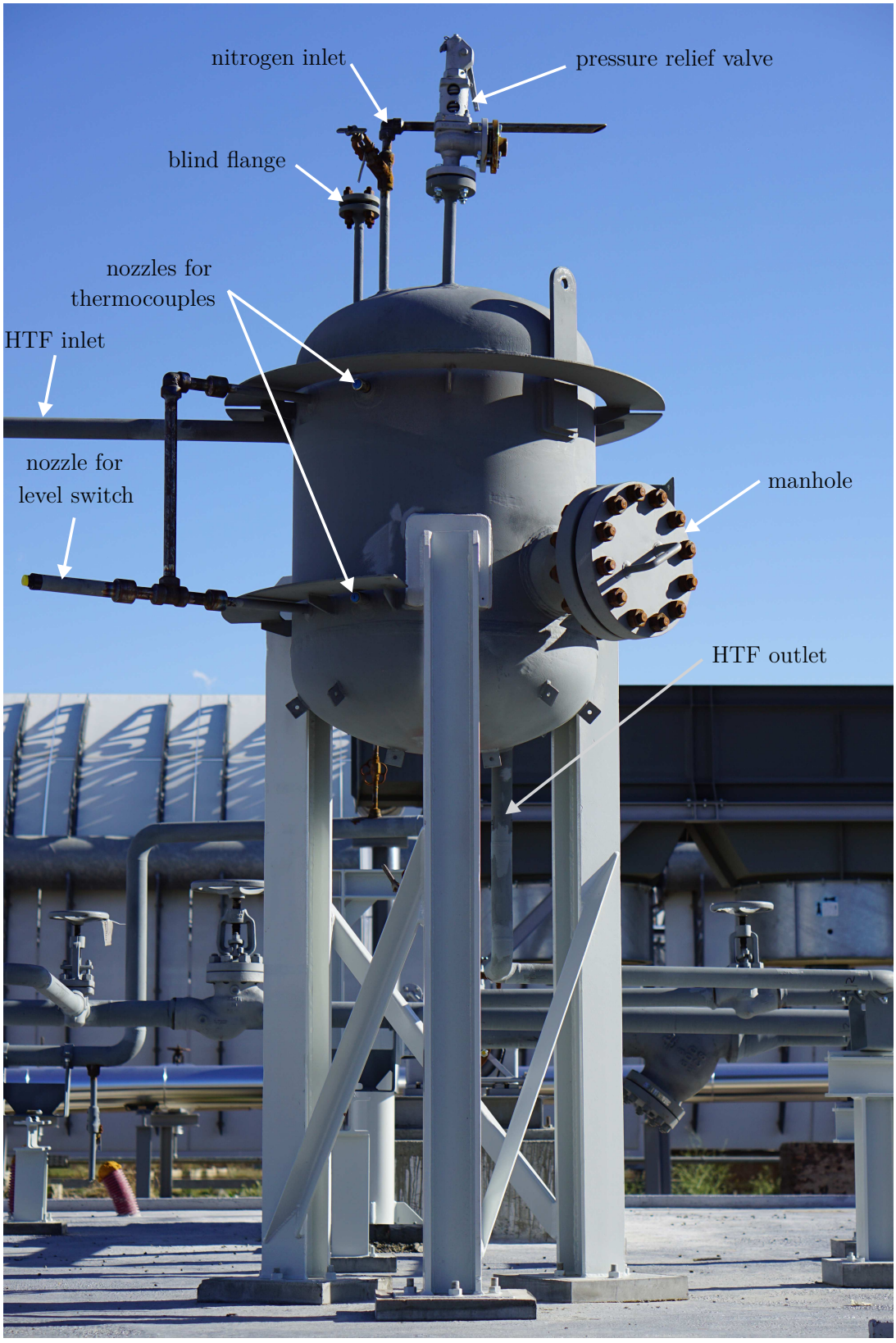

Figure E.3: Photo of the expansion vessel